UNIVERSITY OF PADUA

DEPARTMENT OF INDUSTRIAL ENGINEERING

Department Of Industrial Engineering

Master degree on Chemical and Process Engineering

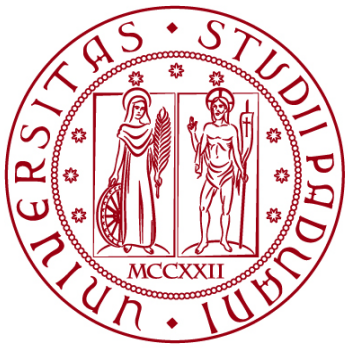

MASTER THESIS

APPLICATION OF THE NON-PARAMETRIC KINETICS (NPK) METHOD TO THE REVERSIBLE SOL-GEL TRANSITION OF GELATIN

Tutor:
Prof. Paolo Canu
Supervisors:
Prof. Rosa Nomen and Prof. Rubén Mercadé

Graduand: Tommaso Palermito
2020225

ACADEMIC YEAR 2022-2023

INDEX

ACKNOWLEDGEMENTS

I would like to thank my Spanish supervisors Rosa Nomen and Rubén Mercadé which helped me on the comprehension of the results obtained and supported me during all the period of work.

I would also like to thank Eduard Serra for the patience and availability during the experimental part, and Julià Sempere for the final revision of the work.

Another acknowledgement goes to professor Canu Paolo for the final revision of the thesis.

ABSTRACT

The kinetic parameters of the melting and gelation phenomena occurring on the reversible sol-gel transition under thermal treatments can be estimated with the classical methods. From a Differential Scanning Calorimetry (DSC) the peaks of the endothermic or exothermic behavior of the relative melting and gelation phenomena can be analysed by calculating the enthalpies of reaction ΔH and the temperatures at which they occur T_m and T_g. It was observed a clear dependence of the thermal treatments of the DSC and the resulting enthalpy and peak temperature. For instance, during cooling the enthalpy and gelation temperature are decreasing by increasing cooling rate.

The purpose of this work is to applicate the Non-Parametric Kinetic (NPK) method on the reversible sol-gel transition to estimate its kinetic parameters. It is observed that this method gives good results and thus it can be used for this kind of reaction.

INTRODUCTION

In this project the purpose is to study the kinetics of denaturation and aggregation of proteins with a Differential Scanning Calorimetry (DSC) through the Non-Kinetic Parameter (NPK) method. Some information needed to be considered as the protein denaturation process and possible aggregation to protein gel formation, the sol-gel transition phenomenoun, the thermal analysis with DSC, and the general application of the NPK method.

The denaturation of a protein is a process that takes place when the protein's folded structure stops working (unfolding and uncoiling of the helix structure), losing for example secondary and tertiary structures. Most denaturation processes are permanent, but it has been observed (in a few cases) that some denaturation processes can be reversed: this is referred to as 'protein renaturation'.

There can be different causes of denaturation: increasing temperature, changing pH, and changing solution's salt composition. In this thesis, it was taken in consideration the denatuation of whey protein isolate (WPI) through thermal treatment under DSC. In facts, WPI samples can denaturates by heat, which should have activated hydrophobic interactions with other proteins (aggregation), leading also to a possible formation of a protein gel.

From the DSC it was observed that the whey proteins analysed were not showing any denaturation effect, thus they were considered as already denatured. The DSC was then used to observe the gelation temperature of a gelatin by heating up in a lower range than the one required for the protein analysis (gelation temperature was almost 20°C while the denaturation temperature should expected to be around 80°C).

For the two DSC analysis, two different kind of pans can be used, medium pressure and aluminium open crucibles, because different were the solution properties and conditions needed for the analysis.

Through the NPK, it could be estimated the kinetic parameters of the reaction occurring in DSC analysis. This method uses the thermal analysis of DSC in order to give

the kinetic parameters of the denaturation and aggregation reactions that could occur under thermal treatments.

From a Matlab code built for the method, the kinetic parameters as the reaction rate constant *k* and the order of reaction *n* were estimated for the sol-gel transition. It was observed that different values were obtained changing the scanning rate of the thermal treatments of the DSC.

The objective of this work is to show how the NPK method can be applied in chemical phenomena related with proteins to achieve the relative kinetic parameters by comparing the results obtained with the ones reported in existing literature.

1.1 Classical methods for kinetic studies

The two most common methods utilized to obtain the kinetic parameter values *k* and *n* are the integral and the differential methods.

The estimation of the reaction rate constant *k* allows to evaluate the value of the activation energy *Ea*. Once it is known the values of *k* at two different temperatures (es: T_1 and T_2), *Ea* can be estimated from the following steps [1]:

$$\frac{k(T_2)}{k(T_1)} = \frac{Ae^{\frac{-Ea}{RT_2}}}{Ae^{\frac{-Ea}{RT_1}}} \tag{1.1}$$

$$k(T_2) = k(T_1)\, e^{\frac{-Ea}{R}(\frac{1}{T_2} - \frac{1}{T_1})} \tag{1.2}$$

$$\frac{-Ea}{R} = \frac{\ln[k(T_2)] - \ln\,[k(T_1)]}{\frac{1}{T_2} - \frac{1}{T_1}} \tag{1.3}$$

Eq. (1.1) is the ratio of $k(T_2)$ over $k(T_1)$, considering $k(T)$ expressed following the Arrhenius equation ($k(T) = Ae^{\frac{-Ea}{RT}}$ with *A* the pre-exponential factor).

Eq. (1.3) shows how the activation energy can be estimated from the slope of the straight line obtained in a plot of *ln(k)* against *1/T*, the so called 'Arrhenius plot' (Figure 1.1).

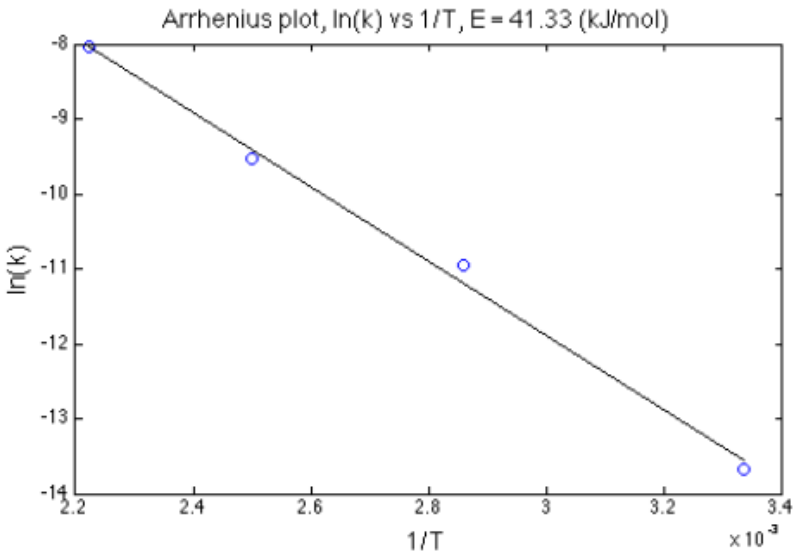

Figure 1.1: Arrhenius plot reporting ln(k) against 1/T. The slope of the straight line has value -Ea/R [1].

In the Arrhenius plot, the slope is given by *-Ea/R*, thus the activation energy can be calculated by multiplying this value (with opposite sign) by gas constant *R*:

$$Ea = -(\frac{-Ea}{R}) \cdot R \tag{1.4}$$

To follow the Arrhenius equation, the *k(T)* data should show a linear behaviour in the Arrhenius plot.

It was already said that there are two different common methods to estimate not only the reaction rate constant *k*, but also the order of reaction *n*.

1.1.1 Integral method

The integral method starts with the functional form of a rate equation [1]. This rate equation may be given, or it can be proposed a functional form, e.g., first-order or second-order. Then the rate equation is put into the balance equation and integrate the balance equation. Finally, it can be determined if the integrated equation can "fit the data" and, if it does fit, it can be determined the values of the rate coefficients.

By "fit the data" it is meant that the rate equation can predict how the experimental data change as reaction time or initial concentrations are changed.

1.1.2 Differential method

The differential method collects some concentration data for each time instant, and then it differentiates them by determining the slopes dC_A/dt (or dX_A/dt) at a series of different times. For a constant volume, for an isothermal batch reactor it can be estimated the reaction rates at known compositions, thus a table of r_A and C_A values. The next step is to find a rate function that can fit the data.

For an essentially irreversible reaction of order *n*:

$$\frac{dC_A}{dt} = r_A = kC_A^n \tag{1.5}$$

$$\ln(r_A) = \ln(k) + n \cdot ln(C_A) \tag{1.6}$$

Eq. (1.6) shows how both the reaction rate constant and the order of reaction can be estimated from a plot of $ln(-dC_A/dt)$ against $ln(C_A)$.

The integral method is based on testing and guessing any reaction order, estimating then the rate coefficient, but it doesn't need to differentiate the data. The differential method, instead, determines both *k* and *n* from one plot by differentiating the data.

It is suggested to know how to do both methods. Eventhough, for complex reaction kinetics, it might be advisable to use the differential method to see how the rate depends on the concentrations of the different components in the reaction mixture. In the example considered previously, only C_A was affecting the rates but, in general, there may be more components involved in a rate equation.

CHAPTER 2: DENATURATION REACTION OF PROTEINS

2.1 General characteristics of proteins

Proteins are large biomolecules and macromolecules that comprise one or more long chains of amino acid residues, and so they differ from one another in their amino acids sequence. This sequence results in protein folding into a specific 3D structure that determines its activity [2]. Proteins perform a vast array of functions within organisms, including catalysing metabolic reactions, DNA replication, responding to stimuli, providing structure to cells and organisms, and transporting molecules from one location to another. Our bodies get this protein from foods such as cheese, milk, nuts, and so on. Proteins differ from one another primarily in their sequence of amino acids, which is dictated by the nucleotide sequence of their genes, and which usually results in protein folding into a specific 3D structure that determines its activity.

Denaturation is a process that takes place when a protein's folded structure stops working. The process disrupts amino acid chains by breaking covalent bonds. For example, in numerous amino acid combinations, high concentrations of alcohol can disrupt hydrogen bonding in amide groups in secondary or tertiary protein structures.

The hydrogen bonds are disrupted as a result of changes in pH, temperature, and chemical structure, resulting in the unfolding of globular proteins and the uncoiling of the helix structure. Denaturation of proteins occurs as a result, and secondary and tertiary structures are lost. A native protein can change its structure and so its properties due to a denaturation process that can be followed by aggregation (Figure 2.1).

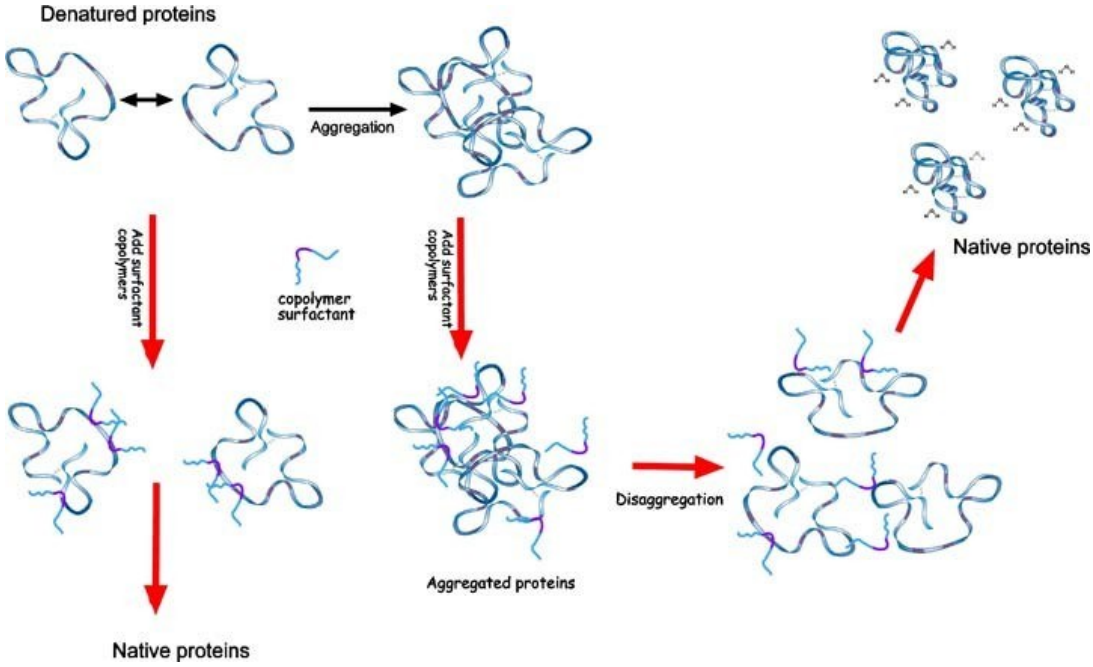

Figure 2.1: three different configurations of proteins: native (folded), denatured (unfolded), and aggregated. Adding surfactant copolymers to denatured proteins, native proteins will be obtained, while adding those after aggregation of the unfolded proteins, aggregated proteins will be achieved which, disgregated, will become native proteins (protein denaturation and aggregation - Bing images).

There can be different causes of protein denaturation:

- hydrogen bonds and non-polar hydrophobic interactions can be disrupted by heat which vibrates the molecules causing an increasing in the kinetic energy. This denaturation disrupts amino acid chains by breaking covalent bonds;
- the hydrogen bonds can also be disrupted as a result of changes in pH;
- heavy salts, like salts and bases, cause protein molecule structure to be disrupted.

Most denaturation processes are permanent, but it has been observed (in a few cases) that some denaturation processes can be reversed; this is referred to as protein renaturation. The coagulation of egg white when an egg is boiled is one of the most common examples of protein denaturation. A change in temperature causes denaturation in this case. Another example of denaturation of proteins is curdling of milk, which occurs when lactic acid is produced by microbial action.

It has to be considered also that the denaturation reactions are considerably influenced by the particular medium in which they take place [3]. The DSC can observe the endothermic phenomenon of the denaturation of proteins (in which heat is

absorbed) and the exothermic one of a possible aggregation (in which heat is released). Nevertheless, the two processes may give rise to only one peak in the DSC curve which is difficult to analyse. With the high scan rates used in most DSC studies (rates above 1°C/min), only one peak is seen [4]. The endothermic peak for denaturation is related to the helix-coil transition [5].

DSC can also calculate the enthalpy of reaction, allowing to measure the residual undenatured protein.

2.2 Thermal denaturation on whey protein isolate WPI

Whey protein is a mixture of proteins isolated from whey (liquid remaining after milk has been curdled and strained, byproduct of manufacturing of cheese or casein). This protein is typically a mixture of beta-lactoglobulin β-LG with variant A and variant B (~65%), alpha-lactalbumin α-LA (~25%), bovine serum albumin BSA (~8%), and immunoglobulins. These are soluble in their native forms, independent of pH. Whey protein is commonly marketed as a protein supplement (muscles growth), and various health claims have been attributed to it. Whey is left over when milk is coagulated during the process of cheese production, and contains everything that is soluble from milk after the pH is dropped to 4,6 during the coagulation process. It is a 5% solution of lactose in water with lactalbumin and some lipid content. Processing can be done by simple drying, or the relative protein content can be increased by removing the lactose, lipids and other non-protein materials.

Whey can be denatured by heat. High heat, such as the sustained high temperatures above 72 °C associated with the pasteurization process (food treated with mild heat to eliminate pathogens), denatures whey proteins. Denaturating the whey proteins activates hydrophobic interactions with other proteins, and the formation of a protein gel.

From the general equation (Eq. 1.5 in Chapter 1) it is possible to arrive to the overall order *n* by the differential method. It is needed an equation that describes the reaction rate at any one moment as a function of the instantaneous protein concentration as

Eq. 1.6 in Chapter 1. With appropriate plots it will be obtained straight lines in which, at any temperature of heating, *n* is the slope.

The B variant is at all temperature less heat stable than the A one [6]. For the experimentally obtained kinetic parameters to be valid over a wide temperature range, it is necessary to have a reliable value for the reaction order. To obtain such a value it is imperative to consider data on degrees of denaturation of up to about 90%.

In order to determine *Ea*, it was utilized an Arrhenius plot (Figure 2.2). It can be observed from the graphic, that there are two temperature regions in which the slope of the straight line is completely different because of the thermal denaturation effect. This break seems to happen at about 90 °C for the β-LG and 80 °C for the α-LA. Calculating *Ea* and *A*, it can accurately be predicted the irreversible denaturation of individual protein fractions after any heat treatment in a wide temperature/holding time range.

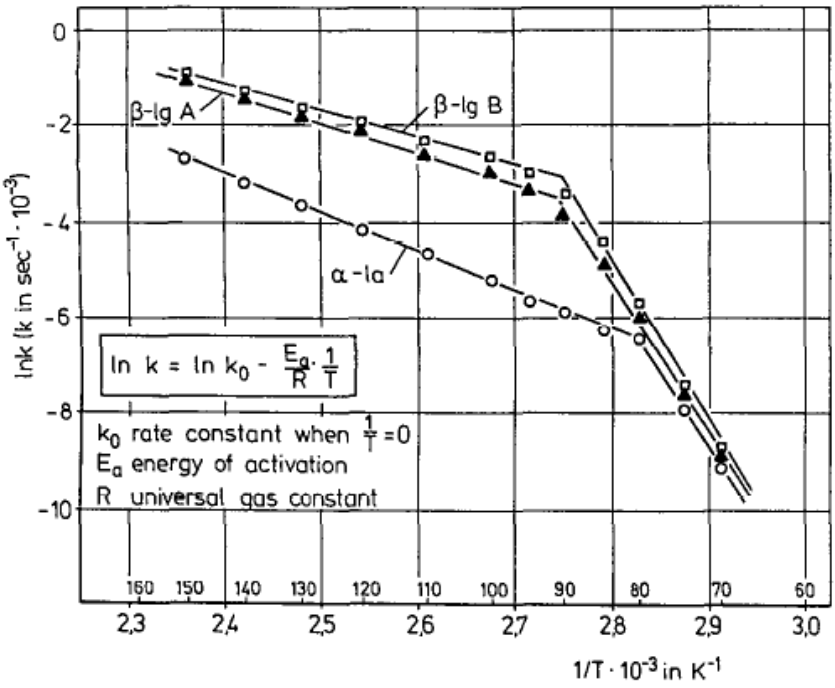

Figure 2.2: Arrhenius plot for whey protein denaturation (DANNENBERG & KESSLER, 1988). The three different compounds can be observed: β-LG with its two variant A and B, and α-LA. Depending on temperature range, the estimation of Ea for the same compound leads to different results (different slopes in the same straight line).

The overall reaction kinetic data for the example denaturation were reported in a table shown in Figure 2.3.

Table 2—Reaction kinetic data for the denaturation of β-LG A and B and α-LA.

	n	Temp [°C]	E_A [kJ/mol]	ln(k_o)	r^{2a}
β-LG A	1.5	70–90	265.21	84.16	0.996
		95–150	54.07	14.41	0.997
β-LG B	1.5	70–90	279.96	89.43	0.995
		95–150	47.75	12.66	0.999
α-LA	1.0	70–80	268.56	84.92	0.997
		85–150	69.01	16.95	0.999

[a] r^2: coefficient of correlation of the straight lines in Fig. 5

Figure 2.3: Reaction kinetic data for the denaturation of β-LG A and B, and α-LA. r^2 is the coefficient of correlation of the straight lines in the Arrhenius plot (DANNENBERG & KESSLER, 1988).

In [4], to cover a wide range of scan rates, it was used two different calorimeters: a Perkin-Elmer DSC 7, which was convenient for high scan rates because of low thermal inertia, and a Hart Scientific DSC 4207, which was preferable with lower scan rates. The curves given from this kind of analysis is showed in Figure 2.4.

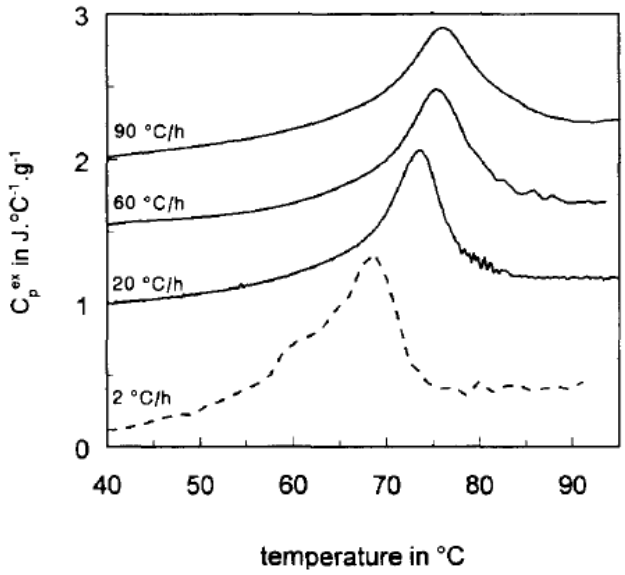

Figure 2.4: Comparison between Hart Scientific DSC 4207 curves with specific heat capacity in J/°C/g against temperature in °C at three different scan rates (20, 60 and 90 °C/h) and the adiabatic calorimeter curve at 2 °C/h, for the 50 g/L β-LG. The curves obtained with the Hart Scientific DSC 4207 have been corrected for thermal lag [4].

The temperature corresponding to maximum heat capacity, the peak temperature, and the shape of the excess heat capacity curve are highly dependent on scan rate. With decreasing scan rate, peak temperature decreases and the curve becomes more

asymmetrical. With the very low scan rate of the adiabatic calorimeter the peak becomes even more asymmetrical and a shoulder at 60 °C could be seen. These results clearly demonstrate that more than one process must have been taking place and that, by lowering the scan rate, these processes can be, at least partially, separated in time.

CHAPTER 3: SOL-GEL TRANSITION

3.1 General characteristics of gelatins

Collagen is the main structural protein found in skin and other connective tissues. It also is the most abundant protein in mammals (25-35% of body protein). Furthermore, this compound is formed from the combination of amino acids. The most common tissues of our body where it can be found collagen are in fibrous tissues such as tendons, ligaments, and skin [7].

The gelatin is a collection of peptides and proteins produced by partial hydrolysis of collagen extracted from the skin, bones, and connective tissues of animals such as domesticated cattle, chicken, pigs, and fish. During hydrolysis, some of the bonds between and within component proteins are broken. Its chemical composition is, in many aspects, closely similar to that of its parent collagen (Figure 3.1).

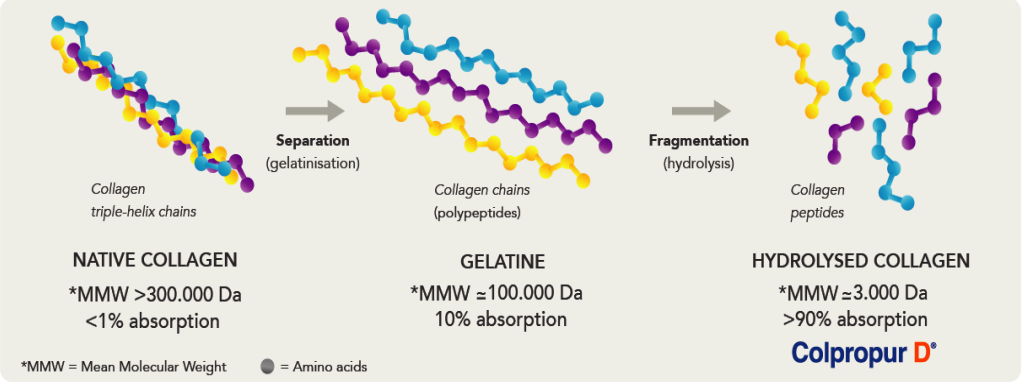

Figure 3.1: Hydrolysis of native collagen to gelatin. Collagen triple-helix chains separates into collagen chains formed by polypeptides and then is fragmented into peptides (hydrolysis of native collagen to gelatin - Bing images).

Gelatin has a gel strength of around 30 to 300 grams Bloom and it declines if it is subjected to temperatures above 100°C, or if it is held at temperatures near 100°C for an extended period of time.

Hydrolyzed collagen contains 19 amino acids, predominantly glycine(Gly) 26–34%, proline(Pro) 10–18%, and hydroxyproline(Hyp) 7–15%, which together represent

around 50% of the total amino acid content. Glycine is responsible for close packing of the chains, while proline restricts the conformation.

Gelatin is classified as a hydrogel, so a crosslinked hydrophilic polymer that does not dissolve in water. It absorbs 5–10 times its weight in water to form a gel and this gel can be melted by reheating (Figure 3.2), and it has an increasing viscosity under stress (thixotropic).

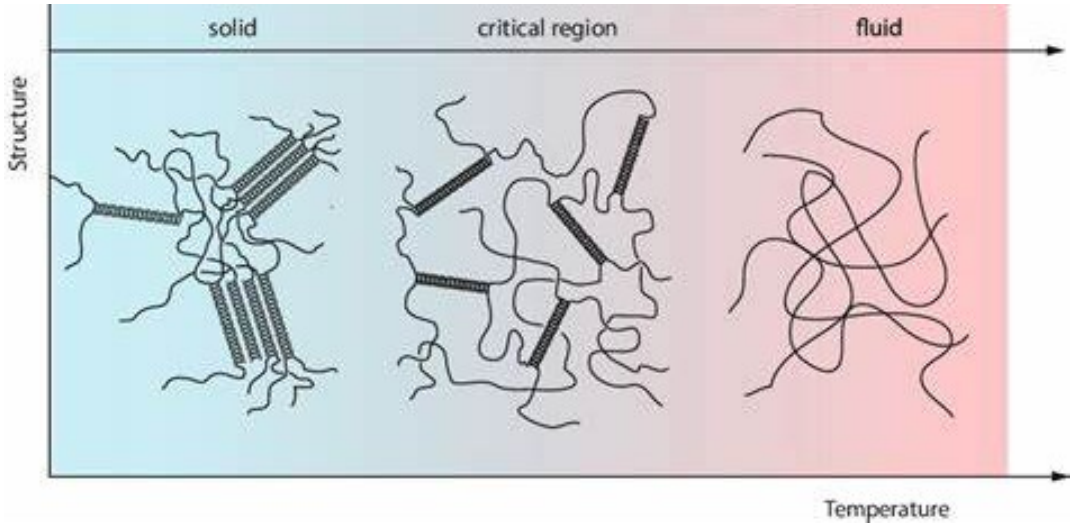

Figure 3.2: Thermal reversible sol-gel transition. Increasing temperature, the solid structure of the gel will melt into a fluid structure (thermal reversible sol-gel transition - Bing images).

3.2 Melting and gelation of gelatins

3.2.1 Gelation temperature and its dependence on sol concentration

A typical indotherm obtained in an experiment is shown in Figure 3.3. It is clearly observed in this figure that the DSC data have three distinct indotherms [8]. The temperature corresponding to the peak of the indotherm occurring at the highest temperature has been designated as T_3, corresponding to the monomer-aggregate transition temperature, the middle as T_2, that is the coil-helix transition temperature, and lowest one as T_1, which is basically the gel transition temperature *Tg.*

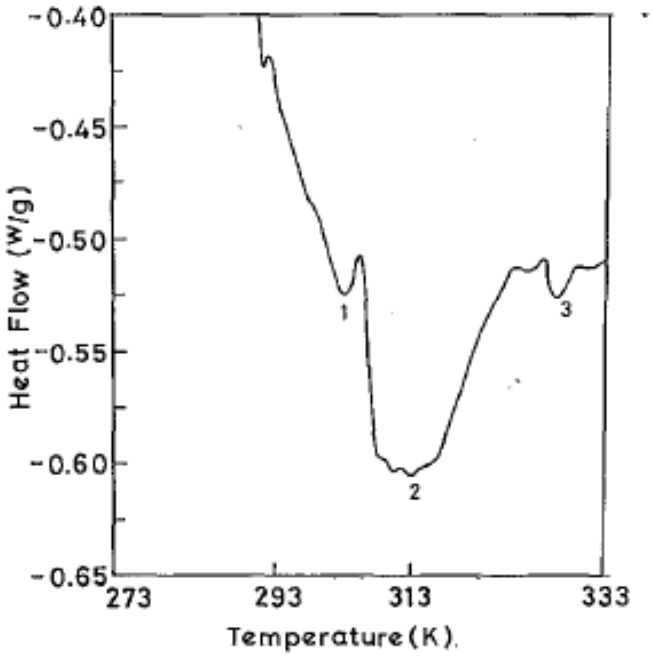

Figure 3.3: Typical DSC indotherm curve for 10 % (w/w) gel with 5 °C/min of heating rate. T_1 is the gel transition temperature, T_2 is the coil-helix transition temperature, and T_3 is monomer-aggregate transition temperature [8].

It was shown that prior to the onset of gelation there are at least two additional conformational phase states in the sol domain.

As the sol is further cooled there is a disorder-order conformational phase transition implying the formation of single helices from random coil chains of gelatin aggregates. It is reasonable to believe that at T_2 the coils undergo a phase transition to the helical state. These single helices are held by intrahelix hydrogen bonds.

As the sol is further cooled, at temperature T_g, triple helices start forming in the system through interchain hydrogen bonds. Multiple triple helices are connected by the random coil segments of the chain. Gelation is basically a single-helix to triple-helix transition state. These triple helices keep reorganizing themselves in the space to minimize the free energy and it can take several weeks before equilibrium is achieved. Solutions of higher conccentrations have a greater tendency to form a gel than those of lower concentrations, therefore, a concentrated solution showed an endothermic peak accompanying gel formation at a lower temperature than dilute solutions [9].

Concentration C (percent) (w/w)	T_g (K)	T_2 (K)	T_3 (K)	t_g (min)
4	298±0.5	307±0.5	317±1	15±2
6	300±0.5	308±0.5	320±1	23±3
8	302±0.5	309±0.5	322±1	28±3
10	303±0.5	310±0.5	323±1	38±3

Figure 3.4: Transition temperatures and gelation time (t_g) as a function of the initial concentration of gelatin. T_g is the gel transition temperature, T_2 is the coil-helix transition temperature, and T_3 is monomer-aggregate transition temperature [8].

It was observed that the concentration of the sol influences the transition temperatures (Figure 3.4). At higher concentrations, the gelation time t_g seems to increase. This may be because of the fact that at higher concentrations there are larger numbers of individual single- to triple-helix transitions, and this is accomplished slowly and a gel network appears only when the triple-helix concentration exceeds a critical value that increases with concentration.

3.2.2 Melting curves of gelatin gels dependence on time of gel formation

In [10], the thermodynamic parameters of the melting of gelatin gels and of collagen denaturation were compared. Differences in these parameters can be used to evaluate defect formation in collagen-like structures in gels.

Three types of gelatin samples were used, differing in the number of interchain crosslinks which are known to strongly affect the process of gel formation: I-gelatin prepared by thermal denaturation of native collagen in a hermetic calorimetric ampoule, the same in which the gel formation process was subsequently studied. In such gelatin, practically all natural interchain crosslinks are preserved that existed in the original collagen. II-α-gelatin, consisting of completely isolated chains.

The curves of the temperature variation of excess heat capacity of sample I (I-gelatin concentration c = 20%) after keeping at 22°C in a thermostat for various periods of time are shown in Figure 3.5. The maximum of heat absorption corresponds to melting of the gels. The curves reflect the development of the gel formation process in time. With increasing time of gel formation, there occurs a transformation of the gel melting

curves: the heat of melting Q_m, increases as well as the melting temperature T_{in}, while the width of the ΔT curve decreases.

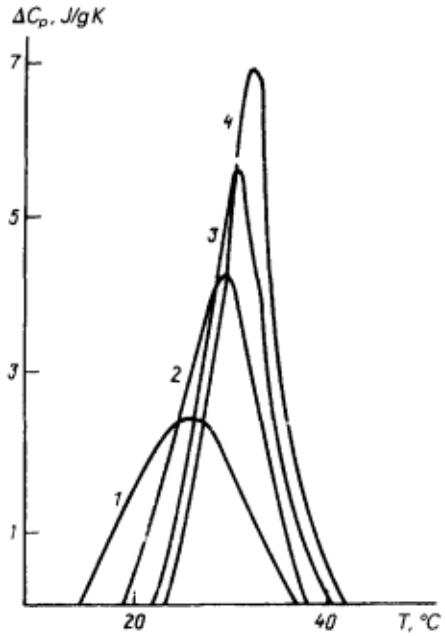

Figure 3.5:Dependence of the melting curves of gels of gelatin I on the time of gel formation: 30 min (1), 3 h (2), 18 h (3) and 7 days (4). Temperature of gel formation 20 °C, rate of heating 1 K/min [10].

3.2.3 Effect of salt on the coil-helix transition of gelatin

It is well known that the triple helix content of gelatin gels, i.e. the renaturation level, can be determined by the measurement of the optical rotation of a given sample [11]. The helices of gelatin in salt solutions with high concentrations grow slowly in the whole gelation process. The kinetics of the coil-helix transition of gelatin at early stages can be described by the following equation:

$$\mathrm{X(t)} = \mathrm{X_0}[1 - \exp\big(-k(t - t_{ind})\big)] \tag{3.1}$$

where

- $\mathrm{X_0}$ represents the amplitude of the early gelation process;
- t_{ind} is an induction period of the early gelation process.

The curves were fitted by using Eq. (3.1) and were also shown by the lines in Figure 3.6. It can be found that Eq. (3.1) gives a fairly good fit. This indicated that the model was suitable for the early stages of gelation.

Figure 3.6 shows the variations of the triple helix content with gelation time at 20 °C for 5,0 wt% gelatin solutions in the presence of different amounts of NaCl salt concentrations.

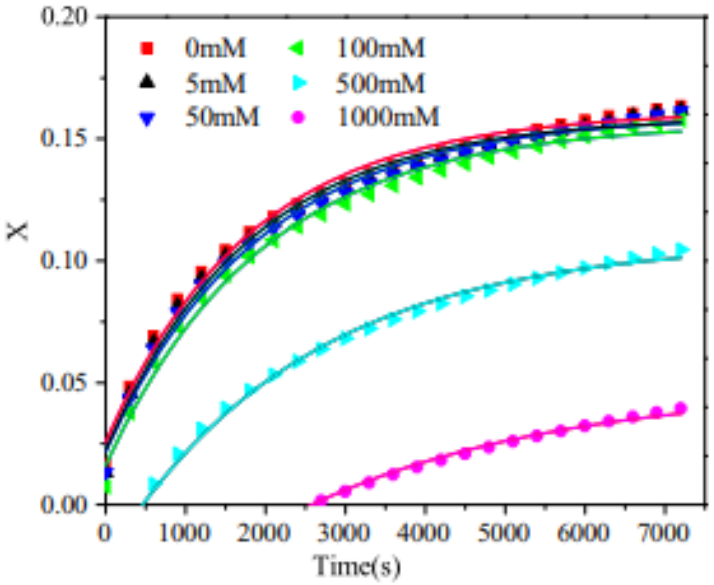

[NaCl]/mmol/L	X_0	$k \times 10^4 (s^{-1})$	t_{ind} (S)	R^2
0	0.161	5.53	N	0.9907
5	0.159	5.51	N	0.9901
50	0.158	5.21	N	0.9914
100	0.156	5.11	N	0.9919
500	0.108	4.07	462	0.9960
1000	0.049	3.17	2581	0.9978

Figure 3.6: The triple helix content as a function of time during gelation process at 20 °C for 5,0 wt% gelatin solutions in the presence of different amounts of NaCl salt concentrations. Continuous lines are calculated using Eq. 3.1 and fitting parameters are reported in table [11].

It is seen from Figure 3.6 that the gelation process of gelatin in salt solutions with low and medium concentrations can be divided into two distinctive stages: an initial rapid increase of the helix content immediately after quenching and a second process with a slow helix growth rate. Similar gelation behaviors have been frequently observed for gelatin solutions with the absence of salts. It can be seen from the relative table that

both X_0 and *k* decreased slightly with an increase in NaCl concentrations, and this declining trend became notable at high salt concentrations.

Generally, the thermal stability of gelatin gels is closely related to the length of the triple helices, and the melting enthalpy is proportional to the triple helix content. As a convenient and widely used method, DSC has already been used to directly exploit the melting temperature of gelatin gels. Both the melting temperature and melting enthalpy of gels in various salts with different concentrations are listed in the table in Figure 3.7.

Salt concentration (mM)	Gelatin/NaCl		Gelatin/$CaCl_2$		Gelatin/$CrCl_3$	
	T_m(°C)	ΔH(J/g)	T_m(°C)	ΔH(J/g)	T_m(°C)	ΔH(J/g)
0	30.7	0.852	30.9	0.852	30.9	0.852
5	30.9	0.826	30.8	1.025	30.2	0.36
50	30.5	0.681	30.3	0.631	–	–
100	30.3	0.636	30.1	0.583	–	–
500	30.2	0.574	–	–	–	–

Figure 3.7: Melting temperature and the corresponding melting enthalpy of gelatin gels in the presence of different amounts of salt concentrations [11].

The melting temperature of gelatin gels was nearly invariable with salt concentration. However, the melting enthalpy has a tendency to decrease with salt addition, especially at high salt concentrations. These results indicate that the electrostatic interactions are important for the coil-helix transition. The additions of salt mainly affect the nucleation of triple helices, but have little effect on its growth.

3.2.4 Helix-coil transition of gelatin

An increase in the melting temperature of a gelatin–water gel is generally accepted to indicate an increase in the stability of the triple helices present. The increase in thermal stability is associated with an increase in the length of the renatured triple helices [12]. It was observed that the melting temperature *Tm* is a measure of the minimum stable triple helix length at a given temperature and concentration, and that *Tm* increases with renaturation temperature. Figure 3.8 shows the enthalpy change on reheating as a function of optical rotation rate θ (directly proportional to the helix concentration) after 30 min. The rotation rate is used instead of the specific rotation

[α], as *ΔH* is not normalized for solution concentration. The dependence of the enthalpy change on helical rotation rate is linear and independent of temperature at low rotation rates in water solutions. The collagen triple helix is stabilized by intermolecular hydrogen bonds. The distance between the donor and acceptor in the one of the two stabilizing hydrogen bonds is too long to be bridged directly. The reduction in the number of stabilizing intermolecular hydrogen bonds leads to a decrease in the enthalpy change per unit helix on melting.

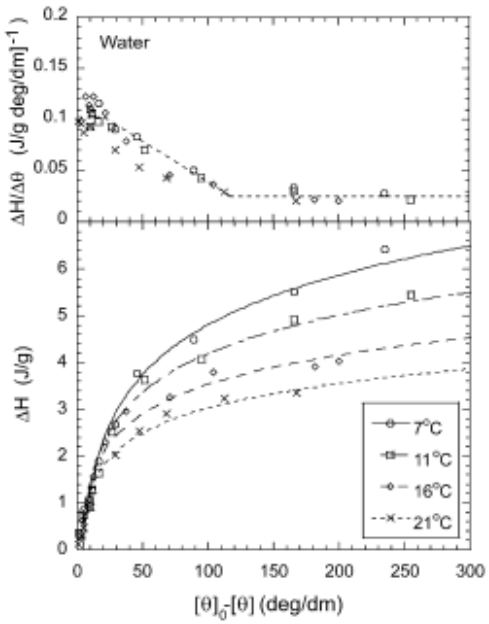

Figure 3.8: (Bottom) Enthalpy change on melting ΔH vs. rotation rate ϑ for gelatin–water solutions after 30 min at various renaturation temperatures labelled on the plot. (Top) Corresponding values of ΔH/ Δϑ [12].

3.3 DSC analysis on gelatins

3.3.1 Sol-gel transition for different cooling rates

To analyse the temperature dependence of sol-gel conversion kinetics in a gelatin-water system, an article of Vyazovkin published in 2009 was firstly taken in consideration [7]. In this paper, the conversion kinetics of an aqueous gelatin solution to gel was studied by temperature modulated and regular DSC under isothermal and continuous cooling conditions. It was taken some information from this paper as the temperature dependence of the sol-gel transition from the regular DSC under continuous cooling conditions, and values of gelation temperature and the activation energy of the transition reaction.

In this article, continuous cooling runs detected a reversing heat flow apparently related to the continuing formation and melting of new gel structures. Isoconversional kinetic analysis of continuous cooling measurements yielded negative activation energy for the whole range of conversions and temperatures suggesting that nucleation remained a rate controlling step throughout the whole gelation process.

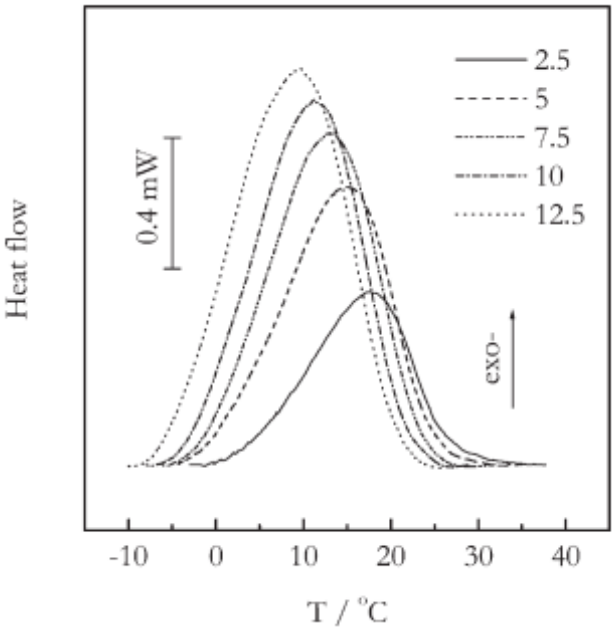

Figure 3.9: Regular DSC curves with heat flow rate in mW against temperature in °C after subtracting a baseline. The numbers by the line types are high cooling rates in °C/min. The gelation phenomenon showed an exothermic behavior [7].

Figure 3.9 displays regular DSC measurements performed at several cooling rates. It can be observed that the gelation phenomenon follows an exothermic behavior. In addition, the peak temperature seems decreasing for higher values of cooling rate and the runs produced markedly larger amounts of heat at slower cooling rates (i.e., for 2,5 °C/min it reached about 16 J/g of gelatin).

To consider also values of cooling rate below 2,5 °C/min, another paper of Vyazovkin published in 2012 was considered as well [13].

The purpose of this paper is to describe the first application of ultrafast scanning calorimetry (UFSC) to the process of gelation in concentrated (40 wt.%) aqueous gelatin solutions.

Nevertheless, the focus for this thesis was on getting the information from the cooling rates below 2,5 °C/min which this article also presents. Isoconversional kinetic analysis is applied to treat the atypical gelation process and to compare it with regular gelation on cooling. Although atypical and regular gelation occur on significantly different time scales, they appear to have common dynamics.

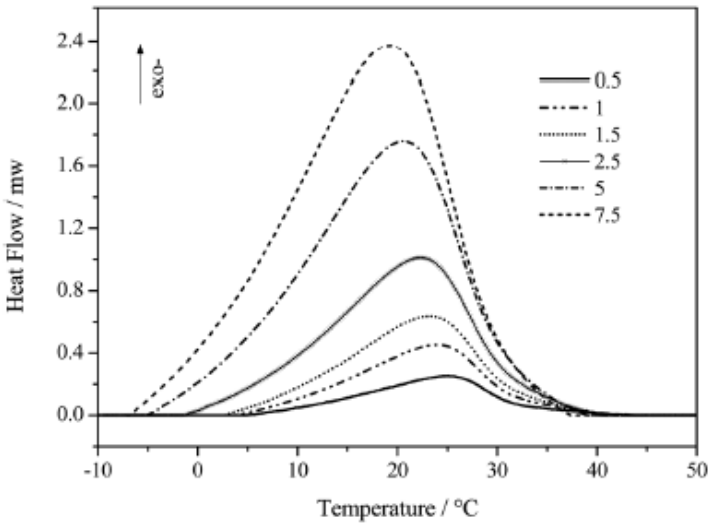

Figure 3.10: Regular DSC curves with heat flow rate in mW against temperature in °C after subtracting a baseline. The numbers by the line types are low cooling rates in °C/min. The gelation phenomenon showed an exothermic behavior [13].

Figure 3.10 presents regular DSC data obtained during cooling. It is seen that an increase in the cooling rate results in shifting the gelation peaks to lower temperature which is a sign of a negative temperature dependence.

3.3.2 Activation energy dependence on conversion

The data have been treated by an advanced isoconversional method developed by Vyazovkin, that allows one to establish a variation in the effective activation energy E_α as a function of conversion α. The latter value is determined as a partial area of a DSC peak. Compared to the popular isoconversional methods of Flynn and Wall, and Ozawa, the advanced method has two important advantages. First, it is capable of treating data obtained under arbitrary variation in temperature, $T(t)$ which allows one to analyze data obtained on cooling as well as to account for self-heating/cooling detectable by the thermal sensor of the instrument. For a set of n experiments performed under different temperature programs, $T_i(t)$, the effective activation energy is evaluated at any given α by finding E_α, which minimizes the function:

$$\Psi(E_\alpha) = \sum_{i=1}^{n} \sum_{j \neq i}^{n} \frac{J[E_\alpha, T_i(t_\alpha)]}{J[E_\alpha, T_j(t_\alpha)]} \tag{3.2}$$

where

$$J[E_\alpha, T_i(t_\alpha)] = \int_{t_{\alpha-\Delta\alpha}}^{t_\alpha} \exp\left[\frac{-E_\alpha}{RT_i(t)}\right] dt \tag{3.3}$$

The second advantage originates from carrying out numerical integration over small time segments (as shown in Eq. 3.3) that eliminates a systematic error found in the Flynn and Wall, and Ozawa methods when E_α varies considerably with α. In Eq. 3.3, α is varied from $\Delta\alpha$ to $1-\Delta\alpha$ with a step $\Delta\alpha = m^{-1}$, where m is the number of intervals chosen for computation. The integral J is evaluated by using the trapezoid rule. The minimization routine is run for each value of α to establish the dependence E_α on α. The obtained E_α on α dependencies are presented in Figure 3.11.

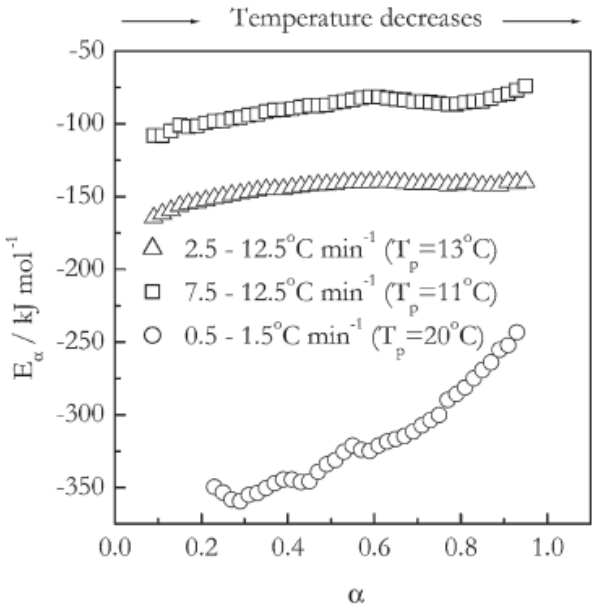

Figure 3.11: The plot of E_α in kJ/mol against α (which increases while temperature decreases) is showing the E_α dependencies obtained by applying an advanced isoconversional method to DSC data on sol-gel conversion. Triangles, squares, and circles denote respectively different intervals of cooling rates. The intervals differ in the mean value of the DSC temperature shown in parentheses [7].

It is seen that all the dependencies demonstrate negative values of the effective activation energy (i.e., temperature coefficient of the sol-gel conversion rate). The E_α values also show a trend to increase with the extent of the sol to gel conversion that can at least partially be explained by the departure from the critical temperature (i.e., T_{gel}) at which the free energy barrier to nucleation of a new phase turns to infinity. Note that a similar type of dependencies (i.e., negative E_α increasing with α) have been reported for crystallization of various polymer melts measured by DSC on continuous cooling, i.e., when an increase in the extent of the melt to crystal conversion reflects the departure from the melting point. The temperature effect on the E_α is more evident when the E_α dependencies are evaluated from DSC data associated with different ranges of the cooling rates.

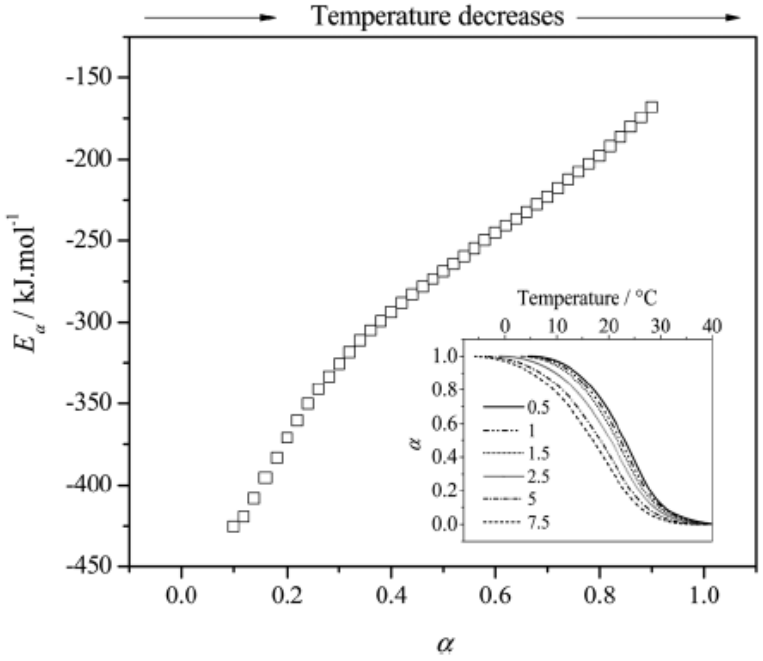

Figure 3.12: Effective activation energy as a function of conversion for gelation of 40 wt.% gelatin solution on cooling. The inset graph shows conversion plots for different cooling rates [13].

As expected, the advanced isoconversional method yields negative values of E_α that increase with the progress of gelation (Figure 3.12). The E_α dependence on α could be converted into E_α dependence on T by replacing the T_α values obtained at different rates of heating (or cooling) with an average value. The parameters of the Hoffman–Lauritzen equation which describes the temperature dependencies of gelation in polymer solutions can be evaluated by fitting the resulting E_α dependence on T to the following equation:

$$E_\alpha(T) = U^* \frac{T^2}{(T-T_\infty)^2} + K_g R \frac{{T_{m,0}}^2 - T^2 - T_{m,0}T}{(T_{m,0}-T)^2 T} \tag{3.4}$$

where

- U^* and K_g are the parameters associated with diffusion and nucleation;
- T_∞ is a hypothetical temperature where polymer chain motion associated with viscous flow ceases (conventionally 30 K below the glass transition temperature);
- $T_{m,0}$ is the equilibrium melting temperature;
- R is the gas constant.

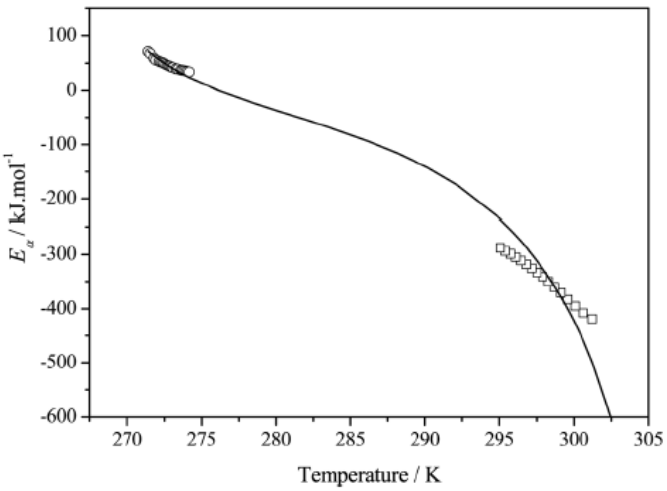

Figure 3.13: Combined E on T dependences for gelation on heating (circles) and on cooling (squares). The solid line is a fit to the Hoffman-Lauritzen equation [13].

Figure 3.13 combines the E_α dependence on T for gelation processes taking place on heating (positive E_α) and cooling (negative E_α). Note that although gelation and gel melting are normally treated as a first order phase transition, the equilibrium melting point of a gel cannot be determined directly because of the nonequilibrium nature of the gel phase. This nature reveals itself in the fact that an experimentally measured value of T_m depends on thermal history of a gel and does not coincide with the value of T_{gel}. The phenomenon is known as thermal hysteresis.

3.3.3 Enthalpy and peak temperature estimation

Both the two articles of Vyazovkin are not reporting the amounts of enthalpy and peak temperature calculated for each cooling rate run, thus the data were analysed through Excel.

To obtain the peak temperatures and the amounts of heat per mass of sample for each cooling rates, the values of the heat flow rate were taken from literature's plots (Figures 3.9 and 3.10).

The range of sample mass is 50-60 mg, so it was studied the data in Excel for 50, 55 and 60 mg obtaining the following plot:

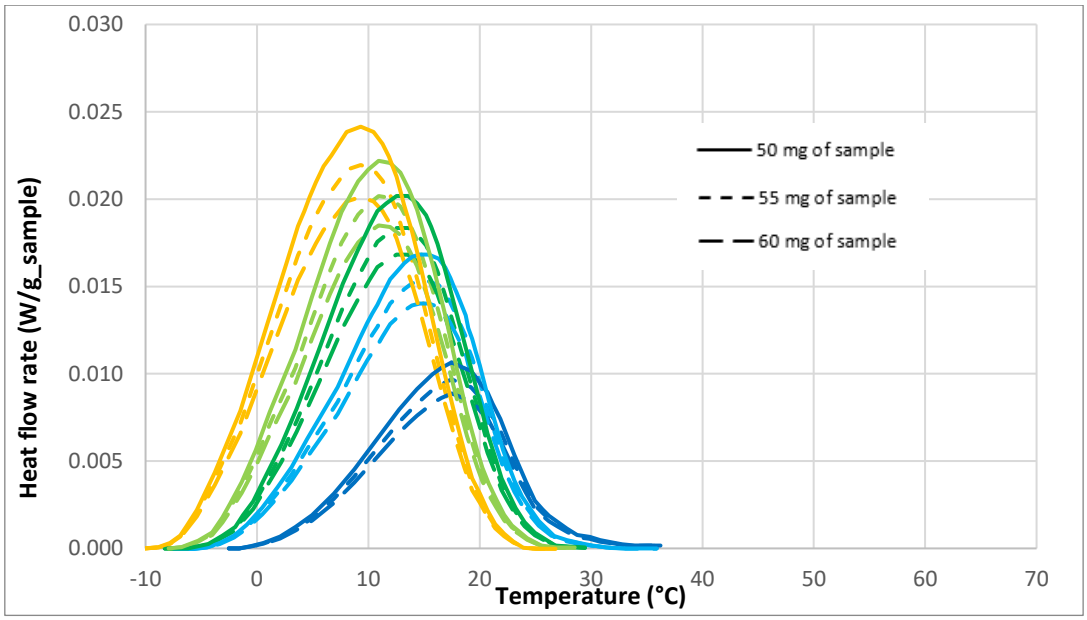

Figure 3.14: DSC subtracted curves with heat flow rate in W/g of sample against temperature in °C, for different mass of sample. The changing in cooling rate is reported by color: blue for 2,5 °C/min, cyan for 5 °C/min, green for 7,5 °C/min, light green for 10 °C/min, and orange for 12,5 °C/min. Data considered are the ones of Vyazovkin's article of 2009.

It has been chosen to take the literature data correspoding to 50 mg of sample.

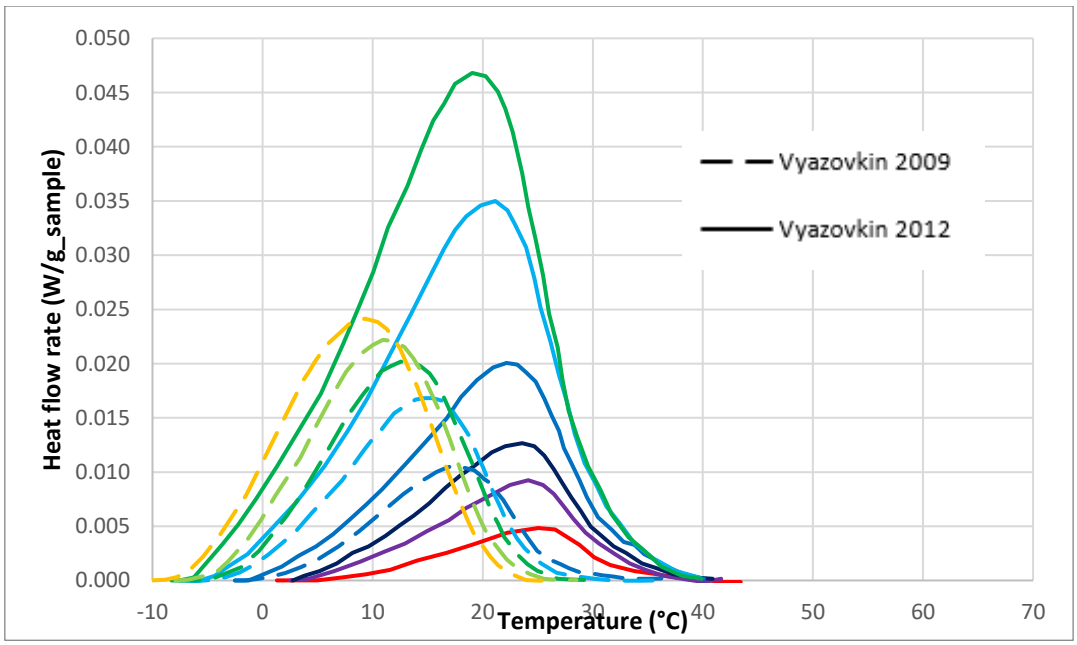

Figure 3.15: DSC subtracted curves comparison for the 50 mg of sample mass between Vyazovkin's articles of 2009 and 2012. The changing in cooling rate is reported by color: red for 0,5 °C/min, violet for 1 °C/min, dark blue for 1,5 °C/min, blue for 2,5 °C/min, cyan for 5 °C/min, green for 7,5 °C/min, light green for 10 °C/min, and orange for 12,5 °C/min.

From Figure 3.15 it can be seen that the peak temperatures shown for this paper have values in an higher range respect the ones plotted in the previous paper.

The area under the curve represents the enthalpy of the gelation and it can be obtained integrating the lines with the 'Trapezium rule':

$$\Delta H\left[\frac{J}{g_{powder}}\right] = \frac{\int_{t_{in}}^{t_{fin}} \frac{d\hat{Q}}{dt}\left[\frac{W}{g_{sample}}\right] dt[s]}{Conc\ [\frac{g_{powder}}{g_{sample}}]} \approx \frac{\sum \frac{(t_b - t_a)(\frac{d\hat{Q}}{dt}|_{t_a} + \frac{d\hat{Q}}{dt}|_{t_b})}{2}}{Conc} \tag{3.5}$$

where

$$(t_b - t_a)\ [s] = \frac{(T|_{t_b} - T|_{t_a})[°C]}{Cooling\ rate[\frac{°C}{s}]} \tag{3.6}$$

The estimated enthalpy and peak temperature for each cooling rate is reported in the following table:

	Vyazovkin 2009		*Vyazovkin 2012*	
Cooling rate [°C/min]	**ΔH [J/g_powder] for 50 mg**	**Peak T [°C]**	**ΔH [J/g_powder] for 50 mg**	**Peak T [°C]**
0,5			21,57	25,03
1			21,23	24,15
1,5			20,49	23,59
2,5	21,96	17,49	21,10	22,15
5	18,37	15,42	19,91	21,15
7,5	14,50	13,58	18,55	19,05
10	11,94	10,93		
12,5	11,01	9,32		

Table 3.1: Comparison between Vyazovkin's articles of 2009 and 2012 in the amount of heat flow released per g of powder ΔH and the relative temperature of gelation peak T calculated for each cooling rates.

The results present in Table 3.1 confirm that the temperature of gelation shifts decreasing for higher cooling rates, and the enthalpy decreases as well with increasing cooling rate.

Both trends can be seen in Figure 3.16, from which a polynomial regression of second order can be considered for the several enthalpy values among cooling rates, obtaining the maximum enthalpy value corresponding to no scanning rate $\Delta H(\beta = 0)$.

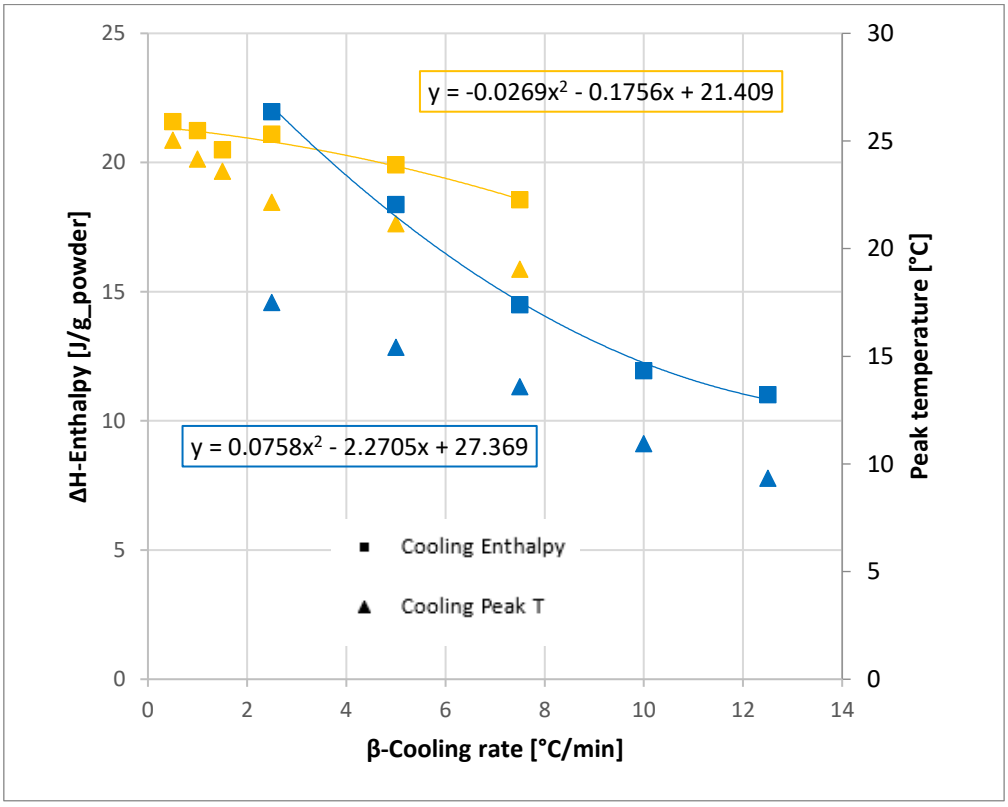

Figure 3.16: Trend of enthalpy ΔH (primary y-axis) and peak T (secondary y-axis) among cooling rates β shown in both Vyazovkin's articles of 2009 (blue) and 2012 (orange). A polynomial regression of second order with relative equation is represented for the two enthalpy curves.

Considering that the conversion curves for each cooling rate can be calculated as:

$$Conversion(t) = \frac{\int_{t_0}^{t} \frac{d\bar{Q}}{dt}\left[\frac{W}{g_{sample}}\right]dt[s]}{\int_{t_0}^{tf} \frac{d\bar{Q}}{dt}\left[\frac{W}{g_{sample}}\right]dt[s]} \tag{3.7}$$

it can be seen from Figure 3.17 that there is a shifting of the conversion trend towards left increasing the cooling rate. This means that the reaction ends at lower temperatures for higher cooling rates, in according with curves in Figure 3.15.

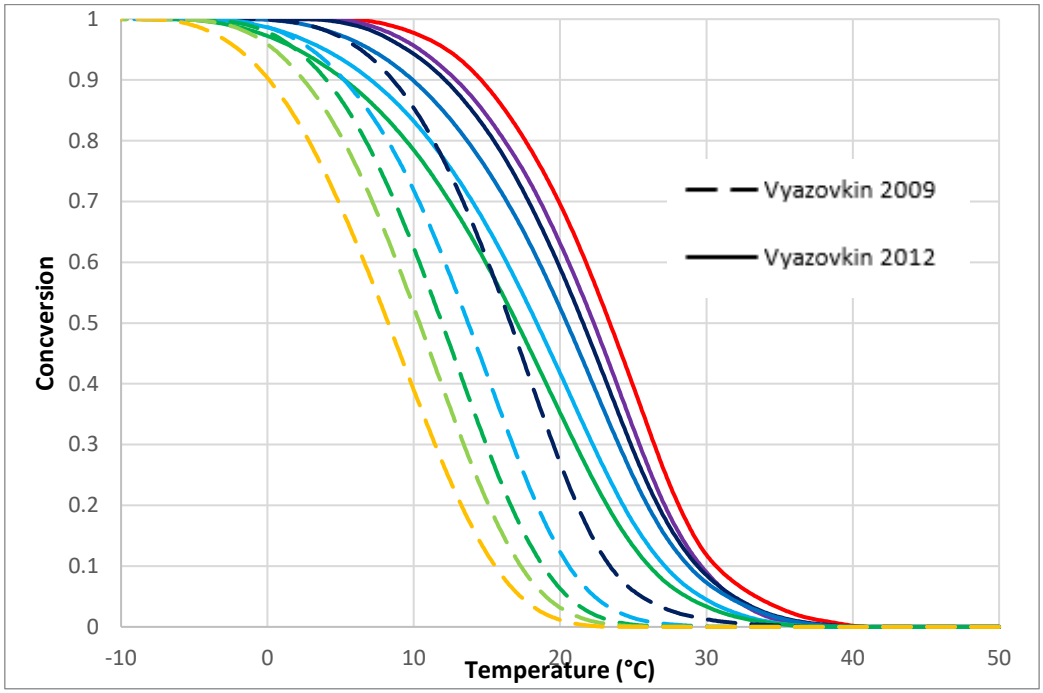

Figure 3.17: Trend of conversion among temperature for each cooling rate in both Vyazovkin's article of 2009 and 2012. The changing in cooling rate is reported by color: red for 0,5 °C/min, violet for 1 °C/min, dark blue for 1,5 °C/min, blue for 2,5 °C/min, cyan for 5 °C/min, green for 7,5 °C/min, light green for 10 °C/min, and orange for 12,5 °C/min.

Considering that the maximum enthalpy value is obtained for no cooling rates, for the other values corresponding to each cooling rate it could not be considered a full conversion of the reaction occurring:

$$Max\ Conversion(\beta) = \frac{\Delta H(\beta)}{\Delta H(\beta=0)} \tag{3.8}$$

where $\Delta H(\beta = 0) = 27{,}369\ J/g$ for Vyazovkin's article of 2009 and $\Delta H(\beta = 0) = 21{,}409\ J/g$ for Vyazovkin's paper of 2012.

Figure 3.18 shows how the maximum value of conversion of the transition sol-gel decreases by increasing the cooling rate because the former is directly proportional to the enthalpy.

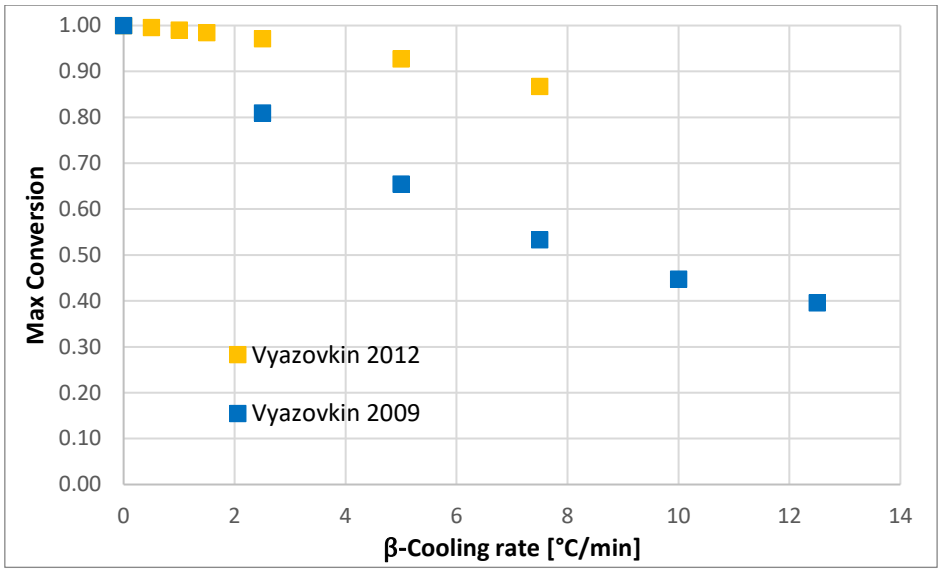

Figure 3.18: Trend of maximum conversion reached for each cooling rate in both Vyazovkin's article of 2009 and 2012. Maximum conversion achieved is lower for higher cooling rates.

Values in Figure 3.18 are obtained applying Eq. 3.8 with $\Delta H(\beta)$ calculated from the polynomial regression expressed in Figure 3.16 for each sanning rate.

It can be said that the fact that the enthalpy was decreasing among cooling rate, could be due to the non maximum conversion achieved in those scanning rates.

4.1 Application of DSC on whey protein denaturation

In order to study the protein denaturation, it was used the *Mettler-Toledo DSC 821* shown in Figure 4.1.

Figure 4.1: Mettler-Toledo DSC 821 utilized for the whey protein isolate denaturation analysis in the laboratory of the IQS.

The studied WPI powder it is likely to be spray-dried at relatively high temperature. A solution of 50 g/L with unchanged pH (6,4) and no salt addition was initally prepared. This amount was chosen to have better signal to noise ratio in the DSC measurements, and no gelation during aggregation.

In order to prepare it, it was measured 100,17 g of distilled water and 5,04 g of protein powder using a mass balance, and then it was mixed them together through a magnetic mixer for almost 1-2 hours. For the protein denaturation investigation, the DSC pans used were stainless steel medium pressure crucibles (Figure 4.2). They

consist of a container for the insertion of the solution, and a cover with a gasket to well close the container. This last one was also well pressed with the cover to avoid any material exchange with the environment during the experiment.

Figure 4.2: WPI solution preparation through a magnetic mixer (left) and medium pressure crucibles pans utilized for the WPI denaturation analysis under DSC (right). The diameters of the crucibles were about 7 mm.

It was put some droplets of the solution in several samples, each with its own mass calculated by a mass balance, while as reference it was used air (as in many papers like [14] or [15]) instead of water (as in papers like [16]). Then, each sample was analysed at different heating rates: 0,5, 1, 5, 10 and 20 °C/min.

All the samples were supposed to be heated up to 120 °C, cooled down to 30 °C, and then heated up again to 120 °C in order to obtain the baselines for the integration calculations.

The point is to subtract these baselines from the first curves obtained (the sample curves) to extract information about the enthalpy values.

It was also checked the weigth of the samples after the DSC measurements confirming that there were no losses or leackages.

Unfortunately, the DSC curves didn't show any peak, thus no denaturation phenomena seem were occurring (Figure 4.3).

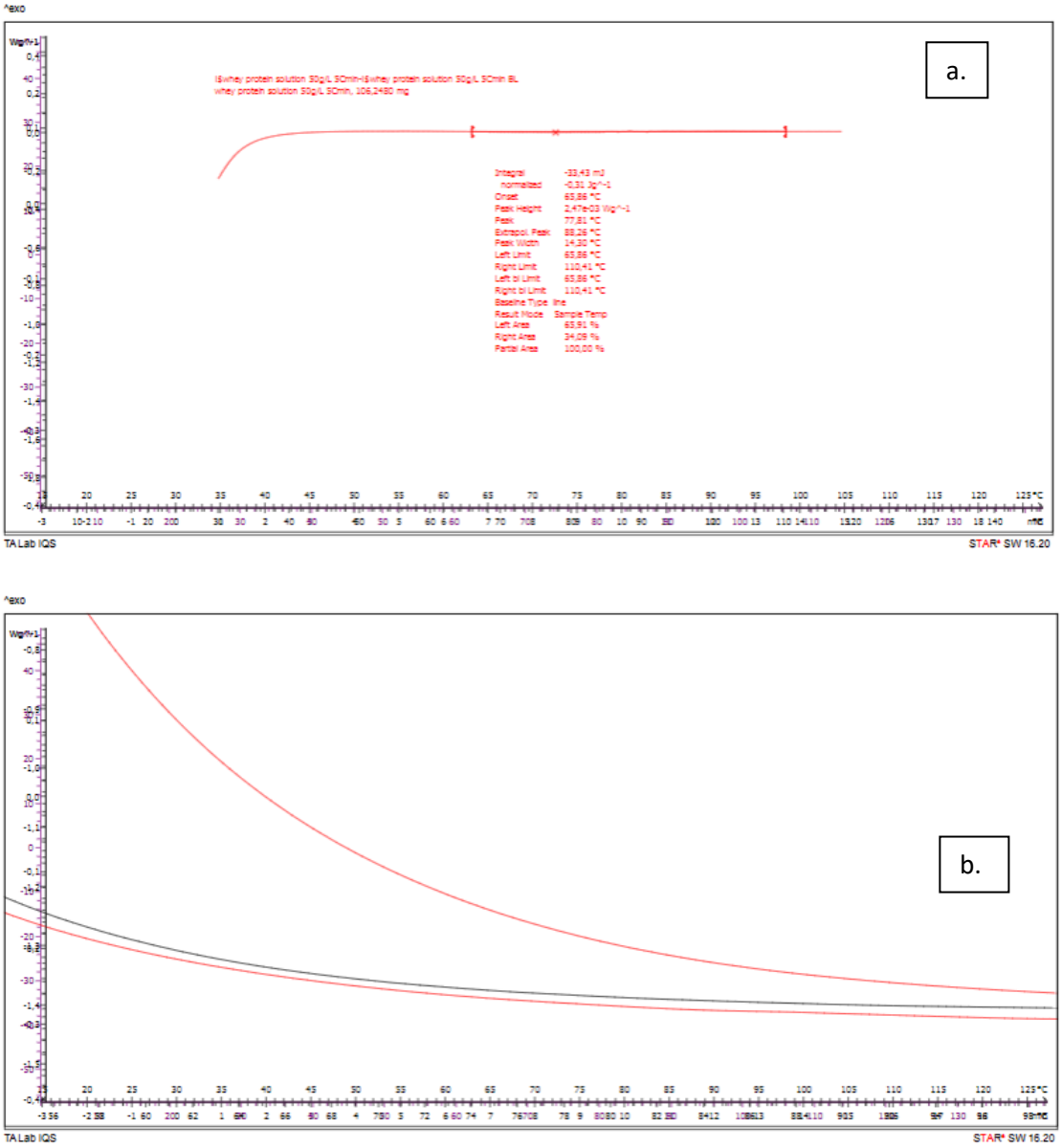

Figure 4.3: DSC curves with heat flow rate in W/g against temperature in °C for the analysed WPI solution of 50 g/L at 5 °C/min (a) and 20 °C/min (b). In the first plot, the subtracted curve is represented, and no peak can be observed. In the second one, both heatings are shown but in none of them the denaturation seems occurring.

The thermal denaturation of a protein solution of 50 g/L seemed not occurring in the common denaturation temperature range of 60-100 °C. It was then decided to prepare another solution, of about 100 g/L to check if at higher concentration the thermal denaturation could occur.

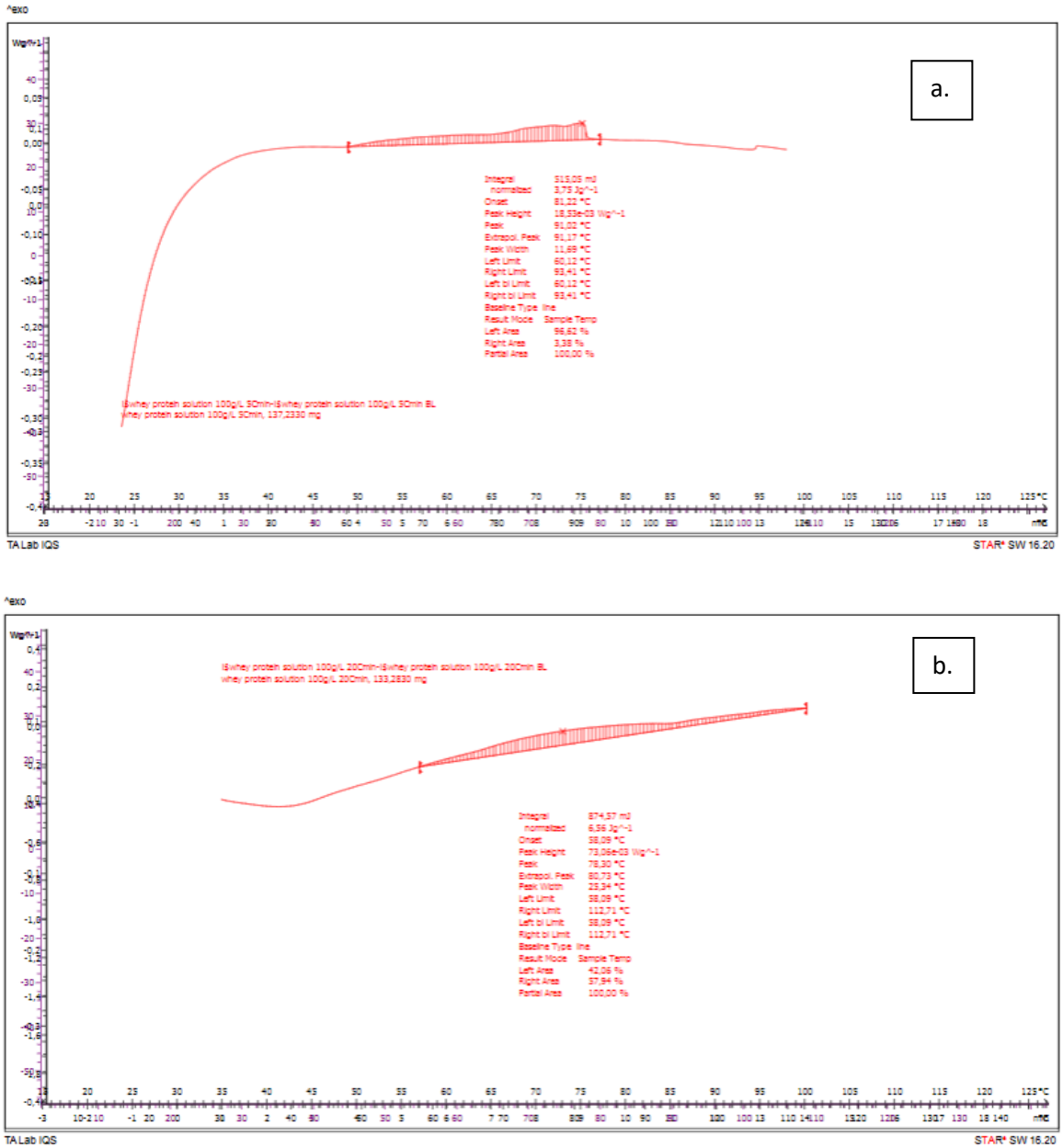

Figure 4.4: DSC curves with heat flow rate in W/g against temperature in °C for the analysed WPI solution of 100 g/L at 5 °C/min (a) and 20 °C/min (b). Both plots are reporting the subtracted curves.

As it can be seen from Figure 4.4, also for higher WPI solution concentration not relevant peaks were determined. In fact, the integration made on the subtracted curve for the 5 °C/min of scan rate was estimating an enthapy value of 3,75 J/g that is not inside the common denaturation enthalpy range of 5-15 J/g.

It was concluded that the lack of extensive denaturation can be due to the spray-dried at relative high temperature method used to prepare the protein powder, thus that the WPI analysed was already denatured.

4.2 Application of DSC on sol-gel transition

Taking a gelatin powder from porcine skin (type A) with strength 175 g Bloom, a solution of 200 g/L (16,67 wt.%) without adding salt nor changing pH was prepared. The solution was obtained through a magnetic mixer in which the powder and the distilled water were put in proportion. The mixer was incorporated with a heater used to achieve a mixing temperature of 50 °C (controlled by a thermometer) to enhance mixing (Figure 4.5).

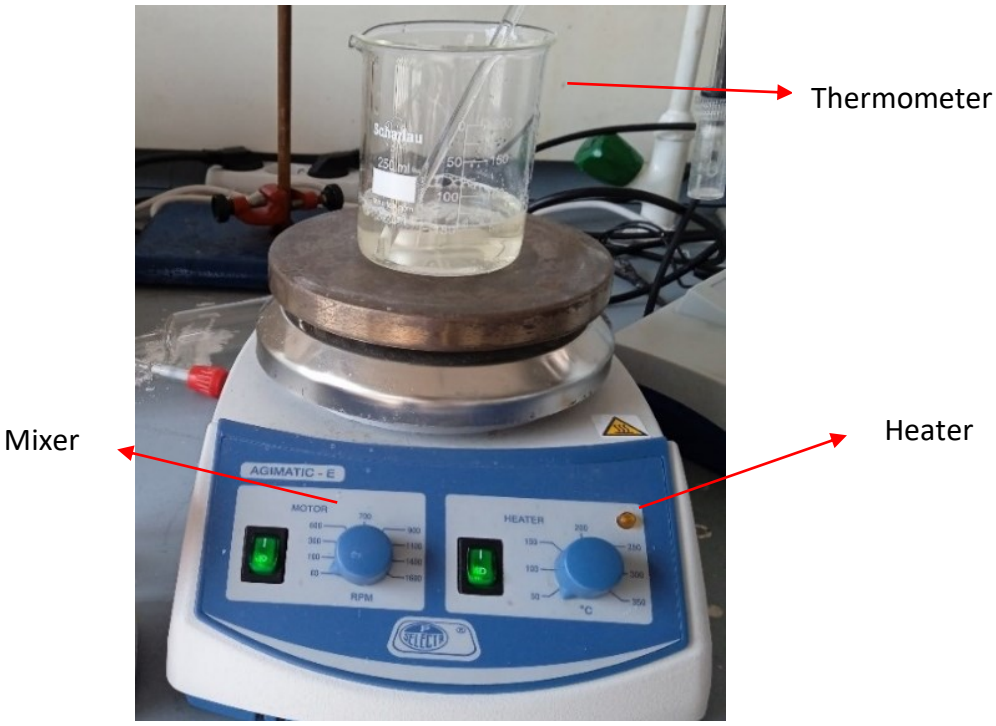

Figure 3.5: Magnetic mixer with heater incorporated to obtain the desired 16,67 wt.% of gelatin solution.

After preparation, the solution was stored in a refrigerator at 5 °C to slow down potential degradation, and it was used for no longer than a week, after which a new gelatin had to be prepared.

The DSC utilized for this experiment was a *Netzch DSC 204* (Figure 4.6), in which temperature, heat and tau-lag calibrations were performed by using indium and zinc standards. All measurements were conducted under nitrogen flow of 20 mL/min.

Figure 4.6: Netzch DSC 204 utilized for the sol-gel transition analysis in the laboratory of the IQS. On the left is shown the machine from the outside, while on the right it can be observed the DSC cell in which the pans and the reference are put.

Gelatin samples were dropped from the solution, put in 100 mL Al pans, and hermetically sealed.

Initially, it was used open crucibles and it was noticed and calculated a loss of mass due to water evaporation. Utilizing closed crucibles instead of open ones it was avoid any possible evaporation effect and thus it was obtained reliable data.

The DSC run procedure was based on two cooling and two heating sections with temperature range between -5 and 70 °C, and with 10 min of holding time between each section. The scanning rates analysed were 0,5, 1, 2, 5, 7,5, 10 and 15 °C/min and several solutions were prepared and experimented: SolA, SolB, SolC and SolD.

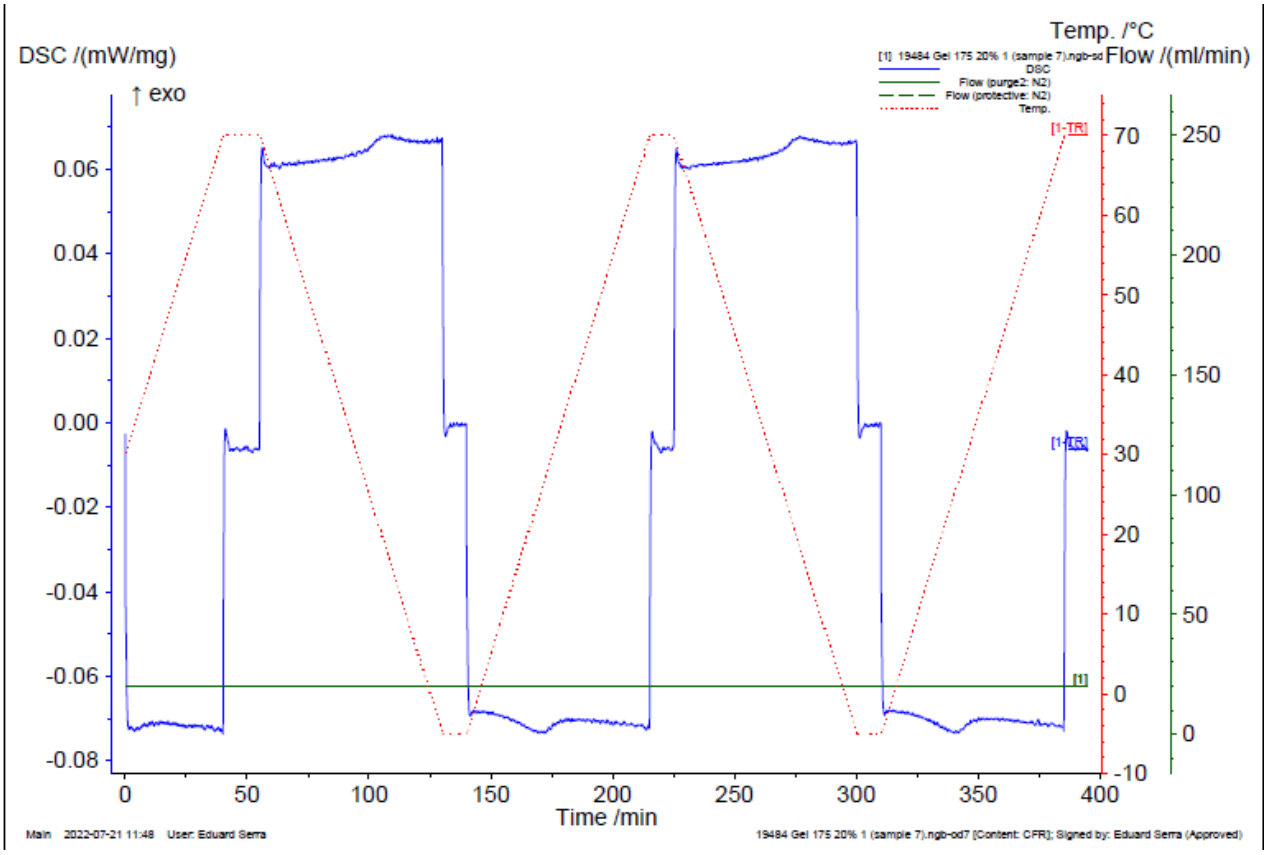
DSC /(mW/mg)
↑ exo
Temp. /°C
Flow /(ml/min)
[1] 19484 Gel 175 20% 1 (sample 7).ngb-sd
DSC
Flow (purge2: N2)
Flow (protective: N2)
Temp.
[1-TR]
[1]
Time /min
Main 2022-07-21 11:48 User: Eduard Serra
19484 Gel 175 20% 1 (sample 7).ngb-od7 [Content: CFR]; Signed by: Eduard Serra (Approved)

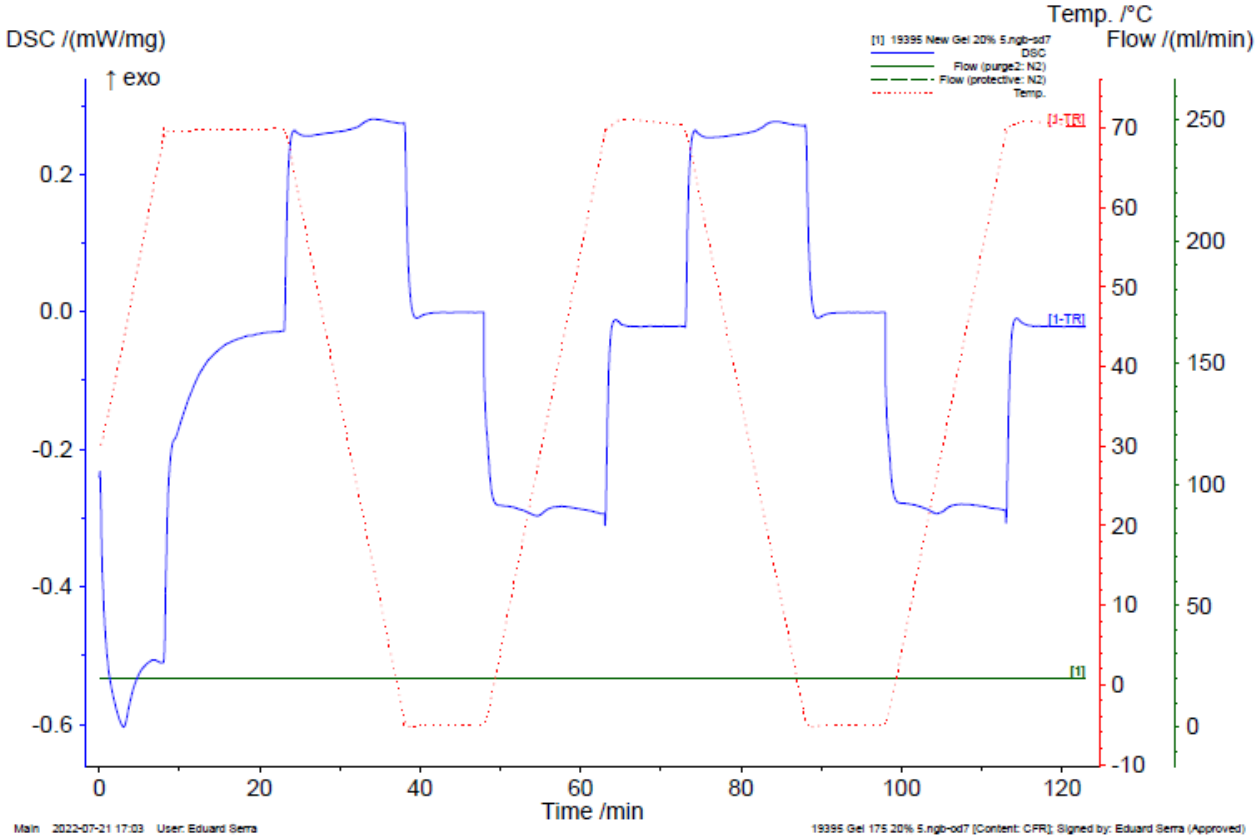
DSC /(mW/mg)
↑ exo
Temp. /°C
Flow /(ml/min)
[1] 19395 New Gel 20% 5.ngb-sd7
DSC
Flow (purge2: N2)
Flow (protective: N2)
Temp.
[1-TR]
[1]
Time /min
Main 2022-07-21 17:03 User: Eduard Serra
19395 Gel 175 20% 5.ngb-od7 [Content: CFR]; Signed by: Eduard Serra (Approved)

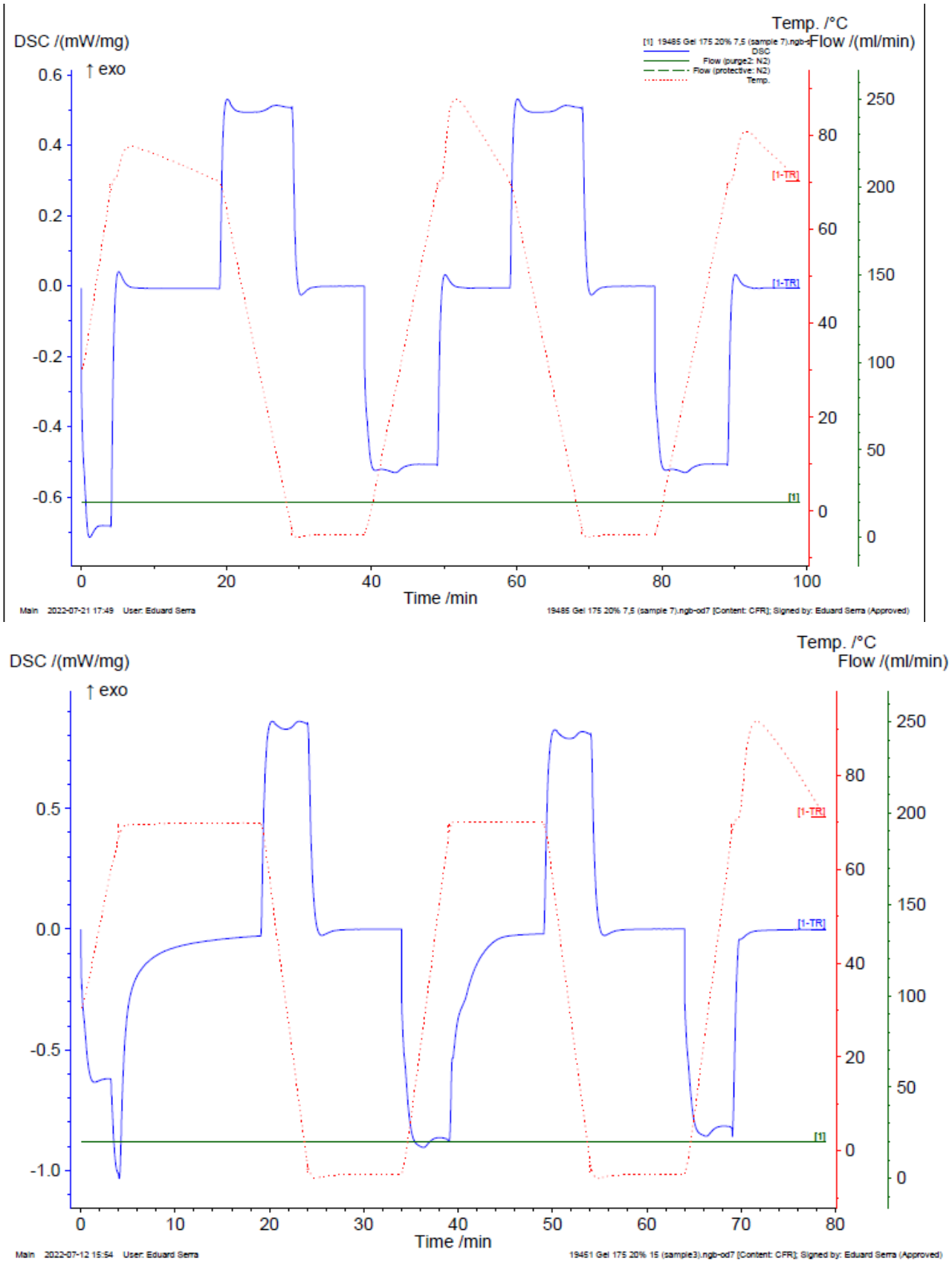

Figure 4.7: DSC runs with closed crucibles at different scanning rates: 1 °C/min (first run), 5 °C/min (second run), 7,5 °C/min (third run), and 15 °C/min (fourth run).

The mass measured before and after each run was reporting the same value. This means that there was no loss of mass, and it can be observed in Figure 4.7 from the fact that the trends during both cooling and heating sections are flat and during the holding step $\frac{\Delta \hat{Q}_{holding}}{\Delta t} = 0 \ \frac{mW}{mg}$. In addition, it is hard to define the peak in the heating sections at 15 °C/min.

The selection of adequate baselines and extreme points for each peak of the DSC curve is important for the NPK method. To work properly, it needs parallel resulting conversion curves, with no crossing in all the range considered (Figure 4.8).

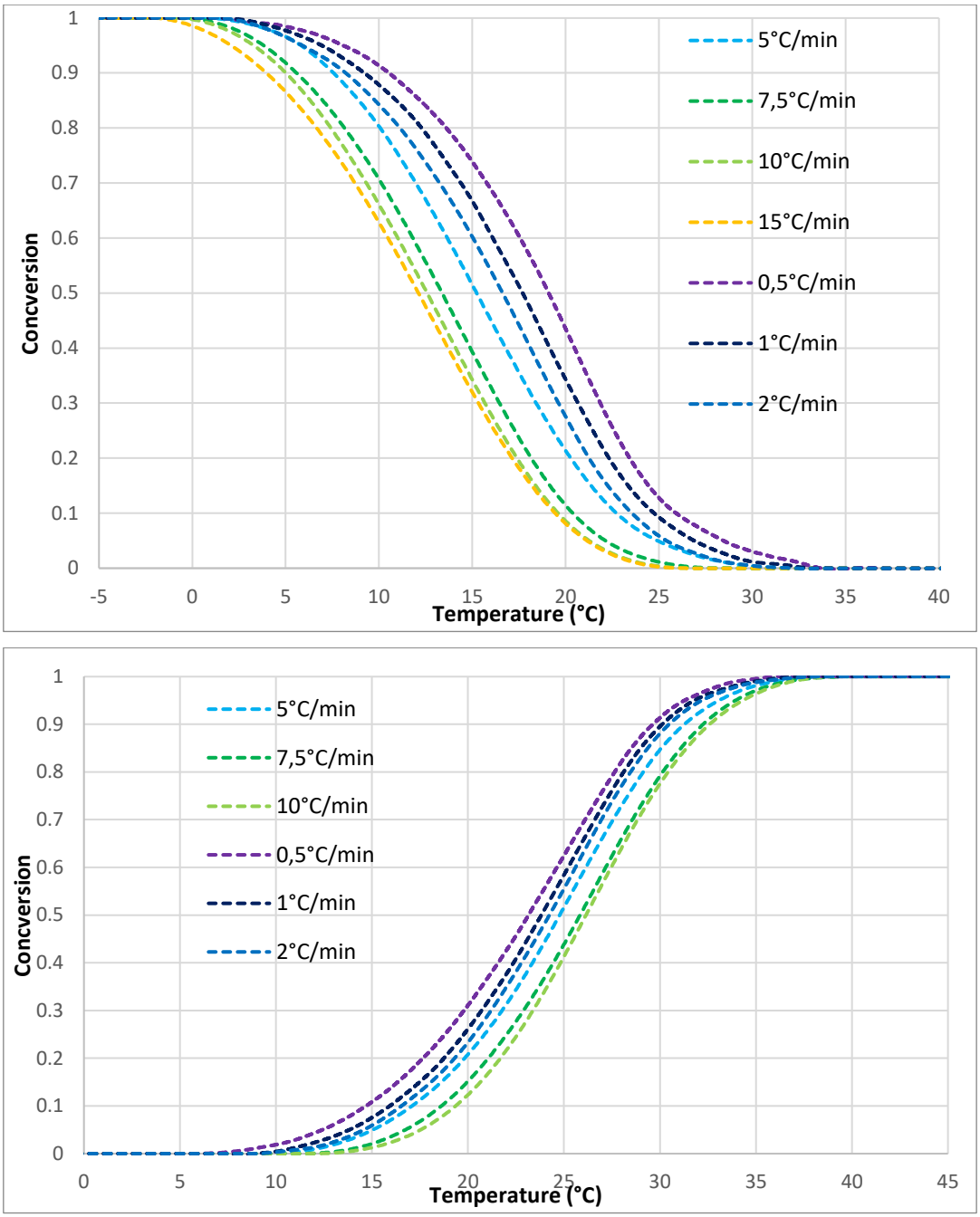

Figure 4.8: DSC conversion curves for each scanning rate in first cooling (first plot) and first heating (second plot) sections.

Considering a baseline, two extreme points were accurately selected in order to obtain parallel conversion curves as shown in the upper figure. Then, the subtracted curves for all the solutions could be drawn and the analysis on them could be made (Figure 4.9).

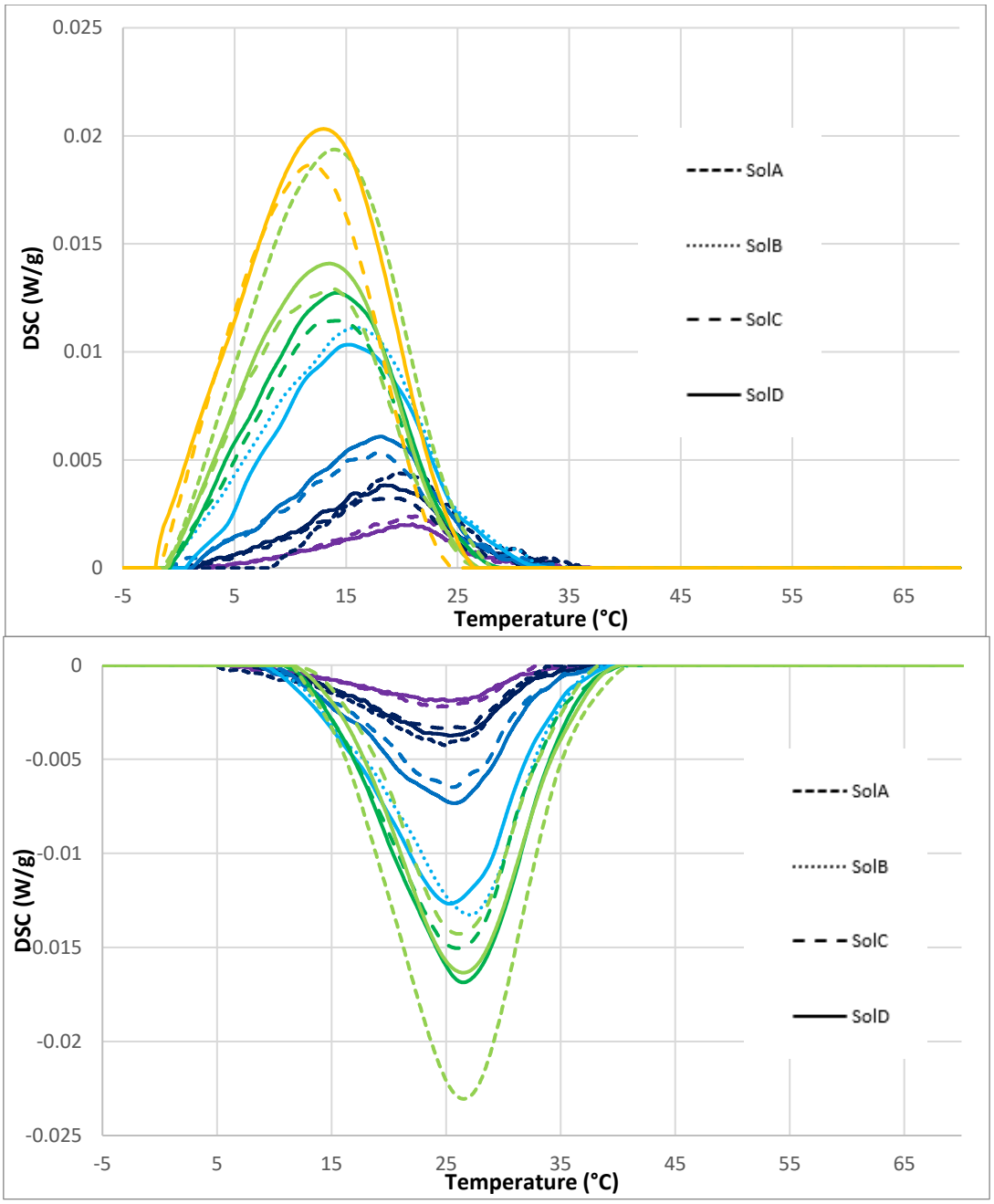

Figure 4.9: DSC subtracted curves for each scanning rate in first cooling (first plot) and in first heating (second plot) sections for several solutions: SolA, SolB, SolC, and SolD. The changing in scanning rate is reported by color: violet for 0,5 °C/min, dark blue for 1 °C/min, blue for 2 °C/min, cyan for 5 °C/min, green for 7,5 °C/min, light green for 10 °C/min, and orange for 15 °C/min.

The 15 °C/min of scanning rate was not considered in heating sections because of the not clear peak present in them (shown in Figure 4.7).

		1° Cooling		*1° Heating*		*2° Cooling*		*2° Heating*	
Scanning rate [°C/min]	**Sol**	**ΔH [J/g]**	**Peak T [°C]**	**ΔH [J/g]**	**Peak T [°C]**	**ΔH [J/g]**	**Peak T [°C]**	**ΔH [J/g]**	**Peak T [°C]**
0,5	SolC	21,68	21,17	-21,87	25,49	19,93	20,69	-20,36	25,71
	SolD	19,40	20,94	-19,64	25,14	19,67	19,60	-20,13	26,13
1	SolA	20,01	19,82	-20,39	24,90	19,85	20,31	-20,24	24,05
	SolC	17,40	19,10	-17,06	24,78	18,36	18,35	-18,48	24,63
	SolD	19,82	18,45	-18,48	25,38	20,27	19,20	-19,28	25,60
2	SolC	14,42	18,05	-15,26	25,63	15,05	17,77	-15,23	25,79
	SolD	16,03	18,14	-17,53	25,70	16,65	16,99	-17,47	25,50
5	SolB	13,15	15,90	-12,53	27,09	14,27	15,62	-13,96	26,30
	SolD	11,51	15,24	-12,39	25,30	11,95	15,63	-12,50	25,91
7,5	SolC	8,39	14,18	-9,49	26,00	9,41	13,53	-9,57	26,05
	SolD	9,26	14,18	-10,73	26,54	9,95	14,33	-10,97	26,40
10	SolA	10,89	13,95	-10,97	26,54	10,88	14,73	-11,01	26,89
	SolC	7,06	13,82	-6,12	26,09	6,62	12,76	-6,66	26,23
	SolC (bis)	6,79	13,53	-6,38	26,00	6,35	12,76	-6,49	26,30
	SolD	7,76	13,48	-7,63	26,50	7,53	12,48	-7,74	26,64
15	SolC	6,59	12,03			6,32	11,80		
	SolC (bis)	8,02	12,38			8,40	12,98		
	SolD	7,71	12,97			7,37	13,18		

Table 4.1: Results of enthalpy and peak temperature in all cooling and heating sections for different solutions in closed crucibles at each scanning rate. The values were obtained from Excel.

Table 4.1 confirms the repeatability of the sol-gel transition by showing quite same results between first and second cooling, and first and second heating sections.

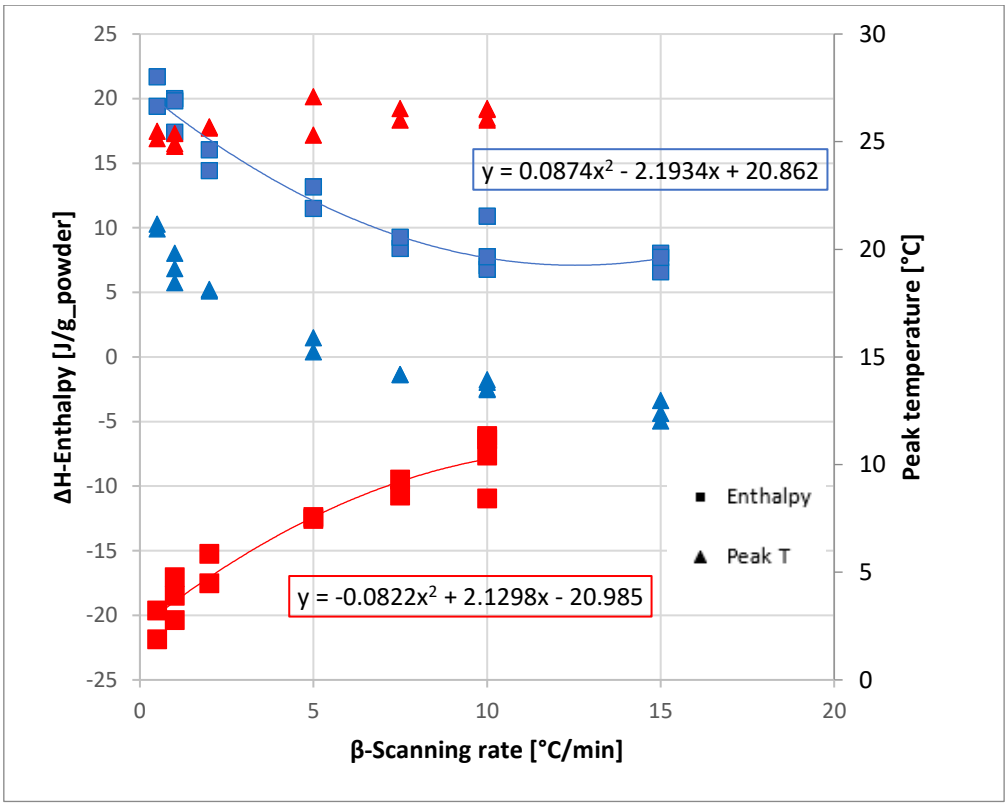

Figure 4.10: Trend of enthalpy ΔH (primary y-axis) and peak T (secondary y-axis) among scanning rates β shown in both first cooling (blue) and first heating (red) sections considering all the solutions prepared.

Observing Figure 4.10 it can be confirmed that also with experimental data both enthalpy and peak temperature are related to scanning rate: heating enthalpies and peak temperatures increase with the scanning rate, while cooling ones decrease with it.

The maximum conversion can be estimated using Eq. 3.8 in Chapter 3 with quite the same enthalpy of reaction ΔH (in absolute value) extrapolated from both cooling and heating sections at $\beta = 0$: $\Delta H(\beta = 0) \sim 21\ J/g$.

Figure 4.11 shows how the maximum value of conversion of the transition sol-gel decreases by increasing the scanning rate, while the one of the reversible transition increases with scanning rate.

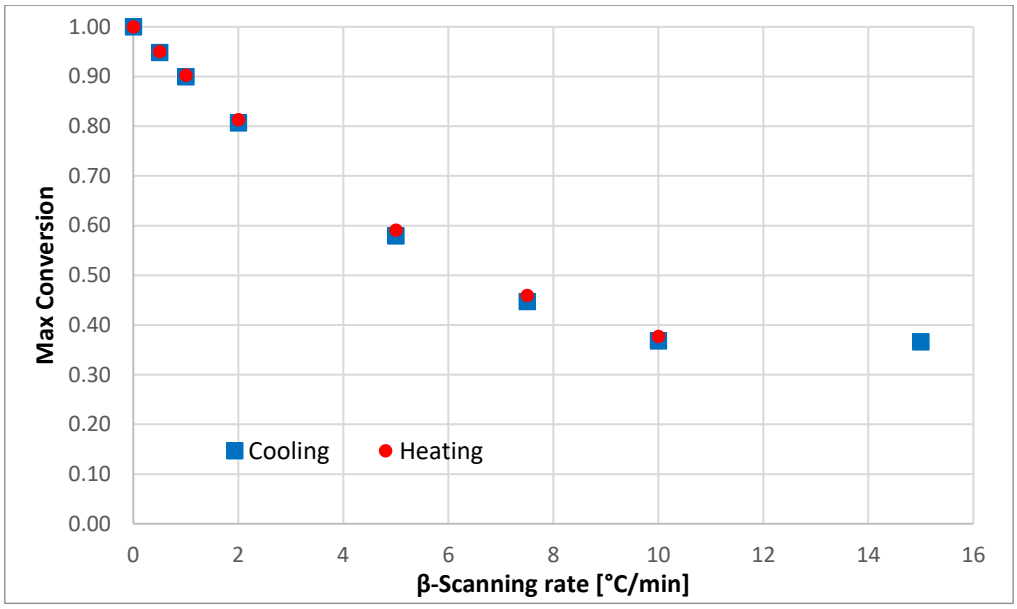

Figure 4.11: Trend of maximum conversion reached for each scanning rate in both cooling and heating of the 175 g Bloom solutions. Maximum conversion achieved during reaction is lower for higher scanning rates.

Values in Figure 4.11 are obtained applying Eq. 3.8 in Chapter 3 with $\Delta H(\beta)$ calculated from the polynomial regression expressed in Figure 4.10 for each sanning rate.

In order to check the reliability of the results reported in Table 4.1 for the 175 g Bloom gel analysed, it was compared those values with the ones calculated for both Vyazovkin's articles of 2009 and 2012 for a 50 mg of sample mass (Table 4.2).

Cooling rate [°C/min]	**ΔH [J/g]**			**Peak T [°C]**		
	175 g Bloom gel	*Vyazovkin 2009*	*Vyazovkin 2012*	*175 g Bloom gel*	*Vyazovkin 2009*	*Vyazovkin 2012*
0,5	21,68		21,57	21,17		25,03
	19,40			20,94		
1	20,01		21,23	19,82		24,15
	17,40			19,10		
	19,82			18,45		
1,5			20,49			23,59
2	14,42			18,05		
	16,03			18,14		
2,5		21,96	21,10		17,49	22,15
5	13,15	18,37	19,91	15,90	15,42	21,15
	11,51			15,24		
7,5	8,39	14,50	18,55	14,18	13,58	19,05
	9,26			14,18		
10	10,89	11,94		13,95	10,93	
	7,06			13,82		
	6,79			13,53		
	7,76			13,48		
12,5		11,01			9,32	
15	6,59			12,03		
	8,02			12,38		
	7,71			12,97		

Table 4.2: Comparison between the results of enthalpy and peak temperature in the first cooling section at each cooling rate of the analysed 175 g Bloom gel and the ones calculated from Vyazovkin's articles data of 2009 and 2012.

It can be seen from Table 4.2 that values of peak temperature and enthalpies for the cooling section obtained from the experiments are around the ones shown in literature.

Even if there are no values for the heating section to compare, it can be considered that the experimental results are reasonable and so further analysis on the kinetics could be done.

It was also analysed the sol-gel transition considering a different strength of the gelatin powder: 300 g Bloom. The procedure applied for the analysis of the 300 g Bloom gel was following the previous one. Some solutions, called SolE, SolF and SolG, were prepared for a concentration of 16,67 wt.% and experimented with closed crucible aluminium pans.

Figure 4.12 is showing the resulting subtracted curves for the 300 g Bloom gel. Again, the 15 °C/min of scanning rate in the heating sections is not considered.

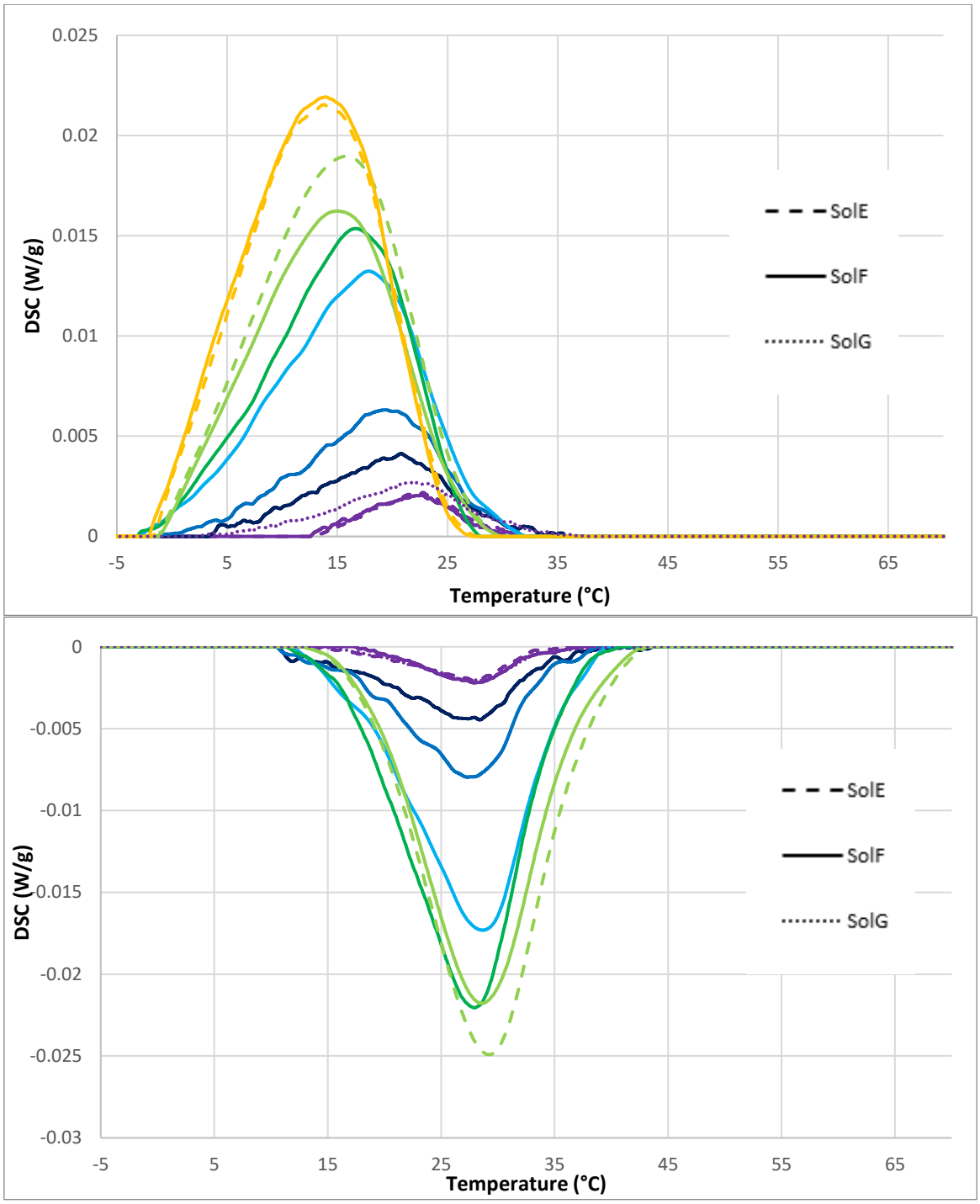

Figure 4.12: DSC subtracted curves for each scanning rate in first cooling (first plot) and in first heating (second plot) sections for several solutions: SolE, SolF, and SolG. The changing in scanning rate is reported by color: violet for 0,5 °C/min, dark blue for 1 °C/min, blue for 2 °C/min, cyan for 5 °C/min, green for 7,5 °C/min, light green for 10 °C/min, and orange for 15 °C/min.

The resulting data from the estimation of the enthalpy and peak temperature in first cooling and heating sections were compared with the ones of the 175 g Bloom gel, and reported in Table 4.3.

	1° Cooling				*1° Heating*			
Scanning rate [°C/min]	**ΔH [J/g]**		**Peak T [°C]**		**ΔH [J/g]**		**Peak T [°C]**	
	175 g Bloom gel	*300 g Bloom gel*	*175 g Bloom gel*	*300 g Bloom gel*	*175 g Bloom gel*	*300 g Bloom gel*	*175 g Bloom gel*	*300 g Bloom gel*
0,5	21,68	24,89	21,17	22,64	-21,87	-14,00	25,49	27,68
		22,72		22,31		-23,48		28,05
	19,40	25,32	20,94	21,98	-19,64	-22,17	25,14	28,37
1	20,01	21,41	19,82	20,80	-20,39	-21,38	24,90	28,43
	17,40		19,10		-17,06		24,78	
	19,82		18,45		-18,48		25,38	
2	14,42	15,83	18,05	19,35	-15,26	-17,12	25,63	27,21
	16,03		18,14		-17,53		25,70	
5	13,15	13,52	15,90	17,98	-12,53	-16,13	27,09	28,66
	11,51		15,24		-12,39		25,30	
7,5	8,39	11,08	14,18	16,73	-9,49	-12,49	26,00	27,91
	9,26		14,18		-10,73		26,54	
10	10,89	11,09	13,95	15,80	-10,97	-11,45	26,54	29,24
	7,06		13,82		-6,12		26,09	
	6,79	9,37	13,53	15,00	-6,38	-9,23	26,00	28,58
	7,76		13,48		-7,63		26,50	
15	6,59	8,19	12,03	13,74				
	8,02	8,34	12,38	13,95				
	7,71		12,97					

Table 4.3: Comparison between the results of enthalpy and peak temperature in both first cooling and firs heating sections at each scanning rate calculated for the 300 g Bloom gel and the ones previously estimated for the 175 g Bloom gel.

The values reported in Table 4.3 for the 300 g Bloom gel are around the ones calculated for the 175 g BloomI gel.

In addition, it can be confirmed that also for the first gel both enthalpy and peak temperature are related to scanning rate: heating enthalpies and peak temperatures increase with the scanning rate, while cooling ones decrease with it (Figure 4.13).

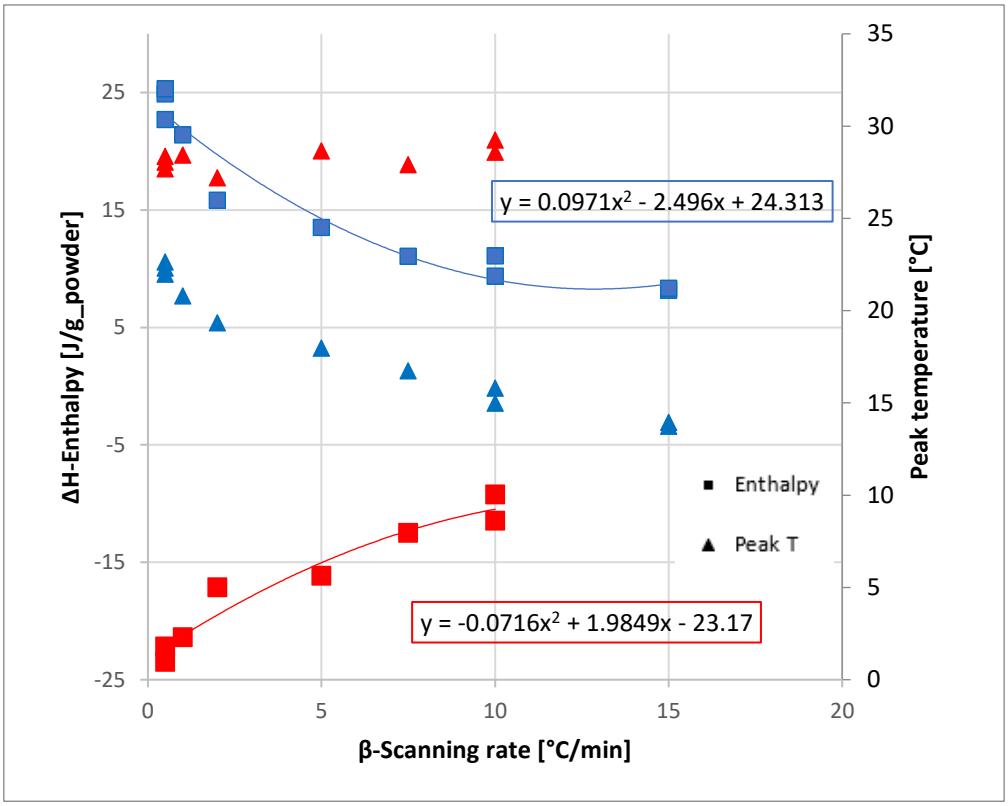

Figure 4.13: Trend of enthalpy ΔH (primary y-axis) and peak T (secondary y-axis) among scanning rates β shown in both first cooling (blue) and first heating (red) sections considering all the solutions prepared for the 300 g Bloom gel.

The maximum conversion can be estimated using Eq. 3.8 in Chapter 3 with quite the same enthalpy of reaction ΔH (in absolute value) extrapolated from both cooling and heating sections at $\beta = 0$: $\Delta H(\beta = 0) \sim 24\ J/g$.

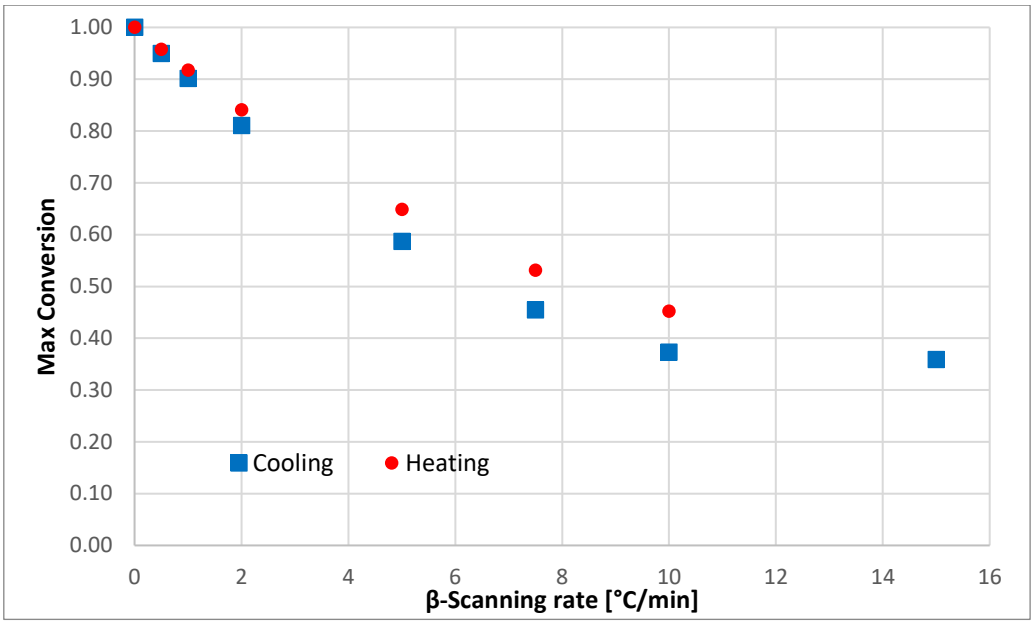

Figure 4.14: Trend of maximum conversion reached for each scanning rate in both cooling and heating of the 300 g Bloom solutions. Maximum conversion achieved during reaction is lower for higher scanning rates.

Values in Figure 4.14 are obtained applying Eq. 3.8 in Chapter 3 with $\Delta H(\beta)$ calculated from the polynomial regression expressed in Figure 4.13 for each sanning rate.

CHAPTER 5: NPK METHOD

5.1 General characteristics of NPK method

The Non-Parametric Kinetic (NPK) method is another technique that allows to estimate the kinetic parameters: are *k* and *Ea*, and the order *n*. It is characterized by the fact that it doesn't use any kinetic model or Arrhenius law, but it utilizes the data obtained from DSC thermal analysis [17].

The general expression for the reaction rate of a simple reaction can be given by the product of two functions:

$$\dot{\alpha} = g(\alpha)f(T) \tag{5.1}$$

where

- $g(\alpha)$ is the function of conversion α, and it is the kinetic model of the process;
- $f(T)$ is the function of temperature *T*, and it accounts for the temperature dependence of the reaction.

Generally, the type of reaction has to be known in advance to apply the appropriate kinetic model.

The improvement that NPK method introduced is that it is able to decouple the two functions without the need of any assumptions about their functionality. From experimental measurements, it provides two independent vectors (**u** and **v**) that contain numerical informations about $g(\alpha)$ and $f(T)$ respectively. The method avoids the problem of the exponential temperature integral because there are no assumption about $f(T)$ and it can be applied to any reaction.

The reaction rate $\dot{\alpha}$ can be expressed in a 3D space as a surface. At any point of this surface, it is determined by the corresponding pair of temperature and degree of conversion, and it does not depend on the previous history of the process. The continuos surface can be discretized and organized as an (*n x m*) matrix, named matrix

A, whose rows correspond to different degrees of conversion (from α_1 to α_n), and whose columns refer to different temperatures (from T_1 to T_m). So, **A** is given by elements $a_{i,j}$ that are the reaction rate at the corresponding pair (α_i, T_j):

$$\boldsymbol{A} = \begin{pmatrix} g(\alpha_1)f(T_1) & \dots & g(\alpha_1)f(T_m) \\ \vdots & \ddots & \vdots \\ g(\alpha_n)f(T_1) & \dots & g(\alpha_n)f(T_m) \end{pmatrix}$$

It can be written as:

$$\boldsymbol{A} = \boldsymbol{g} \text{ x } \boldsymbol{f}^T \tag{5.2}$$

where

- $\boldsymbol{g} = (g(\alpha_1) \dots g(\alpha_n))^T$
- $\boldsymbol{f} = (f(T_1) \dots f(T_m))^T$

The mathematical algorithm used to perform the decomposition of the matrix is the Singular Value Decomposition (SVD) that decomposes any matrix *(n x m)* in the product of three matrices:

$$\boldsymbol{M} = \boldsymbol{U} * \boldsymbol{W} * \boldsymbol{V}^T \tag{5.3}$$

where

- **U** (n x m) and **V** (m x m) are orthonormal matrices;
- **W** (m x m) is a diagonal matrix whose elements are the singular values of matrix **M**.

If only the first singular value $w_1$is significant (bigger than the rest), then $\boldsymbol{M} \cong \mathbf{u} * w_1 * \mathbf{v}^T$ where **u** and **v** are the first columns of matrix **U** and **V** respectively.
Utilizing the general expression $\boldsymbol{M} = \boldsymbol{g} \text{ x } \boldsymbol{f}^T$, it can be said that

$$\boldsymbol{g} = x * \mathbf{u} \tag{5.4}$$

$$\boldsymbol{f} = y * \mathbf{v} \tag{5.5}$$

$$x * y = w_1 \tag{5.6}$$

Thus, there are two vectors **u** and **v** that are proportional to their corresponding vectors ***f*** and ***g*.** It is not feasible to find experimentally all the required elements of matrix **A** for a sufficient range of degrees of conversion and temperature.

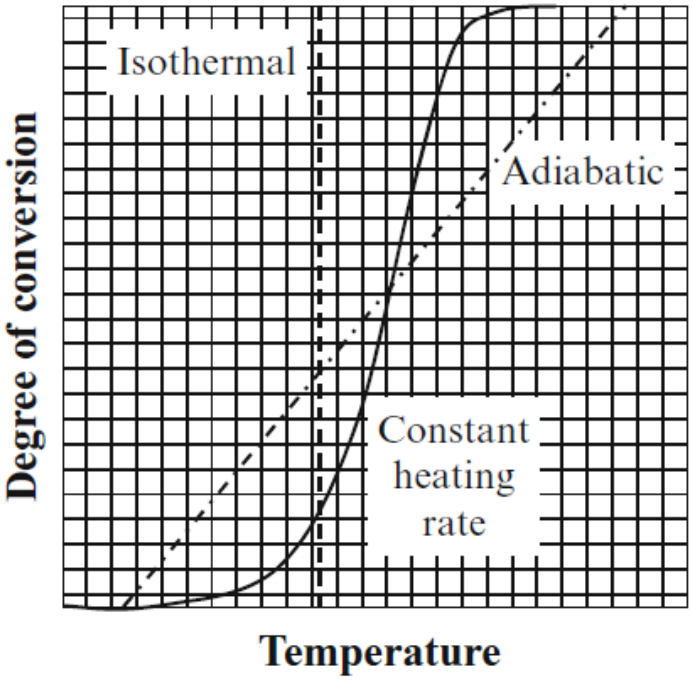

Figure 5.1: Thermal analysis expressed in a plot of degree of conversion against temperature with different possible behaviors [17].

Figure 5.1 shows trajectory of the most common types of thermal analysis experiments on the $T - \alpha$ plane as recorded in matrix **A**, in which few $a_{i,j}$ elements are filled by experimental data. It is possible to define submatrices $\boldsymbol{A_s}$ inside the area between the thermal analysis curves (Figure 5.2):

$$\boldsymbol{A_s} = \begin{pmatrix} g(\alpha_i)f(T_j) & \cdots & g(\alpha_i)f(T_{j+k}) \\ \vdots & \ddots & \vdots \\ g(\alpha_{i+p})f(T_j) & \cdots & g(\alpha_{i+p})f(T_{j+k}) \end{pmatrix}$$

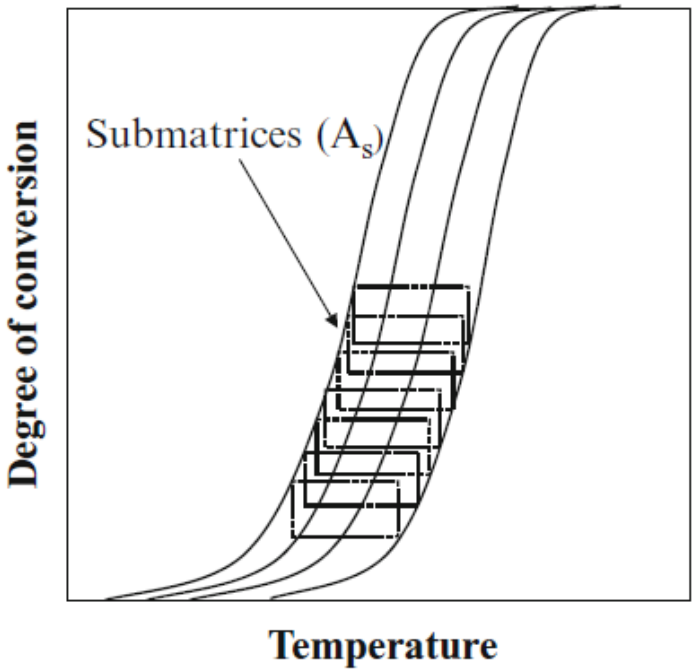

Figure 5.2: Representation of the submatrices As built between the thermal analysis curves obtained from each scanning rate [17].

The submatrices will allow the calculation of the whole vectors **u** and **v.** To build ***As***, the conversion curves must be parallel and should not cross nor overlap. However, it is hard to avoid any crossing for conversion values below 1% or above 99% (or 10% and 90%), thus the calculations and analysis must be made for conversion values between these two limits.

Applicating SVD and assuming that only the first singular value (ω_s) is different from 0:

$$\boldsymbol{A_s} \cong \boldsymbol{\mu_s} \cdot \omega_s \cdot \boldsymbol{v_s}^T \tag{5.7}$$

with $\omega_s = \chi_s \cdot \phi_s$.

To calculate the complete vectors **u** and **v**, a sequential process is applied by formulating first *q* (*s* goes from 1 to *q*), partially overlapped submatrices $\boldsymbol{A_s}$**.** So, it will be obtained *q* vectors $\boldsymbol{\mu}$ and *q* vectors **v**. Vectors **u** and **v** can be recomposed by stacking all the partial vectors and multiplying them by the factors χ_s and ϕ_s respectively:

$$\mathbf{u} = \begin{pmatrix} \chi_1 \cdot \boldsymbol{\mu_1} \\ \vdots \\ \chi_q \cdot \boldsymbol{\mu_q} \end{pmatrix}$$

$$\mathbf{v} = \begin{pmatrix} \phi_1 \cdot \boldsymbol{v_1} \\ \vdots \\ \phi_q \cdot \boldsymbol{v_q} \end{pmatrix}$$

Because of the normalization performed by the SVD algorithm, the resulting ω_s value is different for each matrix $\boldsymbol{A_s}$. As a consequence, the vectors **u** and **v** just defined are not continuos**.** To ensure continuity, each vector $\boldsymbol{\mu_s}$ has to be multiplied by a suitable factor ϕ_s and the corresponding vector $\boldsymbol{v_s}$ has to be divided by the same factor, rendering the product $\boldsymbol{\mu_s} \cdot \omega_s \cdot \boldsymbol{v_i}$ constant. The continuity is achieved because the shared area of any two consecutive matrices *s* and *s+1* forces the corresponding consecutive vectors $\boldsymbol{\mu_s}$ and $\boldsymbol{\mu_{s+1}}$**,** and $\boldsymbol{v_s}$ and $\boldsymbol{v_{s+1}}$, to share half their elements, thus allowing the calculation of the appropriate ϕ_i factor:

$$\mathbf{u} = \begin{pmatrix} \boldsymbol{\mu_1} \\ \vdots \\ \phi_q \cdot \boldsymbol{\mu_q} \end{pmatrix}$$

$$\mathbf{v} = \begin{pmatrix} \omega_1 \cdot \boldsymbol{v_1} \\ \vdots \\ \frac{\omega_q}{\phi_q} \cdot \boldsymbol{v_q} \end{pmatrix}$$

where ϕ_1 is set arbitrarily equal to 1.

Example: assuming the prediction of an experiment at a constant heating rate β, initiating at a temperature T_i. The temperature (T_v), at any time (t_v), is calculated as:

$$T_v = T_i + \beta \cdot (t_v - t_0) \tag{5.8}$$

Then, $g(\alpha_v)$ and $f(T_u)$ are obtained interpolating in vectors **u** and **v**, respectively. Finally, the rate of conversion change ($\dot{\alpha_v} = (\frac{d\alpha}{dt})_{t=t_v}$), is calculated through Eq. 5.1, and the

result is used in the selected solver of ordinary differential equations. If the simple Euler's method were used, the next value of conversion would be estimated as:

$$\alpha_{v+1} = \alpha_v + \dot{\alpha_v}(t_{v+1} - t_v) \quad (5.9)$$

To obtain accurate kinetic data there are some suggestions:

- use the sample temperature (not the reference one) for the analysis. Using the heating rate β, it is assumed that the rate of change of temperature of the sample doesn't deviate from the rate of the reference temperature;
- verify that the sample mass is small enough to avoid temperature gradients inside the sample;
- compare results from experiments done with different sample masses;
- use at least 3 temperatures or temperature programs to determine the kinetic parameters and verify Arrhenius law using 3 or 5 curves;
- replicate the runs to determine the experimental error. All experimental data have error. Smoothing of data is useful for aesthetic purposes, but it can dramatically distort a kinetic analysis;
- use the same type of baseline for all the temperature programs;
- use blank curves as baselines when possible.

Representing *ln(v)* against *1/T* informations about $f(T)$ are given. If the data fit in a straight line, it means that $f(T)$ can well be described by the Arrhenius equation, thus *v* corresponds to *k* and the slope of the line gives *-Ea/R* from which the activation energy of the process can be estimated following Eq. 1.4 in Chapter 1.
Representing instead normalized vector *u* against conversion *α* informations about $g(\alpha)$ are given. The normalized vector *u* is obtained by multiplying the vector by a factor *F*. If the data fit in a straight line, it means that the reaction order is 1, while a parabolic shape suggests an autocatalytic (Sestak-Bergren SB) behaviour.

The curvatures can follow several models like [18]:

$$g(\alpha) = (1-\alpha)^n \quad (5.10)$$

$$g(\alpha) = (1-\alpha)^n \alpha^m \quad (5.11)$$

$$g(\alpha) = (1-\alpha)^n \alpha^m \cdot [-\ln(1-\alpha)]^r \quad (5.12)$$

The NPK method doesn't need any priori assumption of the temperature or conversion functions. However, functions of temperature and conversion of a process can be easily deducted and fit using the primary results of NPK. When a single transformation dominates the kinetics of a process, NPK is capable of reproducing the DSC curves and predicting the evolution of the process in different programs of temperature [19]. In addition, fitting functions of temperatures such as the Arrhenius law, NPK provides activation energies consistent with those obtained with traditional methods of kinetic analysis. So, the function of conversion or kinetic model can also be deducted from NPK results.

5.2 Application of the NPK method on literature data of sol-gel transition

As it was said previously, the NPK method needs numerical information about conversion and temperature. These two types of information can be given by DSC experiments, which obtains temperature and heat flow rate data of the reaction occurring. To be more precise, the heat flow rates used from NPK are the ones of the subtracted curves. This method is based on a MatLab code which needs some variables in input as the instant times with relative temperatures and heat flow rates of the subtracted curve of each scanning rate, giving in output the kinetic parameters of the analysed reaction (activation energy and order of reaction). The code is based on interpolation functions, thus it is important to obtain good subtracted curves which are not giving any crossing in the relative conversion curves. That's why the type of baseline and extreme points choosing are a crucial issue for the analysis.

It is now applied the NPK method to the two literatures' data to check if it gives the same values of order of reaction and activation energy. It will then also be applied on the experimental data for the sol-gel transition to obtain the values of those kinetic parameters with the gel analysed. Vyazovkin's papers have not the baseline issue because, as it can be seen from Figure 3.17 in Chapter 3, the conversion curves of each article are good (no crossing) for the NPK method application. The method in facts, tends to select a range of conversion values where there is no crossing, and within this range it does all the analysis.

5.2.1 NPK results from literaure data focused at high cooling rates on sol-gel transition

Starting from Vyazovkin's paper of 2009, the data of instant times with relative temperatures and heat flow rates of the subtracted curve of each cooling rate were reported in an Excel file which was then uploaded as input in the MatLab code. The range of conversion values settled for the analysis was between 10 and 90%.

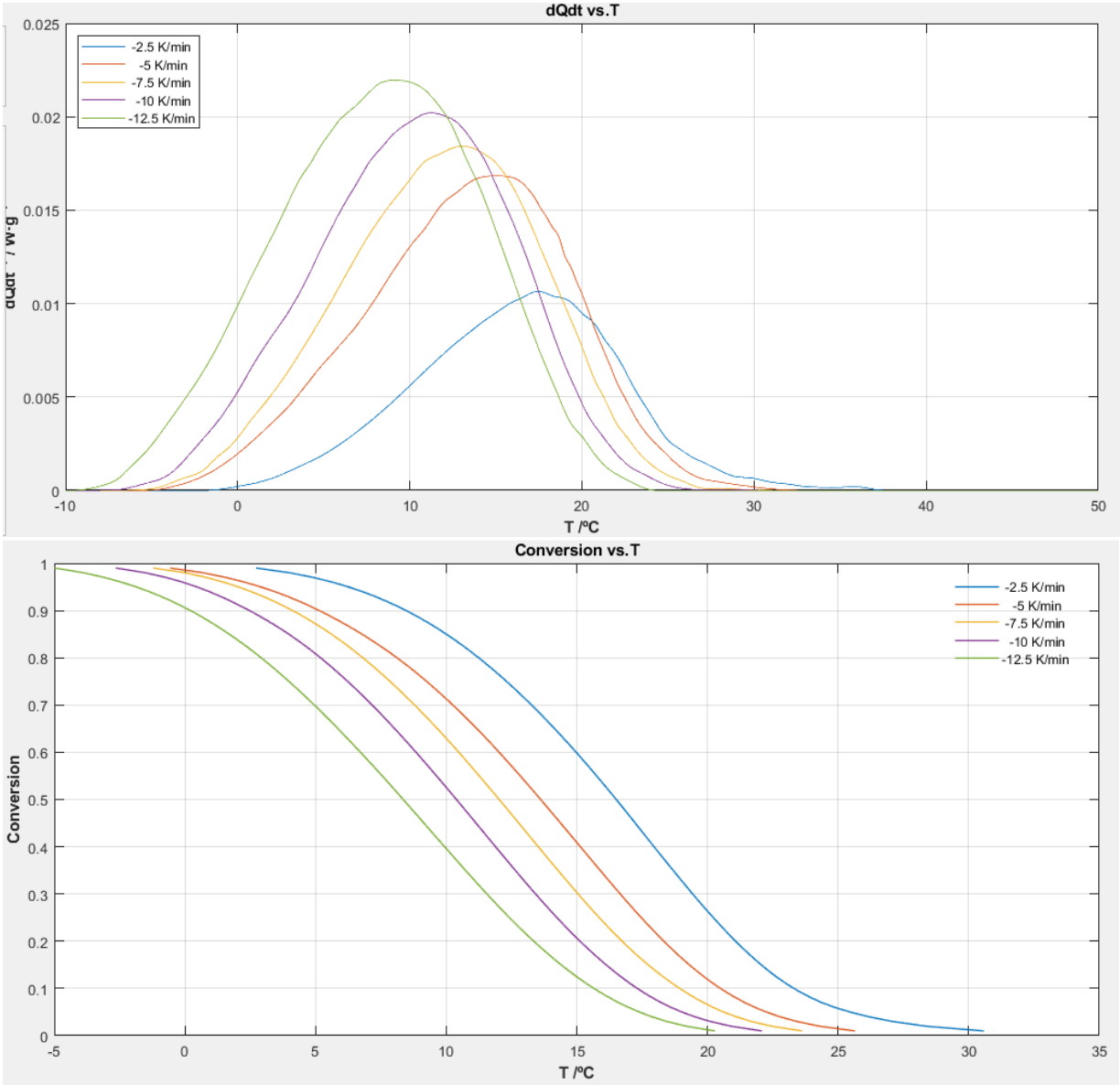

Figure 5.3: Input NPK data of Vyazovkin 2009's article: subtracted curves and relative conversion curves for each cooling rate.

Figure 5.3 reports the subtracted and conversion curves obtained in NPK code from the input Excel data uploaded. Even if vector calculations were made for a settled conversion range of 10-90%, the input values are reported considering values between 1 and 99%. The two vectors (*u* and *v*) resulting from the application of the method, are shown in following:

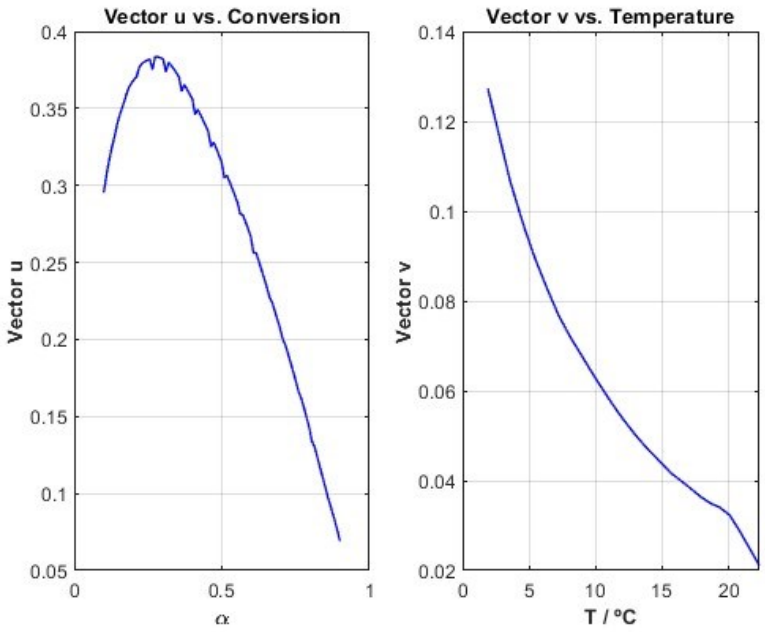

Figure 5.4 Vector u and vector v obtained from data of Vyazovkin 2009's article.

Figure 5.4 represents vector *u* and vector *v* that will be used for the estimation of the relatively order of reaction and activation energy.

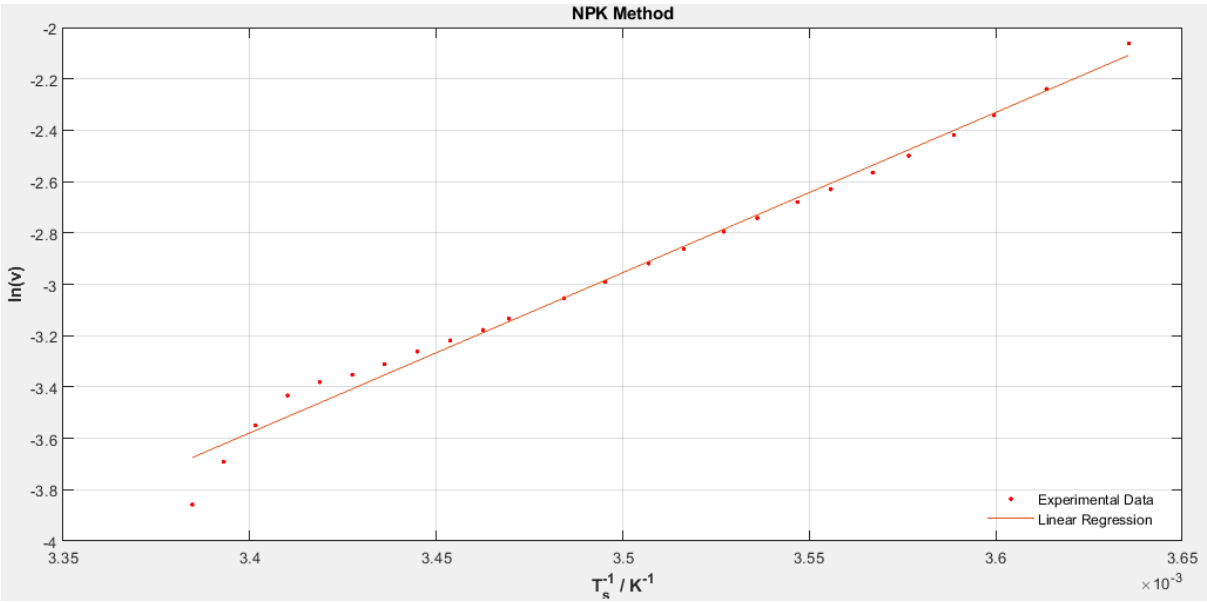

Figure 5.5: NPK Arrhenius plot obtained from data of Vyazovkin's 2009 article.

Analysing vector *v*, the activation energy can be obtained building an Arrhenius plot (Figure 5.5). It is showing a linear regression curve that explains that the reaction rate coefficient *k* is function of temperature following Arrhenius equation.

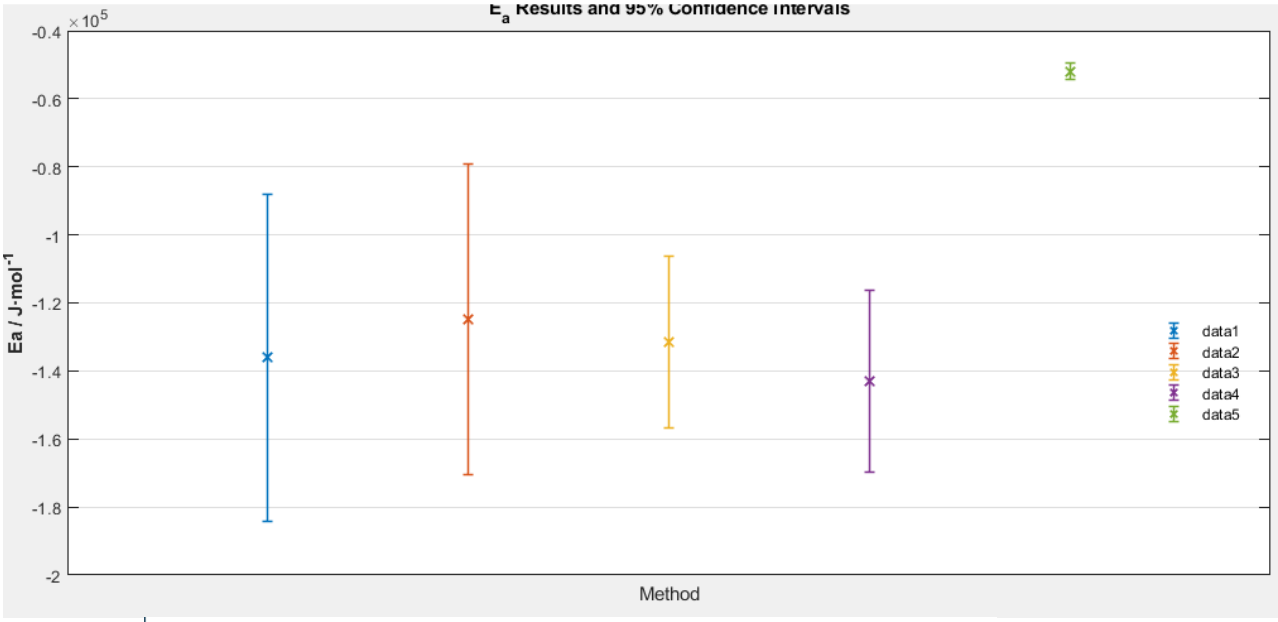

Table of Results

	Ea	error	R2
Kissinger	-1.3609e+05...	4.8008e+04...	0.9644...
Ozawa (peak)	-1.2483e+05...	4.5597e+04...	0.9620...
Ozawa (iso)	-1.3147e+05...	2.5272e+04...	0.9723...
Kiss-Aka-Sun	-1.4305e+05...	2.6609e+04...	0.9741...
NPK	-5.1891e+04...	2.4815e+03...	0.9879...

Figure 5.6: Ea results from Vyazovkin 2009 data with 95% of confidence interval estimated through several methods: Kissinger (cyan), Ozawa (red for peak and orange for isoconversional method), Kiss-Aka-Sun (violet), and NPK (green).

It can be noticed from Figure 5.6 that the activation energy value obtained with NPK for Vyazovkin's article of 2009 is not under the range of values calculated with the other methods.

It was then compared the energy amount calculated with the one reported in literature. Figure 3.11 in Chapter 3 showed that the average value of activation energy was depending on the range of scanning rates considered.

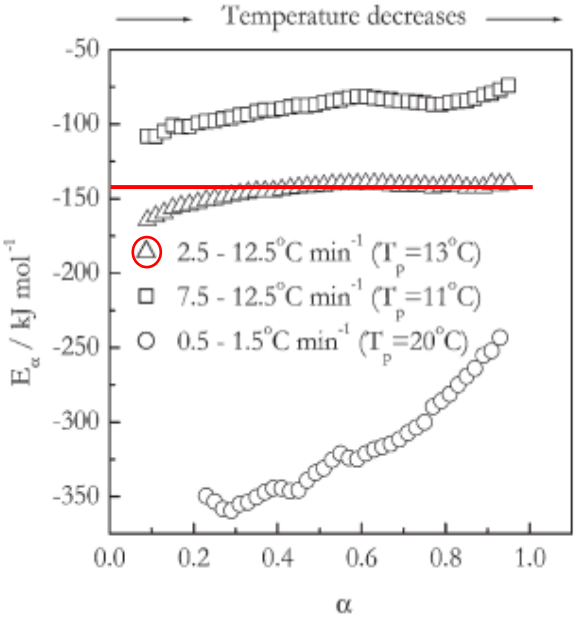

Figure 5.7: Activation energy detected value for cooling rate range 2,5-12,5 °C/min in Vyazovkin's article of 2009.

From Figure 5.7 it can be detected the activation energy value for cooling rate range 2,5-12,5 °C/min which resulted to be around -150 kJ/mol. This value is quite different from the one calculated from NPK, but very similar to the ones obtained from the other methods. Thus, this method seems not reporting the actual value of activation energy estimated for Vyazovkin's article of 2009 data.

Analysing vector *u*, it seems in Figure 5.4 that it is following an autocatalytic (Sestak-Bergren SB) behaviour. The curvature can follow several models: with one parameter, two parameters, and three parameters, following relatively Eq. 5.10 (one parameter *n*), 5.11 (two parameters *n* and *m*) and Eq. 5.12 (three parameters *n*, *m*, and *r*).

The normalized vector *u* is obtained by multiplying the vector by a factor *F*. The value of this factor, as the ones of the parameters, was estimated through the solver in Excel which was minimizing the objective function defined as the sum of the squared errors between $F \cdot u$ and $g(\alpha)$, thus between the normalized vector *u* and the values obtained from the model.

From Figure 5.8 it can be seen the normalized vector *u* fitting the three models considered.

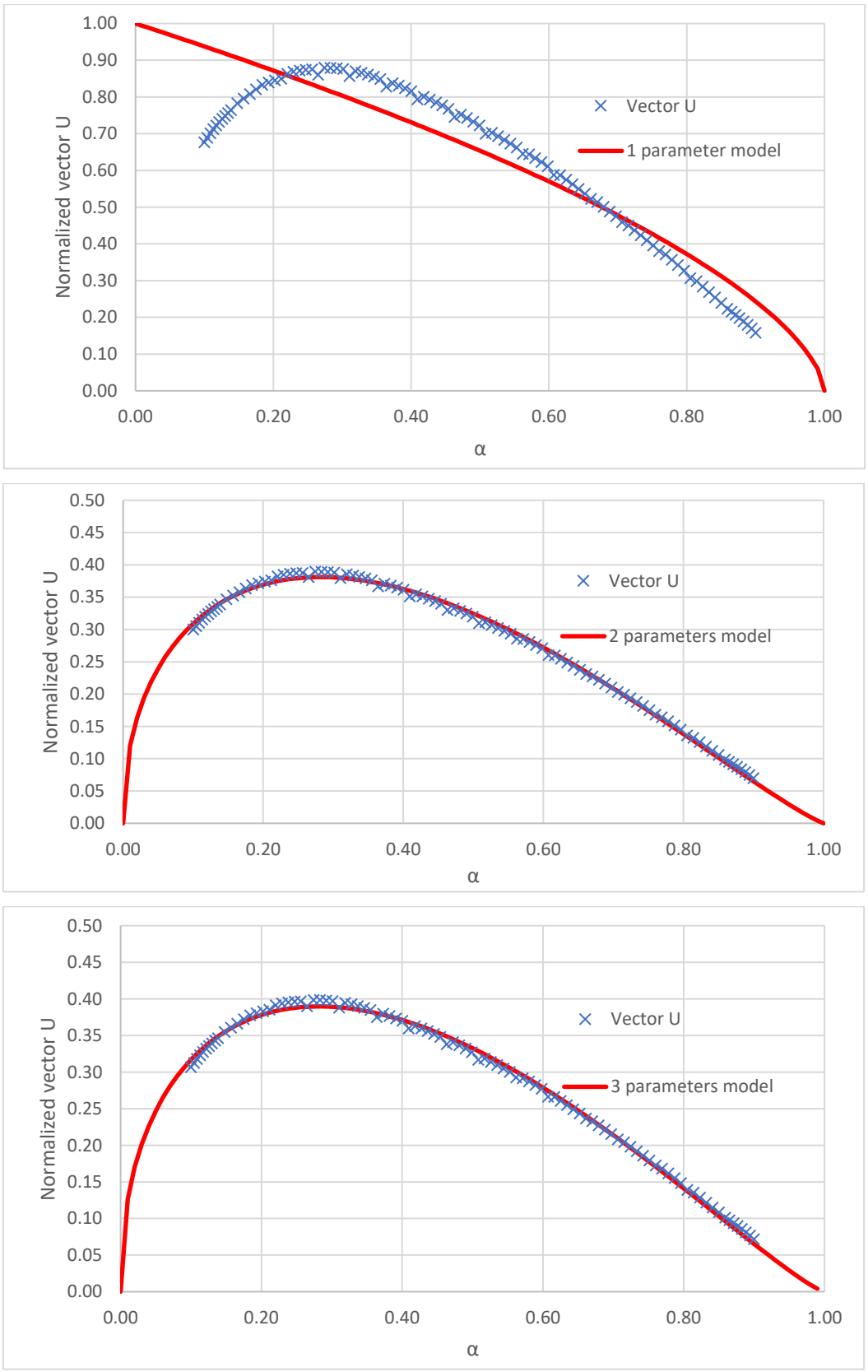

Figure 5.8: Fitting of normalized vector u to three different models: with one parameter n, with two parameters n and m, and with three parameters n, m, and r. The data are the ones of Vyazovkin's article of 2009.

From Figure 5.8 it can be noticed that the one parameter model seems not having a good fitting. The other models instead, appears acceptables.

Table 5.1 is showing the obtained values for factor F and parameters for each model, with relative squared errors (SQ Error).

Models	Factor F	n	m	r	SQ Error
1 parameter	2,29	0,61			0,737
2 parameters	1,02	1,17	0,46		2,25e-3
3 parameters	1,04	1,32	0,07	0,38	2,72e-3

Table 5.1: Values of factor F and parameters for each of the three considered models with relative minimized objective function (SQ Error) from data of Vyazovkin's article of 2009.

Considering the model which is giving the less SQ Error, thus the one with two parameters, the reaction seems quite of first order (Figure 5.9), according to the fact that the sol-gel transition is typically a first-order like phase transition because it involves enthalpy changes (Bohidar & Jena, 1993).

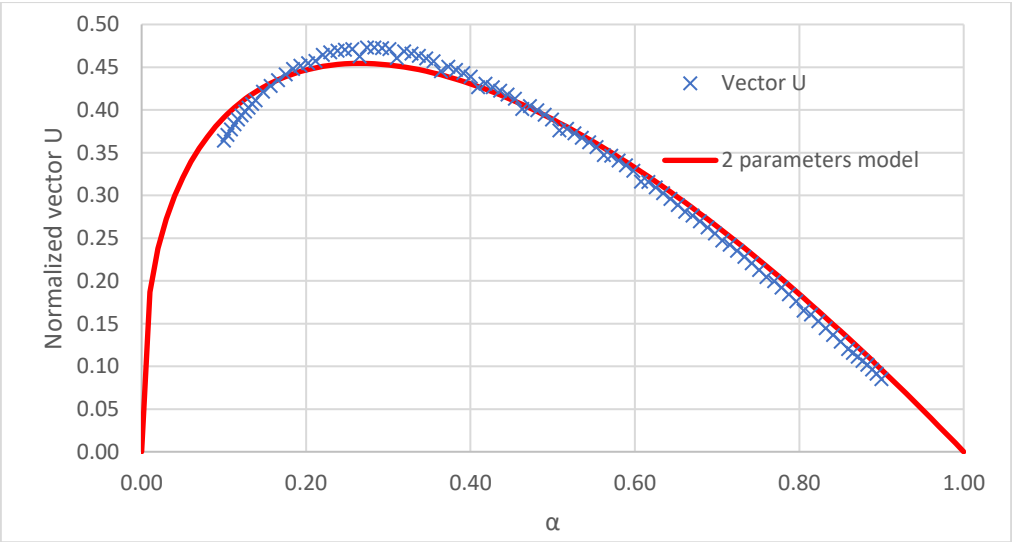

Figure 5.9: Fitting of normalized vector u to the two parameters model with n=1, m=0,36, and factor F=1,23. The data are the ones of Vyazovkin's article of 2009.

5.2.1 NPK results from literaure data focused at low cooling rates on sol-gel transition

It was then applied the NPK method on Vyazovkin's paper of 2012. Also in this case, the data of instant times with relative temperatures and heat flow rates of the subtracted curve of each cooling rate were reported in an Excel file and then uploaded as input in the MatLab code. The range of conversion values settled for analysis was between 10 and 90%.

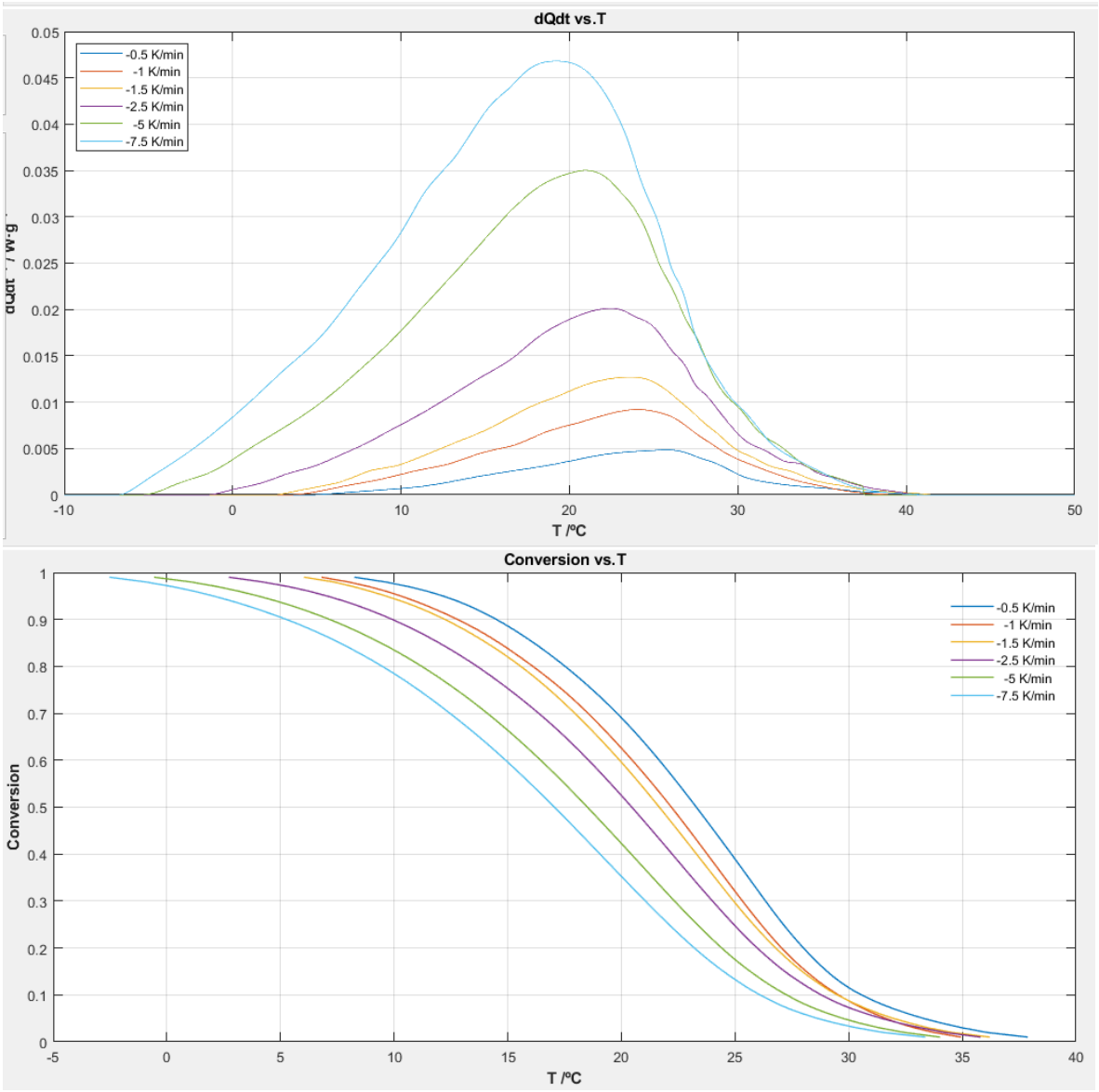

Figure 5.10: Input NPK data of Vyazovkin 2012's article: subtracted curves and relative conversion curves for each cooling rate.

Figure 5.10 reports the subtracted and conversion curves obtained in NPK code from the input Excel data uploaded. Even if vector calculations were made for a settled

conversion range of 10-90%, the input values are reported considering values between 1 and 99%. It can be seen in this case that there is a crossing between conversion curves for a value of conversion below 0,1, thus a selected range of 1-99% would not work for the NPK method. The two vectors (*u* and *v*) resulting from the application of the method, were compared to the ones of the previous article (Figure 5.12).

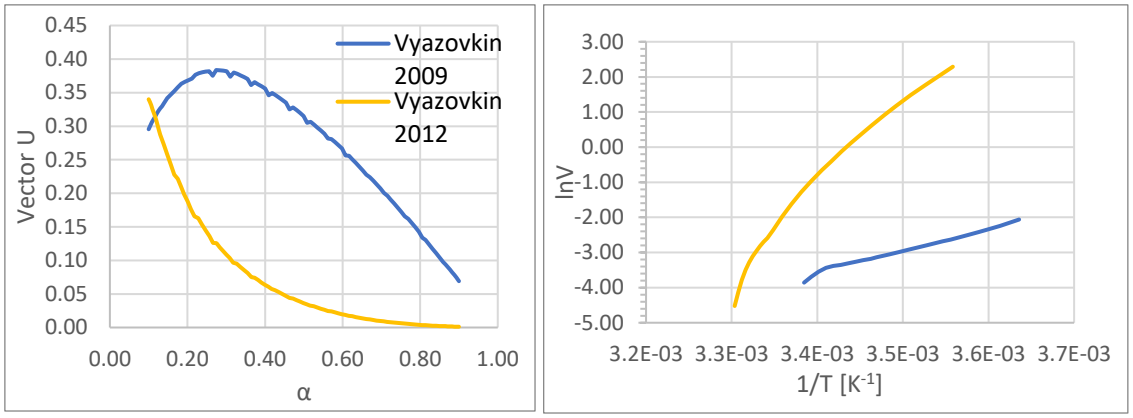

Figure 5.11: Vectors' comparison between the ones obtained from data of Vyazovkin's article of 2009 and the ones from data of Vyazovkin's article of 2012. Vector v is reported as logarithmic to compare the difference in the slopes (thus in Ea).

Plots reported in Figure 5.11 are showing different trends, thus they are presenting different order of reaction and activation energy. The second one is not surprising because it was already said that the activation energy value was depending on the scanning rate range: at higher scanning rates it was estimated a lower (in absolute values) value of activation energy. While the Vyazovkin's article of 2009 was considering a higher range, the Vyazovkin's article of 2012 was analysing a lower one, thus the slope of the latter is higher.

Analysing vector *v*, it can be seen from Figure 5.11 that also for this paper the plot of *lnV* against *1/T* is presenting a straight line, thus the reaction rate coefficient *k* is following the Arrhenius equation. The value of activation energy was again estimated from the slope of the line.

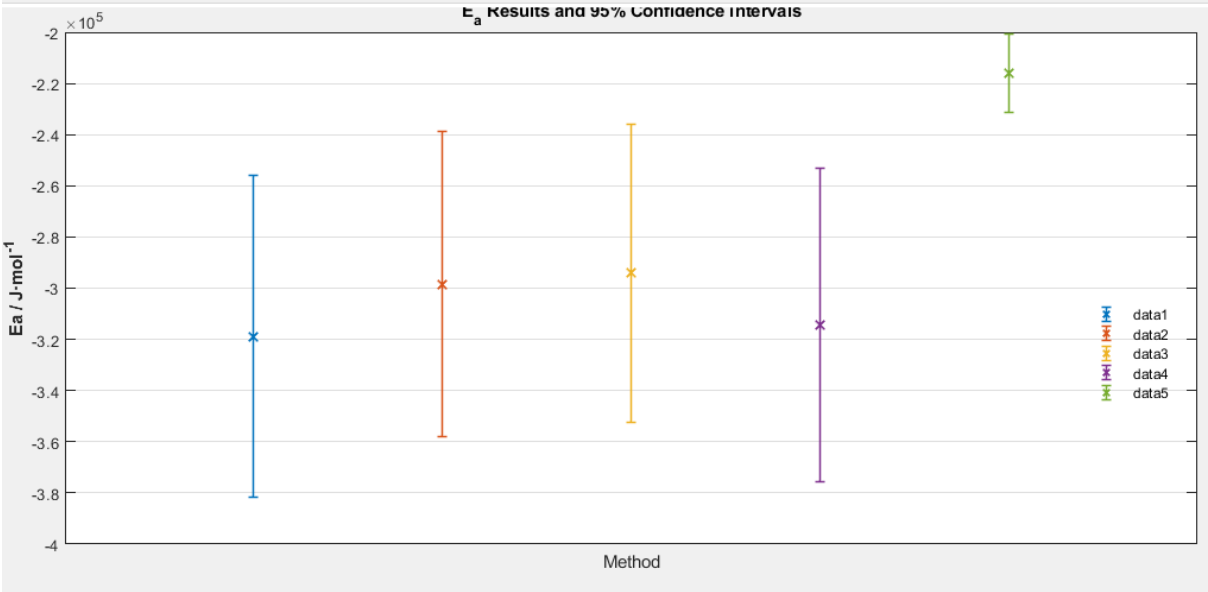

Table of Results

	Ea	error	R2
Kissinger	-3.1884e+05...	6.2775e+04...	0.9803...
Ozawa (peak)	-2.9841e+05...	5.9654e+04...	0.9797...
Ozawa (iso)	-2.9419e+05...	5.8102e+04...	0.9669...
Kiss-Aka-Sun	-3.1436e+05...	6.1135e+04...	0.9679...
NPK	-2.1592e+05...	1.5316e+04...	0.9724...

Figure 5.12: Ea results from Vyazovkin 2012 data with 95% of confidence interval estimated through several methods: Kissinger (cyan), Ozawa (red for peak and orange for isoconversional method), Kiss-Aka-Sun (violet), and NPK (green).

It can be noticed from Figure 5.12 that also the activation energy value obtained with NPK for Vyazovkin's article of 2012 is not under the range of values calculated with the other methods.

As expected, the value obtained from Vyazovkin 2012 data analysis with NPK method for the activation energy is quite different from the one estimated from Vyazovkin 2009 data analysis with that method (-216 kJ/mol for the former against -52 kJ/mol for the latter). It was then compared the energy amount calculated with the one reported in literature. From Figure 3.11 in Chapter 3 it can be detected the activation energy value for cooling rate range 0,5-7,5 °C/min which resulted to be from -425 to -175 kJ/mol. In this case, the value of the energy obtained from the NPK method is inside this range. Thus, the amount estimated from this method can be considered valid for Vyazovkin's 2012 article data.

Analysing vector *u*, it seems in Figure 5.11 that the curve is very different from the one obtained for Vyazovkin's article of 2009, thus the reaction has not a first-order like behavior. Considering again the previous three different models, the solver in Excel could minimize the objective function giving good fittings.

Table 5.2 is showing the obtained values for factor F and parameters for each model, with relative squared errors (SQ Error).

Models	Factor F	n	m	r	SQ Error
1 parameter	1,90	4,33			1,91e-2
2 parameters	1,00	5,32	0,25		1,09e-2
3 parameters	1,00	5,34	0,21	0,04	1,09e-2

Table 5.2: Values of factor F and parameters for each of the three considered models with relative minimized objective function (SQ Error) from data of Vyazovkin's article of 2012.

Considering the model which is giving the less SQ Error, thus it can be the one with two or three parameters, the reaction seems quite of fifth order (Figure 5.13).

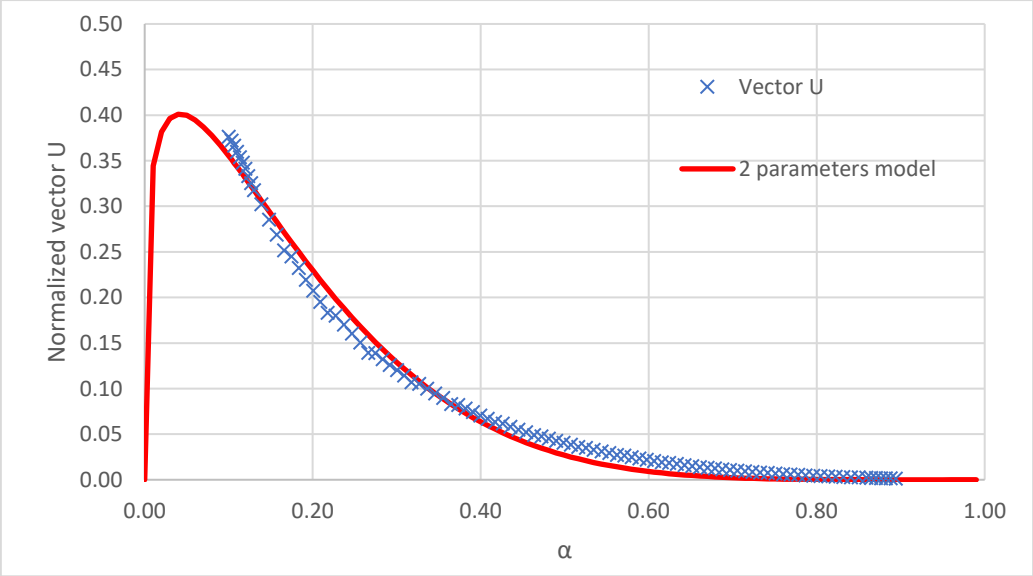

Figure 5.13: Fitting of normalized vector u to the two parameters model with n=5, m=0,22, and factor F=1,11. The data are the ones of Vyazovkin's article of 2012.

5.3 Application of the NPK method on experimental data of sol-gel transition

It is now applied the NPK method on the experimental data. Taking into account that the scanning rate is important for this method, at least four values help it for a better analysis and to obtain better results. According to this, not all the solutions were considered because not all were experimented under four or more scanning rates. Thus, the analysis were based only on SolC and SolD for the 175 g Bloom gel, and SolB for the 300 g Bloom gel.

5.3.1 NPK results for the 175 g Bloom sol-gel transition

Considering both SolC and SolD for the 175 g Bloom gel, the range of conversion values settled for analysis was still between 10 and 90%, and only the first sections of cooling and heating were considered.

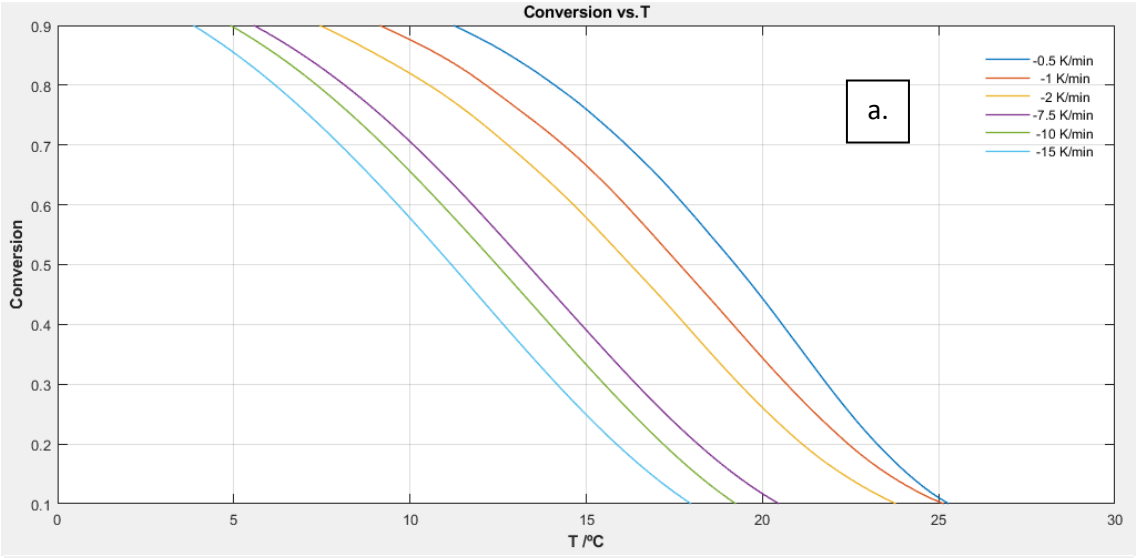
Conversion vs.T
Conversion
T /ºC
-0.5 K/min
-1 K/min
-2 K/min
-7.5 K/min
-10 K/min
-15 K/min
a.

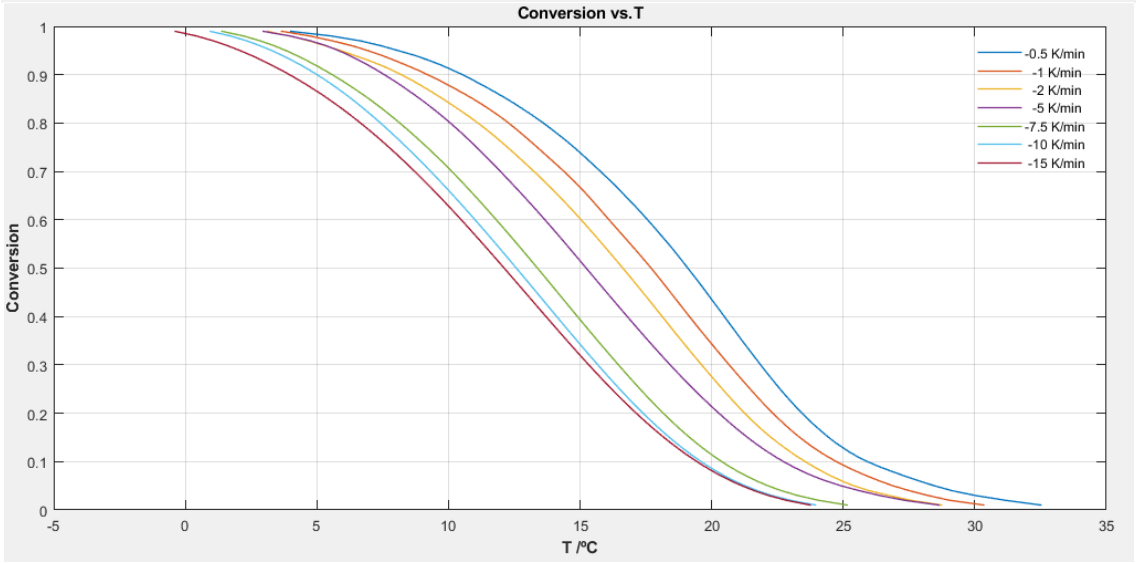
Conversion vs.T
Conversion
T /ºC
-0.5 K/min
-1 K/min
-2 K/min
-5 K/min
-7.5 K/min
-10 K/min
-15 K/min

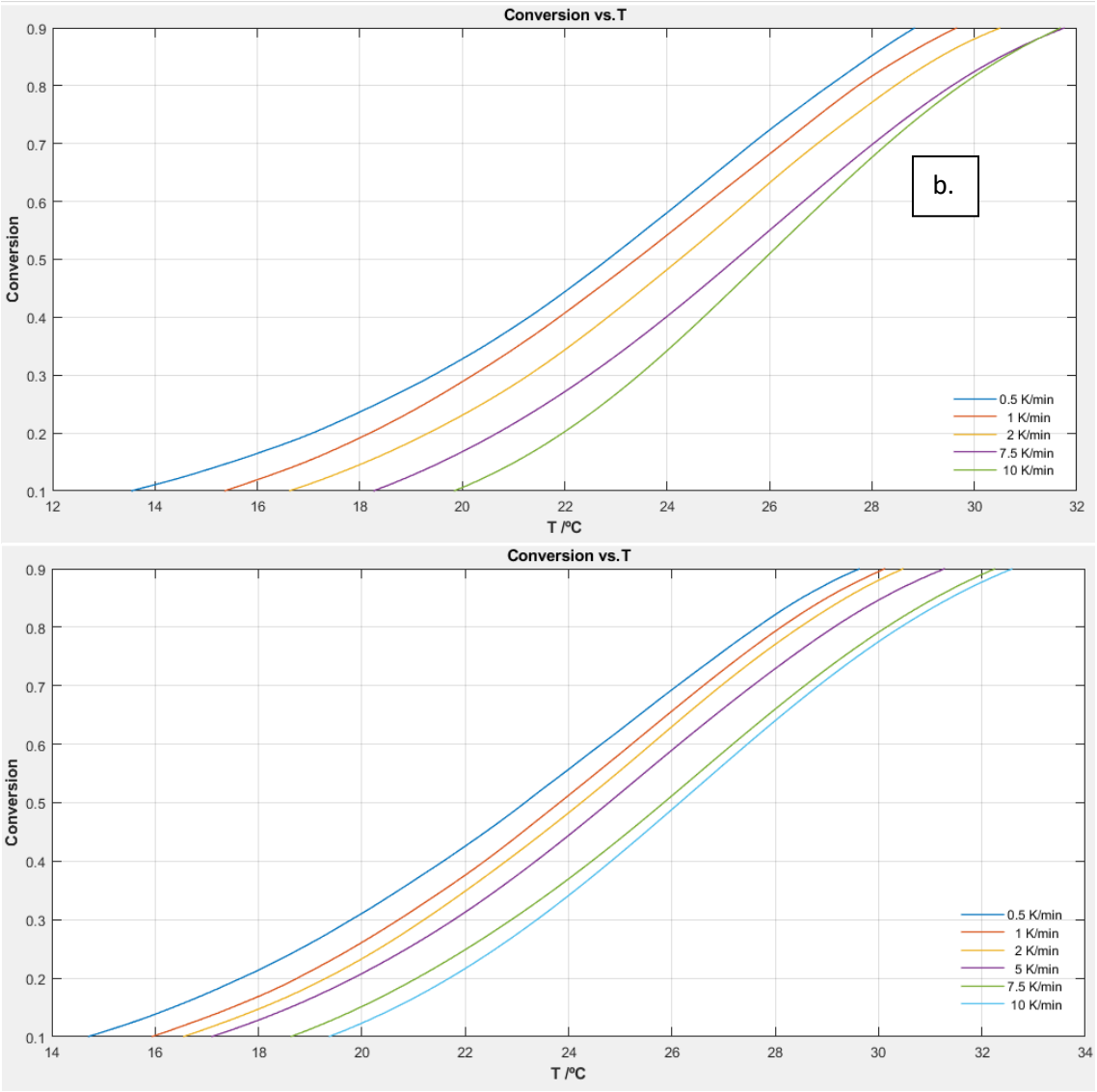

Figure 5.14: NPK conversion curves for each scanning rate for SolC (first plot) and SolD (second plot) in both first cooling (a) and first heating (b) sections.

Figure 5.14 reports the conversion curves of the two solutions (SolC and SolD) for both first cooling and first heating sections obtained in NPK code from two input Excel data uploaded. It was noticed that the conversion curve at heating rate 5 °C/min for SolC was showing an overlap, thus it was not considered.

The two vectors (*u* and *v*) resulting from the application of the method for both first cooling and first heating, are shown in following:

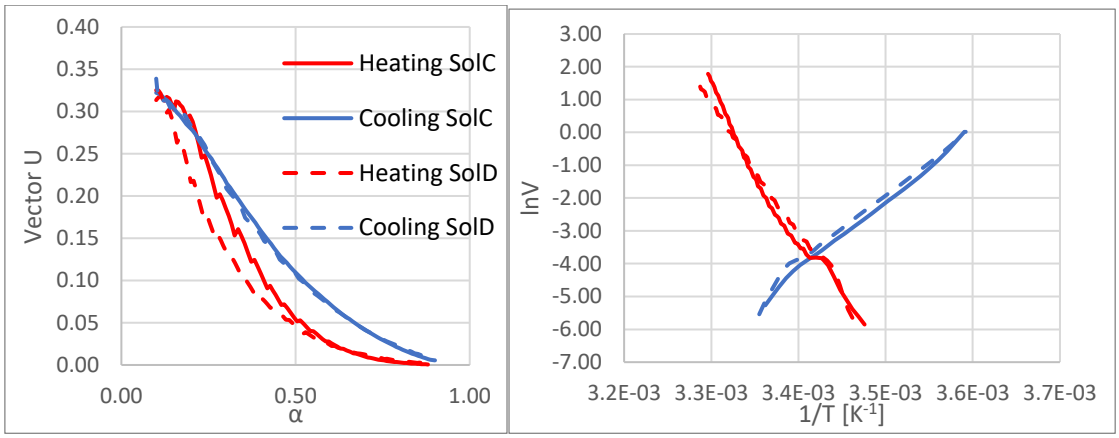

Figure 5.15: Comparison between the obtained vectors for SolD and the ones for SolC. Vector v is reported as logarithmic to compare the difference in the slopes (thus in Ea).

Analysing vector *v*, it can be seen in Figure 5.15 that SolC and SolD in both first cooling and first heating sections have very similar trends. Thus, it will be expected that SolD will have the same *Ea* values of SolC in both the two steps.

It can be already noticed that the sign of the energy value for the heating section will be the opposite of the one for the cooling section (thus, it will be positive).

Table of Results

	Ea	error	R2
Kissinger	-2.7016e+05...	2.6768e+04...	0.994...
Ozawa (peak)	-2.5222e+05...	2.5429e+04...	0.994...
Ozawa (iso)	-2.8975e+05...	2.9635e+04...	0.990...
Kiss-Aka-Sun	-3.0961e+05...	3.1185e+04...	0.990...
NPK	-1.7606e+05...	5.0005e+03...	0.995...

a.

Table of Results

	Ea	error	R2
Kissinger	-2.9675e+05...	4.6017e+04...	0.9821...
Ozawa (peak)	-2.7750e+05...	4.3744e+04...	0.9815...
Ozawa (iso)	-3.1517e+05...	5.0963e+04...	0.9688...
Kiss-Aka-Sun	-3.3636e+05...	5.3623e+04...	0.9697...
NPK	-1.7567e+05...	7.9382e+03...	0.9886...

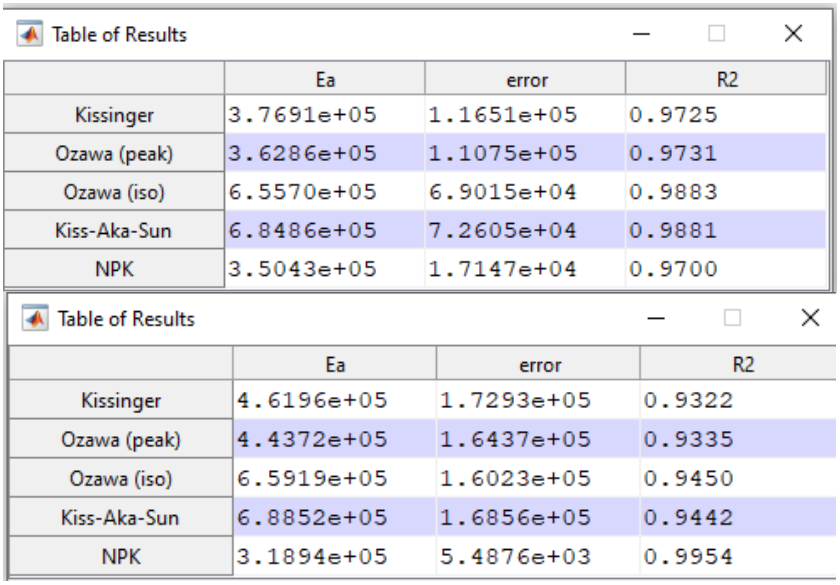

Table of Results

	Ea	error	R2
Kissinger	3.7691e+05	1.1651e+05	0.9725
Ozawa (peak)	3.6286e+05	1.1075e+05	0.9731
Ozawa (iso)	6.5570e+05	6.9015e+04	0.9883
Kiss-Aka-Sun	6.8486e+05	7.2605e+04	0.9881
NPK	3.5043e+05	1.7147e+04	0.9700

Table of Results

	Ea	error	R2
Kissinger	4.6196e+05	1.7293e+05	0.9322
Ozawa (peak)	4.4372e+05	1.6437e+05	0.9335
Ozawa (iso)	6.5919e+05	1.6023e+05	0.9450
Kiss-Aka-Sun	6.8852e+05	1.6856e+05	0.9442
NPK	3.1894e+05	5.4876e+03	0.9954

b.

Figure 5.16: Ea results for SolC (first table) and SolD (second table) in both first cooling (a) and first heating (b) sections with 95% of confidence interval estimated through several methods: Kissinger (cyan), Ozawa (red for peak and orange for isoconversional method), Kiss-Aka-Sun (violet), and NPK (green).

It can be seen from Figure 5.16 that the activation energy obtained during cooling has the same value for both solutions: -176 kJ/mol. Instead, the one estimated during heating has a little difference between +350 kJ/mol for SolC and +320 kJ/mol for SolD.

The fact that the heating step presents a very different energy amount (in absolute value) than the one calculated for the cooling section, is given by the difference in the two phenomena occurring: during heating there is unfolding and melting, while during cooling there is folding and gelation.

For activation energy comparisons, it is indifferent to take vector *v* of SolC or SolD. Thus, the resulting Arrhenius plot of SolD for cooling could be compared to the ones obtained from Vyazovkin's papers (Figure 5.17).

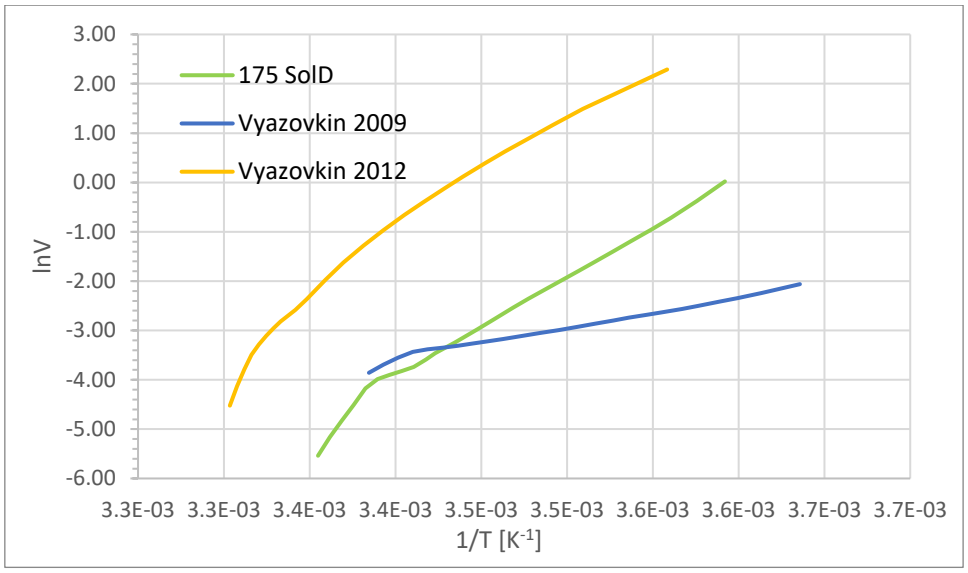

Figure 5.17: Arrhenius plot comparing vector v data of SolD of the 175 g Bloom gel with the ones of Vyazovkin's articles of 2009 and 2012.

It can be seen from figure that the activation energy obtained for SolD (-176 kJ/mol) is pretty similar to the one calculated for Vyazovkin's article of 2012 (-216 kJ/mol), thus different from the one estimated for Vyazovkin's paper of 2009 (-52 kJ/mol). Anyway, the latter could be considered bad for comparison because it was not giving acceptable NPK results (the amount of energy was not according to the one reported in literature: around -150 kJ/mol).

Analysing vector *u,* it can be seen in Figure 5.15 that SolC and SolD in both first cooling sections have very similar trends, while in both first heating steps there are some differences. Thus, it will be expected that SolD will have the same *n* values of SolC during cooling, but different order of reactions during heating (higher for SolD).

Considering the previous three different models, the solver in Excel could minimize the objective function giving good fittings.

Table 5.3 is showing the obtained values for factor F and parameters for each model, with relative squared errors (SQ Error).

SolC - Cooling					
Models	**Factor F**	**n**	**m**	**r**	**SQ Error**
1 parameter	2,42	1,91			1,37e-2
2 parameters	1,82	2,17	0,13		1,63e-3
3 parameters	1,82	2,17	0,13	0	1,63e-3
SolD - Cooling					
Models	**Factor F**	**n**	**m**	**r**	**SQ Error**
1 parameter	2,42	1,91			2,45e-2
2 parameters	1,59	2,35	0,18		8,48e-3
3 parameters	1,60	2,35	0,18	0	8,49e-3
SolC - Heating					
Models	**Factor F**	**n**	**m**	**r**	**SQ Error**
1 parameter	2,06	2,88			9,50e-2
2 parameters	1,00	3,70	0,31		6,59e-3
3 parameters	1,00	3,85	0	0,31	6,52e-3
SolD - Heating					
Models	**Factor F**	**n**	**m**	**r**	**SQ Error**
1 parameter	2,05	3,53			1,07e-2
2 parameters	1	4,55	0,28		6,38e-3
3 parameters	1	4,55	0,28	0	6,38e-3

Table 5.3: Values of factor F and parameters for each of the three considered models with relative minimized objective function (SQ Error) for the 175 g Bloom gel solutions during both cooling and heating.

Considering the model which is giving the less SQ Error, thus it can be the one with two or three parameters, the gelation reaction seems quite of second order in both SolC and SolD, while the melting one can follow a reaction of third (for SolC) or fourth (for SolD) order (Figure 5.18).

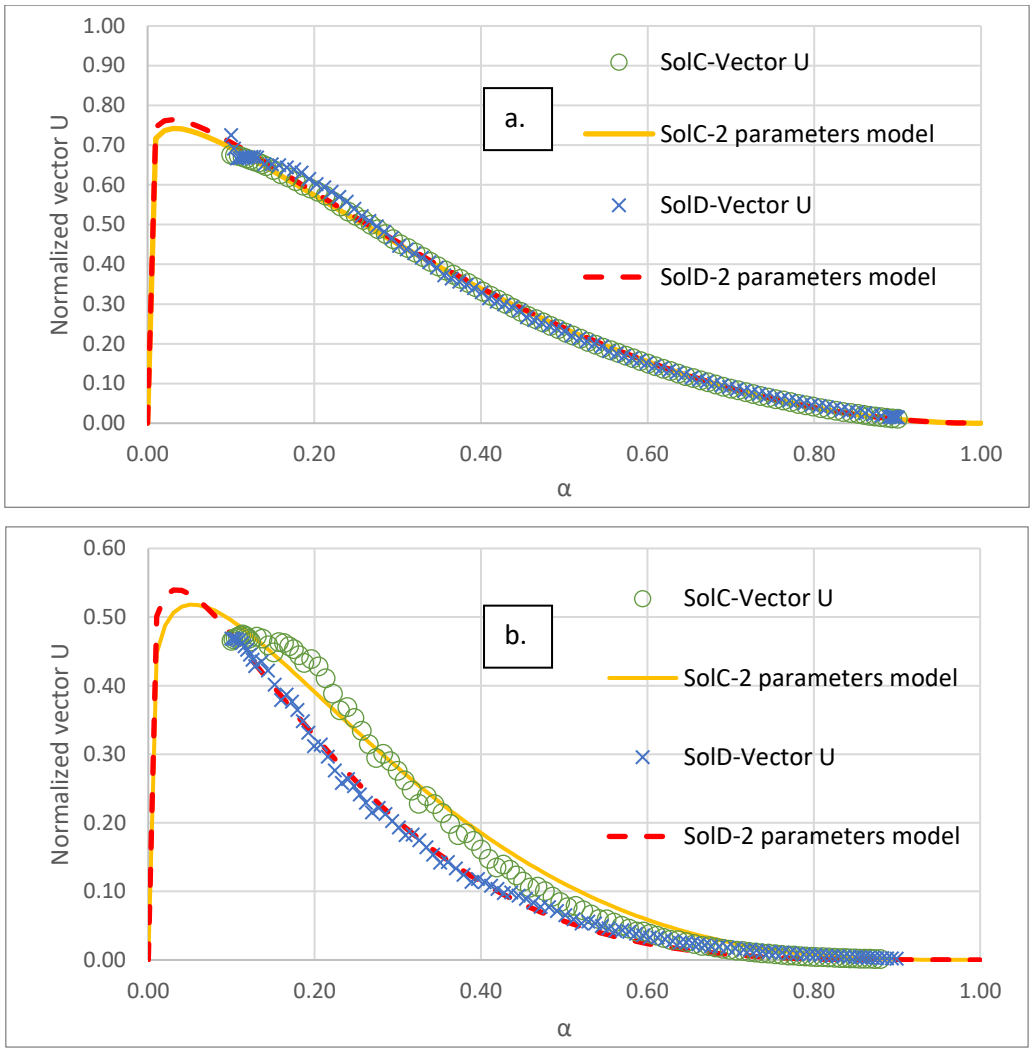

Figure 5.18: Fitting of normalized vector u to the two parameters model. In cooling section (a) both SolC and SolD vector u data are fitted with n=2, while in heating section (b) SolC vector u data are fitted with n=3 and SolD ones with n=4.

For reaction order comparisons, it is indifferent to take vector *u* of SolC or SolD during cooling. Thus, the vector data of SolD could be compared to the ones obtained from Vyazovkin's papers (Figure 5.19).

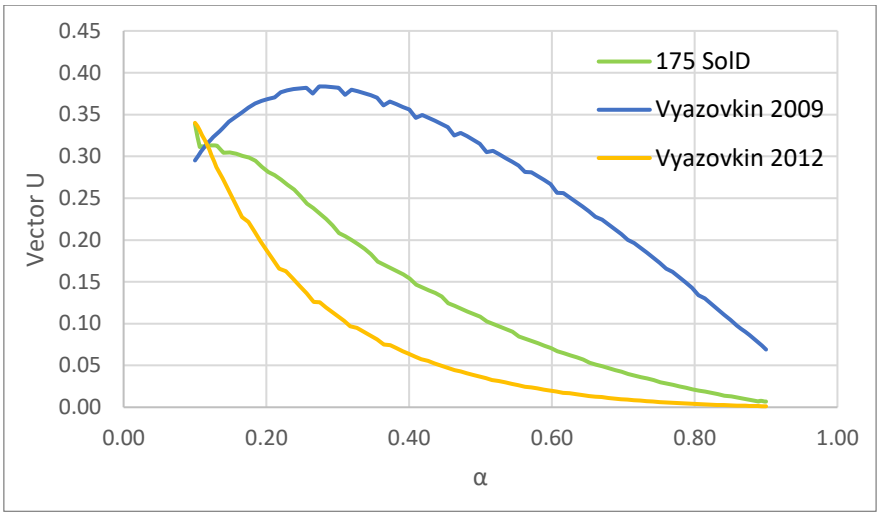

Figure 5.19: Comparison between vector u of SolD of the 175 g Bloom gel and the ones of Vyazovkin's articles of 2009 and 2012.

It is confirmed from Figure 5.18 that the reaction order of SolD during gelation (second order) is between the ones of Vyazovkin 2012 (fifth order) and Vyazovkin 2009 (first order).

5.3.2 NPK results for the 300 g Bloom sol-gel transition

Considering now SolB for the 300 g Bloom gel, the range of conversion values settled for analysis was still between 10 and 90%, and only the first sections of cooling and heating were considered.

Figure 5.20 reports the conversion curves of the 300 g Bloom SolB for both first cooling and first heating sections obtained in NPK code from two input Excel data uploaded. It was noticed that the heating rates 0,5 and 7,5 °C/min were showing an overlap, thus they were not considered.

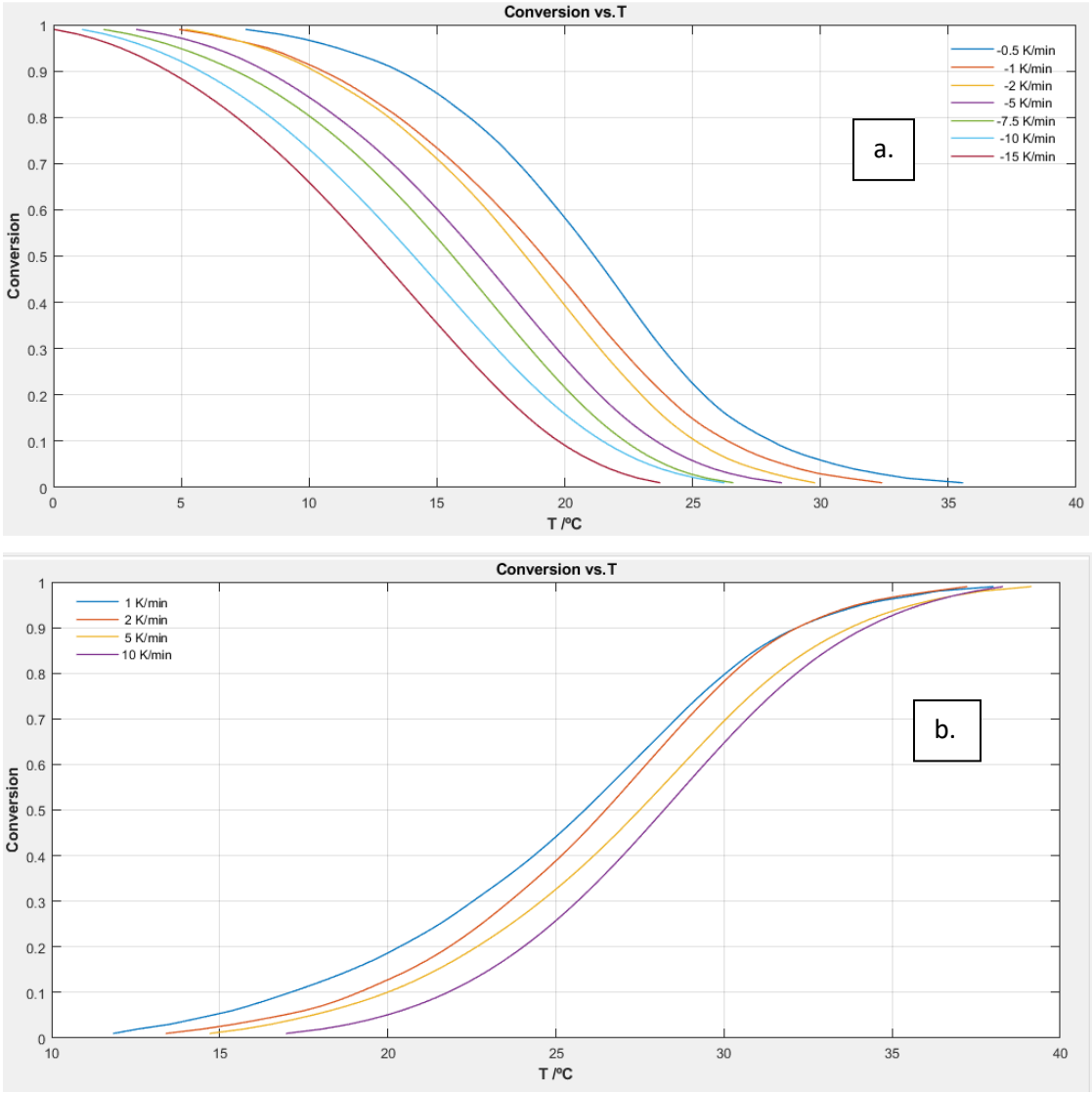

Figure 5.20: NPK conversion curves for each scanning rate for SolB in both first cooling (a) and first heating (b) sections.

The 300 g Bloom SolB can be compared to either SolC or SolD of the 175 g Bloom gel. For instance, the two vectors (*u* and *v*) resulting from the application of the method for both first cooling and first heating were compared to the ones obtained for SolD:

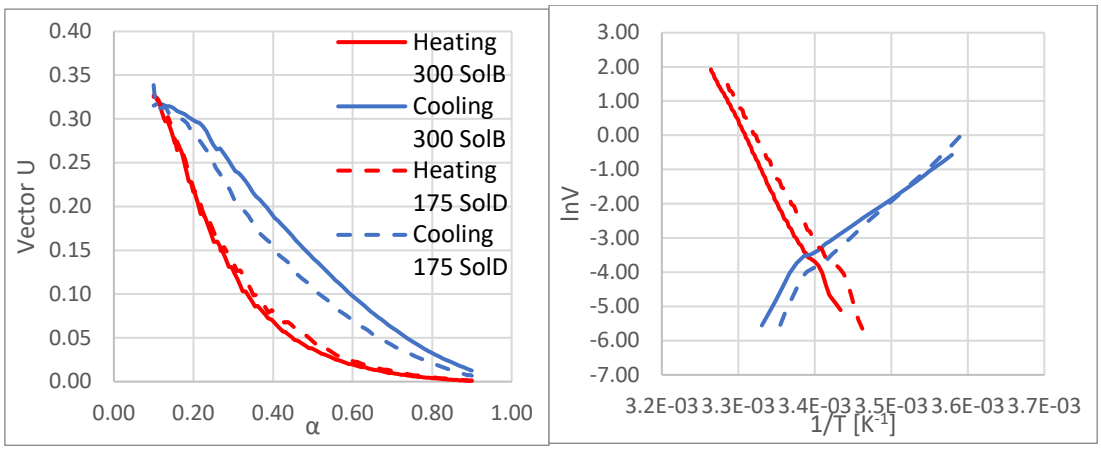

Figure 5.21: Comparison between the obtained vectors for SolB of the 300 g Bloom gel and the ones for SolD of the 175 g Bloom gel. Vector v is reported as logarithmic to compare the difference in the slopes (thus in Ea).

Analysing vector *v*, it can be seen in Figure 5.21 that SolB and SolD in both first cooling and first heating sections have very similar trends. Thus, it will be expected that SolB will have quite the same *Ea* values of SolD in both the two steps.

Table of Results

	Ea	error	R2
Kissinger	-2.0418e+05...	2.9959e+05...	0.3804...
Ozawa (peak)	-1.8948e+05...	2.8479e+05...	0.3691...
Ozawa (iso)	-1.8973e+05...	2.2583e+05...	0.3579...
Kiss-Aka-Sun	-2.0442e+05...	2.3757e+05...	0.3690...
NPK	-1.4824e+05...	1.0391e+04...	0.9719...

a.

Table of Results

	Ea	error	R2
Kissinger	-2.9675e+05...	4.6017e+04...	0.9821...
Ozawa (peak)	-2.7750e+05...	4.3744e+04...	0.9815...
Ozawa (iso)	-3.1517e+05...	5.0963e+04...	0.9688...
Kiss-Aka-Sun	-3.3636e+05...	5.3623e+04...	0.9697...
NPK	-1.7567e+05...	7.9382e+03...	0.9886...

Table of Results

	Ea	error	R2
Kissinger	-2.1486e+04	1.6138e+05	0.1410
Ozawa (peak)	-1.5689e+04	1.5337e+05	0.0883
Ozawa (iso)	6.0767e+05	1.5137e+05	0.9721
Kiss-Aka-Sun	6.3428e+05	1.5924e+05	0.9717
NPK	3.5475e+05	4.9463e+03	0.9965

Table of Results

	Ea	error	R2
Kissinger	4.6196e+05	1.7293e+05	0.9322
Ozawa (peak)	4.4372e+05	1.6437e+05	0.9335
Ozawa (iso)	6.5919e+05	1.6023e+05	0.9450
Kiss-Aka-Sun	6.8852e+05	1.6856e+05	0.9442
NPK	3.1894e+05	5.4876e+03	0.9954

b.

Figure 5.22: Ea results for SolB (first table) and SolD (second table) in both first cooling (a) and first heating (b) sections with 95% of confidence interval estimated through several methods: Kissinger (cyan), Ozawa (red for peak and orange for isoconversional method), Kiss-Aka-Sun (violet), and NPK (green).

It can be seen from Figure 5.22 that the activation energies obtained during both cooling and heating have little differences: between -150 kJ/mol for SolB and -176 kJ/mol for SolD during cooling, and between +355 kJ/mol for SolB and +320 kJ/mol for SolD during heating.

Analysing vector *u,* it can be seen in Figure 5.21 that SolB and SolD in both first cooling and first heating sections have very similar trends. Thus, it will be expected that SolD will have the same *n* values of SolB during both cooling and heating.

Considering the previous three different models, the solver in Excel could minimize the objective function giving good fittings.

Table 5.4 is showing the obtained values for factor F and parameters for each model, with relative squared errors (SQ Error).

SolB - Cooling					
Models	**Factor F**	**n**	**m**	**r**	**SQ Error**
1 parameter	2,50	1,49			4,22e-2
2 parameters	1,66	1,88	0,19		3,43e-3
3 parameters	1,66	1,96	0	0,19	3,60e-3
SolB - Heating					
Models	**Factor F**	**n**	**m**	**r**	**SQ Error**
1 parameter	1,96	3,88			1,03e-2
2 parameters	1,00	4,83	0,26		4,04e-3
3 parameters	1,00	4,96	0	0,26	4,08e-3

Table 5.4: Values of factor F and parameters for each of the three considered models with relative minimized objective function (SQ Error) for the 300 g Bloom gel solution during both cooling and heating.

Considering the model which is giving the less SQ Error, thus it can be the one with two or three parameters, the gelation reaction seems quite of second order in both SolB and SolD, while the melting one is following a reaction of fourth order as in SolD (Figure 5.23).

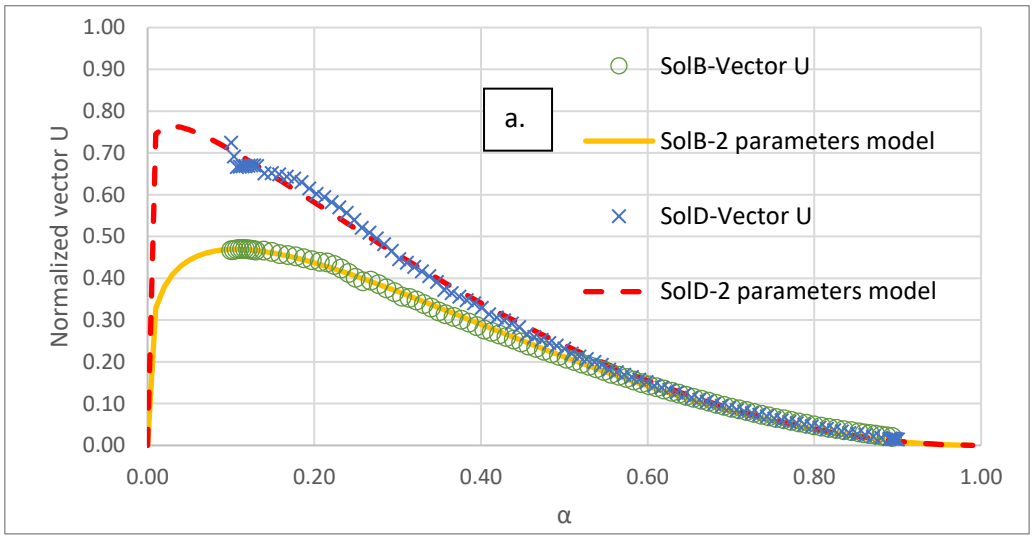

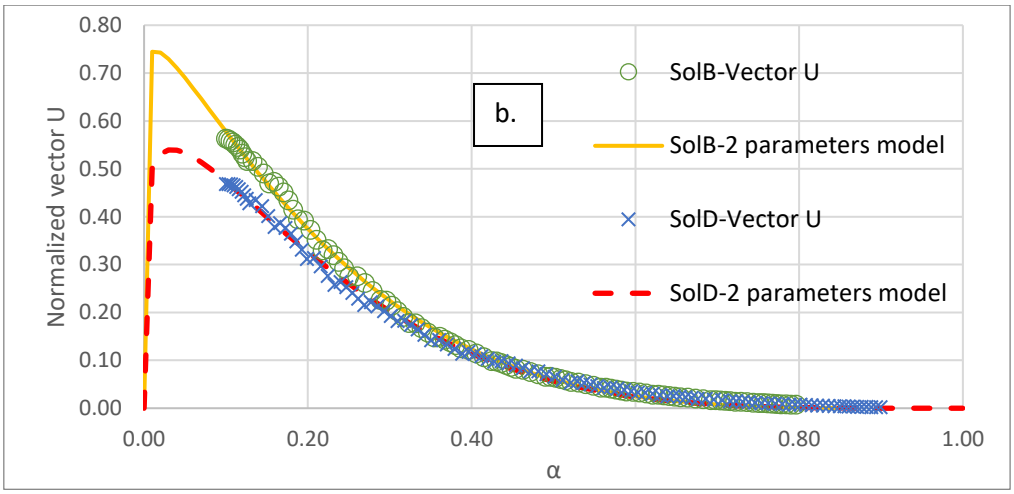

Figure 5.23: Fitting of normalized vector u to the two parameters model. In cooling section (a) both SolB and SolD vector u data are fitted with n=2, while in heating section (b) they are fitted with n=4.

5.4 NPK further analysis on sol-gel transition

5.4.1 NPK analysis of activation energy dependence on scanning rate in sol-gel transition

As it was observed from the two literature's papers, the activation energy was changing with different ranges of scanning rates. Thus, it was questioned if the selection of scanning rates was important for the NPK method.

According to Figure 3.11 in Chapter 3, the activation energy for Vyazvokin's article of 2009 has three different values depending on three different ranges of cooling rate: 0,5-1,5 °C/min, 7,5-12,5 °C/min, and 2,5-12,5 °C/min. In order to check if also the NPK method is considering this activation energy dependence on the cooling rate range considered, the code was changed by putting a cycle that was calculating vector *v* for each possible combination of scanning rates.

For instance, the overall SolD cooling rate range 0,5-15 °C/min was subdivided in all possible groups of three and five different rates, giving several vectors *v* (Figure 5.24).

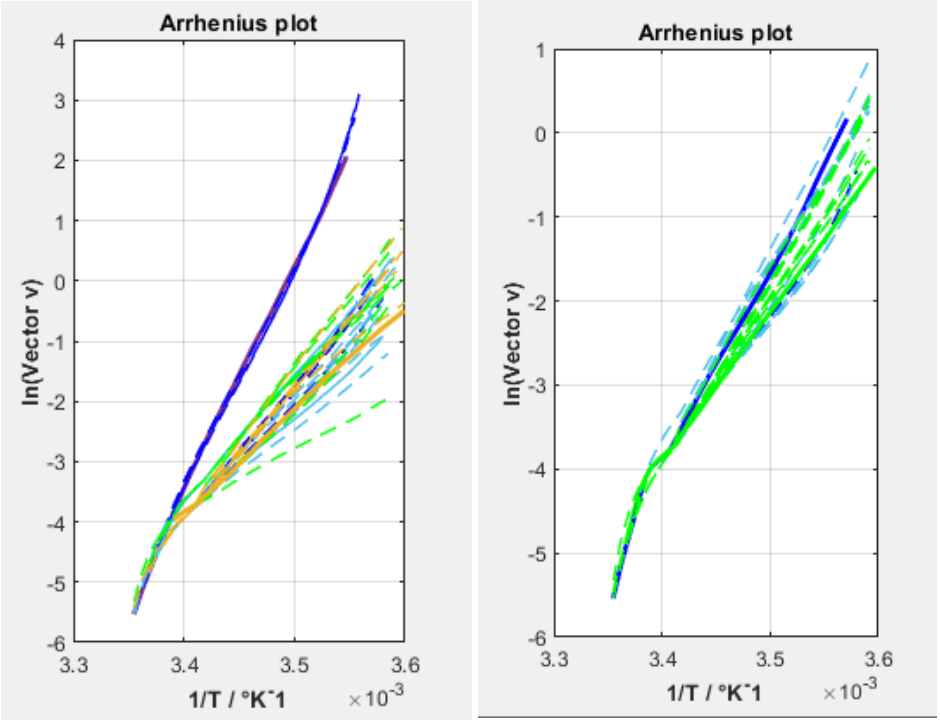

Figure 5.24: All possible Arrhenius curves from vectors v for combinations of three (left) and five (right) cooling rates from SolD data of the 175 g Bloom gel. The colors are referred to several ranges of averaged cooling rate values obtained from each combination: violet [0-2], blue [2-4], cyan [4-6], green [6-8], yellow [8-10], orange [10-12] and red [12-14]. The curves obtained for the lowest and the highest cooling rate ranges in both combinations of three and five rates are reported as continuous lines, while the other curves are dashed.

It can be detected from Figure 5.24 on the left the lowest cooling rate range as a violet continuous curve, while the highest one as an orange continuous line. In fact, the former is composed by 0,5, 1 and 2 °C/min which gives an average value of 1,17 that is inside the range [0-2], while the latter contains 7,5, 10 and 15 °C/min and has a mean of 10,83 that is inside the range [10-12].

Considering the right side of the figure, the lowest cooling rate range is plotted as a blue continuous curve, while the highest one as a green continuous line. In fact, the former is composed 0,5, 1, 2, 5 and 7,5 °C/min which gives an average value of 3,20 that is inside the range [2-4], while the latter contains 2, 5, 7,5, 10 and 15 °C/min and has a mean of 7,9 that is inside the range [6-8].

It can be confirmed from the figure that the trend of the activation energy is following an increasing in value for lower values of cooling rates considered.

To correctly compare the SolD activation energies of the 175 g Bloom gel (which are similar to the ones of SolC of the same gel, and to the ones of SolB of the 300 g Bloom

gel) with the ones of the two Vyazovkin's articles of 2009 and 2012, different cooling rate ranges were selected and analysed: two ranges of three (one containing 0,5, 1 and 2 °C/min, and the other with 7,5, 10 and 15°C/min) and two ranges of five (one containing 0,5, 1, 2, 5 and 7,5 °C/min, and the other with 2, 5, 7,5, 10 and 15 °C/min).

Cooling rate range [°C/min]	**Ea from literature [kJ/mol]**		**Ea from NPK method [kJ/mol]**		
	Vyazovkin 2009	*Vyazovkin 2012*	*Vyazovkin 2009*	*Vyazovkin 2012*	*SolD*
0,5-2	From -350 to -250				-321
7,5-15	-100		-35		-143
0,5-7,5		From -425 to -175		-216	-120
2-15	-150		-52		-146
0,5-15					-176

Table 5.5: Table comparing activation energy in each range of cooling rates from Vyazovkin 2009, Vyazovkin 2012 and SolD data.

Table 5.5 is summarizing all the activation energies obtained for each cooling rate range from the two articles data (Vyazovkin 2009 and Vyazovkin 2012) and from the experimental data (SolD) through the NPK method, and the ones reported in literature. It can be noticed that even if the amounts reported in Vyazovkin's article of 2009 for different cooling rate ranges are quite comparable to the ones obtained for SolD with the NPK method selecting the same ranges, the energy value estimated with this method for SolD is not falling into the range of values shown in Vyazovkin's article of 2012 at the same cooling rate range.

5.4.2 NPK analysis of activation energy dependence on conversion in sol-gel transition

Both Vyazovkin's papers were also reporting a dependence of activation energy on conversion (Figure 3.11 and Figure 3.12 in Chapter 3). Taking for instance Vyazovkin's article of 2009 data, the NPK code was run with two cooling rate ranges (overall 2,5-12,5 and 7,5-12,5 °C/min) for several conversion ranges: [0,1-0,25], [0,2-0,35], [0,3-0,45], [0,4-0,55], [0,5-0,65], [0,6-0,75], [0,7-0,85], and [0,8-0,9].

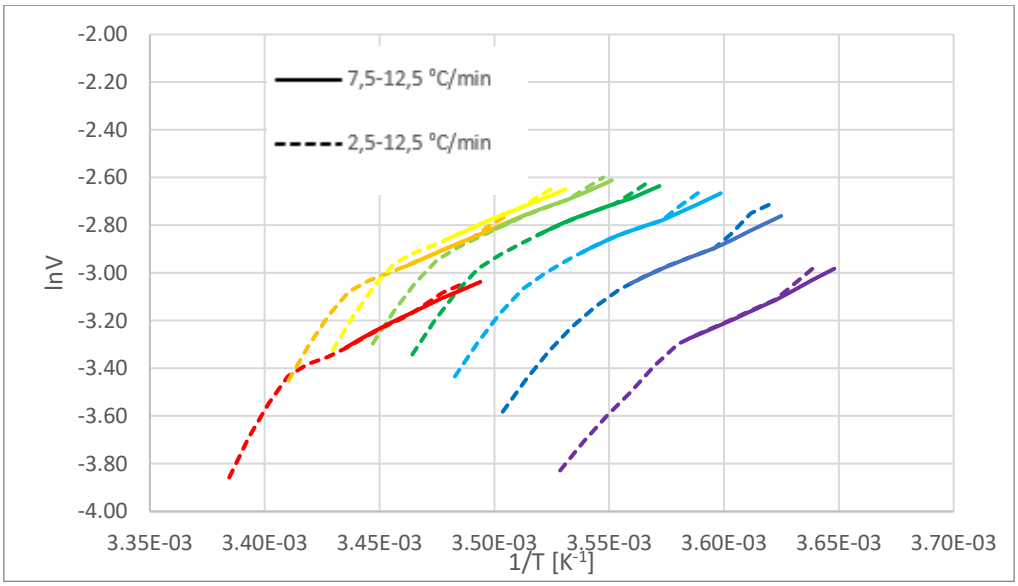

Figure 5.25: Arrhenius plot for Vyazovkin's article of 2009 with two different cooling rate ranges for several conversion ranges defined by colors: red (0,1-0,25), orange (0,2-0,35), yellow (0,3-0,45), light green (0,4-0,55), green (0,5-0,65), cyan (0,6-0,75), blue (0,7-0,85), and violet (0,8-0,9).

It seems from Figure 5.25 that the change of slope along the same curve, is given by the cooling rate range influence, according to the fact that for different scanning rate ranges the activation energy calculated is different.

It can be seen from Table 5.6 that the values of the activation energy among conversion are very similar between each other in the two cooling rate ranges considered. Thus, it seems that the amount of energy is not dependent on conversion in the overall and at higher scanning rates (Figure 5.26).

Conversion range	Ea [kJ/mol]	
	2,5-12,5 °C/min	*7,5-12,5 °C/min*
0,1-0,25	-58	-40
0,2-0,35	-52	-35
0,3-0,45	-51	-33
0,4-0,55	-51	-32
0,5-0,65	-52	-31
0,6-0,75	-54	-32
0,7-0,85	-56	-35
0,8-0,9	-60	-38
0,1-0,9	-52	-35

Table 5.6: Activation energies obtained from each conversion range from Vyazovkin's article of 2009 data with two different cooling rate ranges.

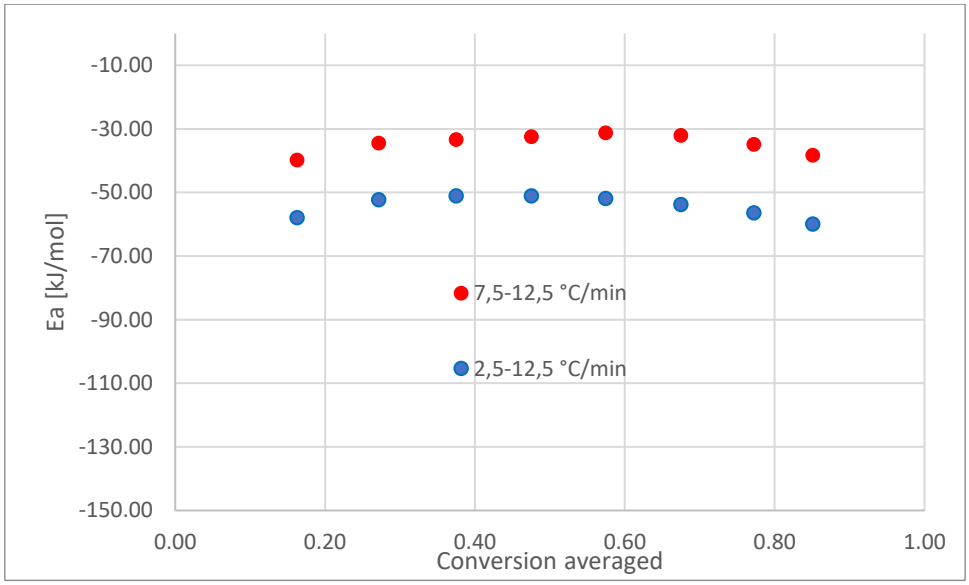

Figure 5.26: Activation energy against conversion at different cooling rate ranges. As conversion values in x-axis, it was taken an average value for each conversion range.

From Figure 5.26 it can be confirmed that the activation energy values obtained are following the trend in Figure 3.11 in Chapter 3 for the two cooling rate ranges considered.

A clear dependence of *Ea* on conversion is shown at lower scanning rate range, which can be better analysed through Vyazovkin 2012's article data.

In this case, the NPK code was run with 0,5-7,5 °C/min of cooling rate range for several conversion ranges: [0,1-0,25], [0,2-0,35], [0,3-0,45], [0,4-0,55], [0,5-0,65], [0,6-0,75], [0,7-0,85], and [0,8-0,9].

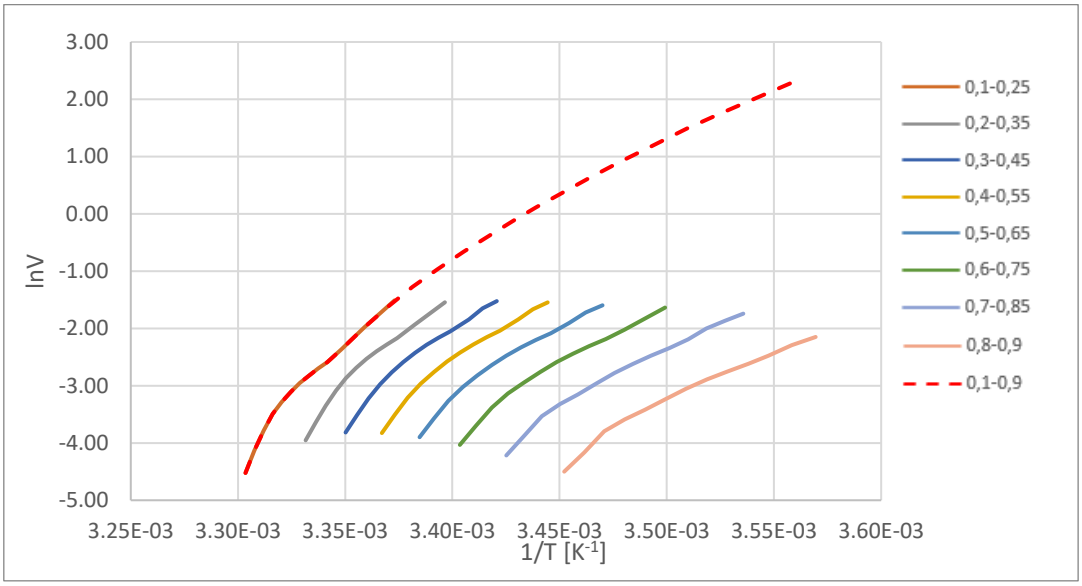

Figure 5.27: NPK Arrhenius plot for several conversion ranges obtained from data of Vyazovkin's 2012 article.

In Figure 5.27 it can be seen the original curve obtained considering the overall conversion range 0,1-0,9 compared to the ones estimated from several conversion ranges. It seems the lines are showing decreasing values of the slopes for higher conversion ranges, thus the activation energy will be lower (in absolute values) for higher conversion values.

Table 5.7 is representing the values of the activation energy obtained for each range through the NPK method, showing that in this case these values are very different between each other and actually increasing (in absolute values) for lower conversion ranges according to Figure 3.12 in Chapter 3 (Figure 5.28). Thus, it seems following that the amount of energy is dependent on conversion.

Conversion range	T averaged [K]	Ea [kJ/mol]
0,1-0,25	300	-334
0,2-0,35	298	-296
0,3-0,45	296	-256
0,4-0,55	294	-232
0,5-0,65	292	-191
0,6-0,75	290	-198
0,7-0,85	287	-175
0,8-0,9	285	-157
0,1-0,9		-216

Table 5.7: Activation energies and averaged temperature obtained from each conversion range from Vyazovkin's article of 2012 data.

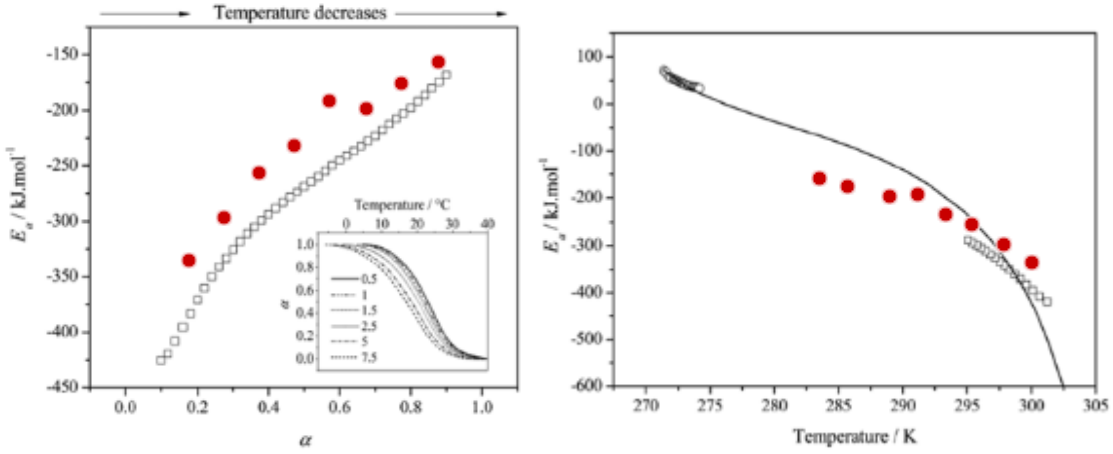

Figure 5.28: Plot of Ea against conversion (left) and temperature (right) with data obtained through NPK method (pointed in red) compared to the ones reported in literature.

In Table 5.7 is also reported the estimated averaged temperature for each conversion range which is related to the conversion. Thus, *Ea* is not only dependent on conversion, but also on temperature according to Figure 3.13 In Chapter 3 (Figure 5.28).

Once it was tested that NPK method is giving comparable results with the ones of the two literatures regarding the activation energy dependence on both scanning rate and conversion, it is now analysed the behaviour of the energy calculated from the experimental data.

The procedure followed for the two Vyazovkin's papers was then repeated for the SolC data of the 175 g Bloom gel (which are similar to the ones of SolD of the same gel, and to the ones of SolB of the 300 g Bloom gel).

Running the NPK code for several conversion ranges and for different cooling rate ranges, the following plot was obtained:

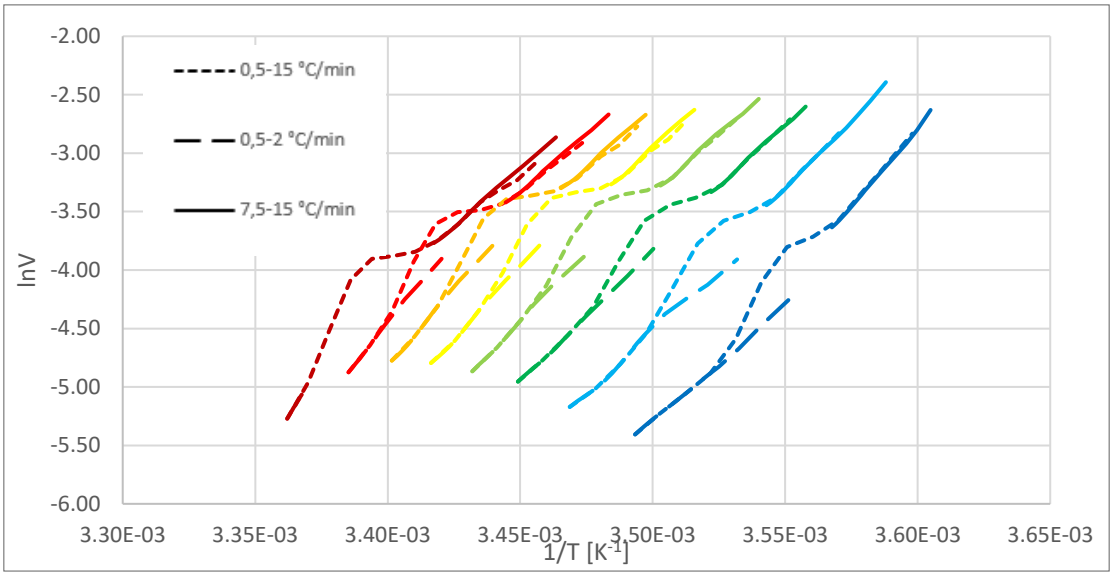

Figure 5.29: Arrhenius plot for SolC data of 175 g Bloom gel with different cooling rate ranges and several conversion ranges defined by colors: dark red (0,1-0,25), red (0,2-0,35), orange (0,3-0,45), yellow (0,4-0,55), light green (0,5-0,65), green (0,6-0,75), cyan (0,7-0,85), and blue (0,8-0,9).

It seems from Figure 5.29 that the change of slope along the same curve, is again given by the cooling rate range influence, according to the fact that for different scanning rate ranges the activation energy calculated is different.

It seems from Table 5.8 that the amount of energy is quite constant among conversion in both 0,5-15 °C/min and 7,5-15 °C/min of cooling rate ranges, while it is dependent on conversion in the 0,5-2 °C/min one.

Conversion range	Ea [kJ/mol]		
	0,5-15 °C/min	*0,5-2 °C/min*	*7,5-15 °C/min*
0,1-0,25	-169	-308	-166
0,2-0,35	-171	-234	-164
0,3-0,45	-170	-222	-169
0,4-0,55	-172	-210	-175
0,5-0,65	-191	-197	-170
0,6-0,75	-176	-186	-174
0,7-0,85	-196	-174	-193
0,8-0,9	-211	-163	-221

Table 5.8: Activation energies obtained from each conversion range from SolC data of 175 g Bloom gel with different cooling rate ranges.

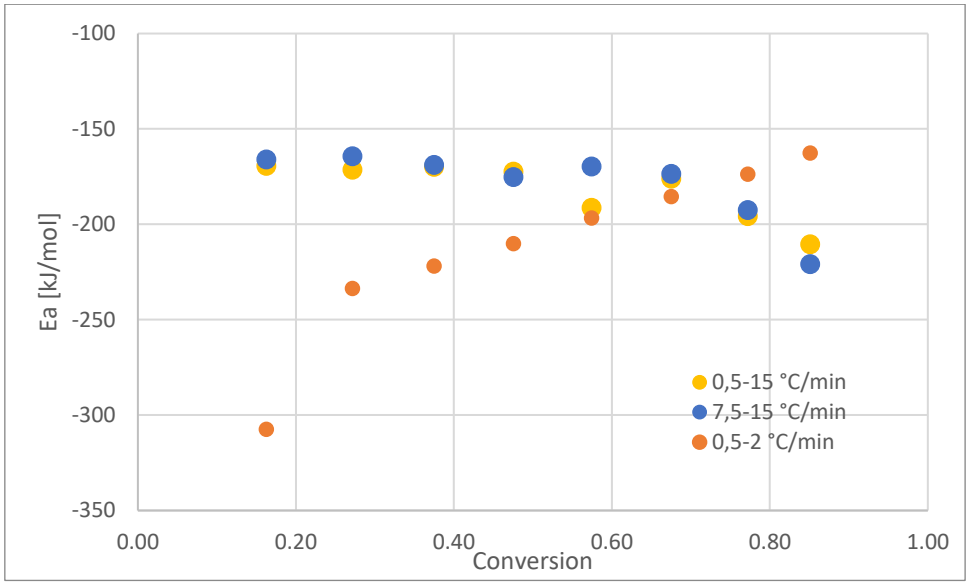

Figure 5.30: Activation energy against conversion at different cooling rate ranges. As conversion values in x-axis, it was taken an average value for each conversion range.

It can be seen also from Figure 5.30 that the values for the largest scanning rate range and the ones for the range with the highest cooling rates are quite constant and pretty similar, while the amount of energy for the lower scanning rate range is following the trend discussed before: it is increasing among conversion. It can be concluded then, that the experimental NPK results are according with literature observations, even for some difference in values.

CONCLUSION

In this work, two types of gelatin solutions are analysed under DSC, the 175 and 300 g Bloom gels.

The thermal treatments are based on a scanning rate range from 0,5 to 15 °C/min for the gelation, and from 0,5 to 10 °C/min for the melting phenomena.

For both of them, the peak curve obtained during gelation is shifting towards lower temperature with higher cooling rates (from 22 to 13 °C), and the one during melting presents higher temperature with increasing heating rates (from 26 to 28 °C). It is noticed that the enthalpy of reaction, thus the estimated area under the DSC peak curve, is following the same trend of the peak temperature among scanning rates (from 21 to 7 J/g during cooling, and from -21 to -7 J/g during heating). In addition, the fact that the enthalpy values during gelation and during melting are the same, shows the reversibility of the sol-gel transition.

By applying the NPK method to the DSC data it is estimated the activation energy and the kinetic model of the reversible gelation phenomenoun for both gels. It is observed a clear dependence of the activation energy on the DSC thermal treatments and on conversion at low scanning rates. The results obtained are in good agreement with the reported values from similar gelatin solutions got through kinetic classical methods. Thus, the NPK method is useful for the kinetic analysis of the gelation process of gelatin solutions.

REFERENCES

[1] R. K. Herz, “Chemical Reaction Engineering-Part 7.”

[2] D. M. Mulvihill and M. Donovan, “Whey Proteins and Their Thermal Denaturation - A Review,” 1987. [Online]. Available: https://about.jstor.org/terms

[3] S. G. Anema and A. B. Mckenna, “Reaction Kinetics of Thermal Denaturation of Whey Proteins in Heated Reconstituted Whole Milk,” 1996.

[4] M. A. M. Hoffmann, J. C. Van Miltenburg, and R. J. M. Van Mil, “therm0chimica acta ELSEVIER The suitability of scanning calorimetry to investigate slow irreversible protein denaturation,” 1997.

[5] M. S. Rahman, G. Al-Saidi, N. Guizani, and A. Abdullah, “Development of state diagram of bovine gelatin by measuring thermal characteristics using differential scanning calorimetry (DSC) and cooling curve method,” *Thermochim Acta*, vol. 509, no. 1–2, pp. 111–119, Sep. 2010, doi: 10.1016/j.tca.2010.06.011.

[6] F. DANNENBERG and H. -G KESSLER, “Reaction Kinetics of the Denaturation of Whey Proteins in Milk,” *J Food Sci*, vol. 53, no. 1, pp. 258–263, 1988, doi: 10.1111/j.1365-2621.1988.tb10223.x.

[7] K. Chen and S. Vyazovkin, “Temperature dependence of sol-gel conversion kinetics in gelatin-water system,” *Macromol Biosci*, vol. 9, no. 4, pp. 383–392, 2009, doi: 10.1002/mabi.200800214.

[8] H. B. Bohidar and S. S. Jena, “Kinetics of sol-gel transition in thermoreversible gelation of gelatin,” *J Chem Phys*, vol. 98, no. 11, pp. 8970–8977, 1993, doi: 10.1063/1.464456.

[9] K. Nishinari and K. Nishinari, “Rheological and DSC study of sol-gel transition in aqueous dispersions of industrially important polymers and colloids,” 1997.

[10] G. I. Tseretely and O. I. Smirnova, “DSC study of melting and glass transition in gelatins,” *Journal of Thermal Analysis*, vol. 38, no. 5, pp. 1189–1201, May 1992, doi: 10.1007/BF01979179.

[11] C. Qiao, J. Zhang, X. Ma, W. Liu, and Q. Liu, “Effect of salt on the coil-helix transition of gelatin at early stages: Optical rotation, rheology and DSC

studies," *Int J Biol Macromol*, vol. 107, no. PartA, pp. 1074–1079, Feb. 2018, doi: 10.1016/j.ijbiomac.2017.09.079.

[12] J. L. Gornall and E. M. Terentjev, "Helix-coil transition of gelatin: Helical morphology and stability," *Soft Matter*, vol. 4, no. 3, pp. 544–549, 2008, doi: 10.1039/b713075a.

[13] N. Guigo, N. Sbirrazzuoli, and S. Vyazovkin, "Atypical gelation in gelatin solutions probed by ultra-fast calorimetry," *Soft Matter*, vol. 8, no. 27, pp. 7116–7121, Jul. 2012, doi: 10.1039/c2sm25737h.

[14] F. Casanova *et al.*, "Physico-chemical, structural and techno-functional properties of gelatin from saithe (Pollachius virens) skin," *Int J Biol Macromol*, vol. 156, pp. 918–927, Aug. 2020, doi: 10.1016/j.ijbiomac.2020.04.047.

[15] M. S. Rahman, G. S. Al-Saidi, and N. Guizani, "Thermal characterisation of gelatin extracted from yellowfin tuna skin and commercial mammalian gelatin," *Food Chem*, vol. 108, no. 2, pp. 472–481, May 2008, doi: 10.1016/j.foodchem.2007.10.079.

[16] S. M. Ahsan and C. M. Rao, "Structural studies on aqueous gelatin solutions: Implications in designing a thermo-responsive nanoparticulate formulation," *Int J Biol Macromol*, vol. 95, pp. 1126–1134, Feb. 2017, doi: 10.1016/j.ijbiomac.2016.10.103.

[17] Sempere J, Nomen R, Serra E, and Sempere B, *Thermal analysis of Micro, Nano- and Non-Crystalline Materials*, vol. 9. in Hot Topics in Thermal Analysis and Calorimetry, vol. 9. Dordrecht: Springer Netherlands, 2013. doi: 10.1007/978-90-481-3150-1.

[18] J. M. Criado, J. Malek, and F. J. Gotor, "THE APPLICABILITY 0~ THE SESTAK-BERGGREN KINETIC EQUATION IN CONSTANT RATE THERMAL ANALYSIS (CRTA)," Elsevier Science Publishers B.V, 1990.

[19] N. Ferrer, E. Serra, J. Sempere, and R. Nomen, "Non-parametric kinetic analysis of autocatalytic reactions," *J Loss Prev Process Ind*, vol. 49, pp. 357–366, 2017, doi: 10.1016/j.jlp.2017.08.001.